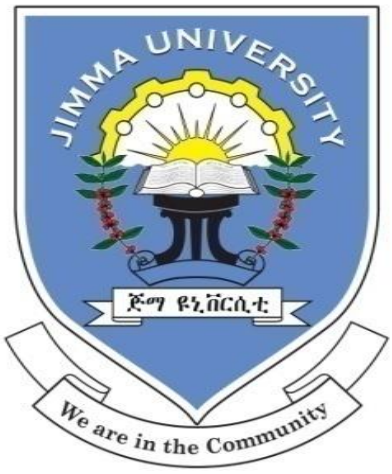

JIMMA UNIVERSITY

JIMMA INSTITUTE OF TECHNOLOGY

FACULTY OF CIVIL AND ENVIROMENTAL ENGONEERING

STRUCTURAL ENGINEERING STREAM

Analytical study of load carrying capacity and torsional behavior of horizontally curved reinforced concrete deep beam

A Research Thesis Submitted to Jimma University in Partial Fulfillment of the Requirements for the Degree of Masters of Science in Structural Engineering.

By: Goshu Kenea

Jimma, Ethiopia

27 / 11/ 2018

JIMMA UNIVERSITY

JIMMA INSTITUTE OF TECHNOLOGY

FACULTY OF CIVIL AND ENVIROMENTAL ENGONEERING

STRUCTURAL ENGINEERING STREAM

Analytical study of load carrying capacity and torsional behavior of horizontally curved reinforced concrete deep beam

A Research Thesis Submitted to Jimma University in Partial Fulfillment of the Requirements for the Degree of Masters of Science in Structural Engineering.

By: Goshu Kenea

Advisor: Ass. Prof. Getachew Kebede

Co-advisor: Asso. Prof. Elmer C. Agon

Jimma, Ethiopia

27 /11/ 2018

DECLARATION

Goshu Kenea

I declare that this thesis entitled "Analytical study of the load carrying capacity and torsional behaviour of horizontally curved reinforced concrete deep beam" is my original work, and has not been presented by any other person for an award of a degree in this or any other University.

Goshu Kenea (Candidate)

Signature_____ Date_____

This thesis has been submitted for examination with my approval as a university advisor.

Advisor: Ass. Prof. Getachew Kebede

Signature_____ Date_____

Co- Advisor: Asso. Prof. Elmer C. Agon

Signature_____ Date_____

ABSTRACT

Currently complex construction industry is drastically growing in the world especially in urban areas. In this progress the demand of constructing different types of structures are increasing. Among those structures, reinforced concrete deep beam is one type of structure that can be constructed in different arrangement in order to increase the resistance to torsion, shear, bending, fire, and temperature. Additionally, it is used to increase the beauty by fitting the geometric limitation of the building. Deep beam can be conventionally straight, horizontally curved, which is mainly used to carry huge concentrated load that act transverse to its plane. Horizontally curved deep beams have large resistance. It is used at rounded corners of buildings, modern highway bridges, construction of stadium and others. Therefore, detail studying of load carrying capacity and torsional behavior of horizontally curved reinforced deep beam is crucial in order to provide safe and economic deep beam structure.

The torsional behaviuor of horizontally curved reinforced concrete deep beam and its load carrying capacitys had been discussed in the lesson of the study. The research focused on the effect of span length to overall depth (L/D) and length to radius (L/R) ratio on the torsional behaviour of horizontally curved reinforced concrete deep beam and its load carrying capacity. 21 samples of reinforced deep beam studied to investigate the load carrying capacity and torsional behavior using non-linear finite element analysis with ABAQUS Software package under concentrated load at mid-span of the beam. From these samples, straight reinforced concrete deep beam are three as control group and others are horizontally curved reinforced concrete deep beam.

Concrete damaged plasticity model has been used to model the beam with C-25 grade concrete and steel reinforcement of having diameter of ϕ4mm, ϕ10mm and ϕ12mm with 568Mpa, 596Mpa, 643Mpa steel yield strength respectively. In addition, eight-noded brick element had been used during modeling.

Finally, from finite element analysis the load carrying capacity, the load deflection and load twisting angle curve had been obtained with respect to different length to depth (L/D) and length to radius (L/R) ratio.

In conclusion, the analysis result showed, significant increase of internal torsion and decrease of load carrying capacity as length to depth (L/D) and length to radius (L/R) ratio increase for horizontally curved deep beam when compared torespective straight deep beam. The study also revealed that, the length to depth (L/D) has more effect when compared to length to radius (L/R) ratio.

Key words: *torsional behaviour, horizontally curved reinforced concrete deep beam, non-linear finite element method.*

ACKNOWLEDGEMENT

First of all I would like to thank God, who enabled me doing this research paper. ThenI would like to express my sincere appreciation and gratitude to my supervisorsto Ass. Prof. Getachew Kebede and Asso.Prof.Elmer C. Agon for their guidance, patience and untiring support. Their constant mentorship and suggestions have not only enriched my technical knowledge, but have also provided me with the confidence and determination needed to pursue and complete this research.

I would also like to use this opportunity to convey my gratitude to my wife Mingot Gutu and my sister Darartu Dheressa for their unlimited assistance.

Finally, I would like thank my classmates in contributing different reference and for sharing experiences.

TABLE OF CONTENTS

LIST OF TABLES

LIST OF FIGURES

ACRONYMS

IS	Indian standard
EBCS	Ethiopian Building Code Standards
GUI	Graphical user interface
HSC	High Strength concrete
ACI	American Concrete Institute
L/R	Length to radius ratio
L/D	Length to depth ratio
FEM	Finite element method
$f_c^{'}$	Ultimate compressive strength of concrete
ε_u	Ultimate strain
ADINA	Automatic Dynamic Incremental Nonlinear Analysis
STM	Strut and Tie Model
E_c	Elastic modulus of concrete
E_s	Elastic Modulus of Steel
f_{ctm}	Peak tensile stress
CFRP	Carbon fiber reinforced polymer
E_{co}	Initial undamaged modulus of elasticity of concrete
f_t	Tensile stress of concrete
SCM	Smeared Crack Model
BCM	Brittle Cracking Model
CDPM	Concrete Damaged Plasticity Model
ε_c^{in}	Inelastic strain of concrete
ε_c	Total compressive strain of concrete
ε_{oc}^{el}	Elastic compressive strain corresponding to the undamaged material
σ_c	Compressive stress of concrete
σ_{oc}	Initial yield of concrete
w	Cracking opening displacement
Gf	Concrete fracture energy

ε_t^{ck}	Cracking strain
ε_t	Total tensile strain
ε_{ot}^{el}	Elastic tensile strain corresponding to the undamaged material
σ_t	Tensile stress
σ_{ot}	Peak tensile stress
w_c	Maximum cracking displacement
ε_c^{pl}	Compression plastic strain
ε_t^{pl}	Tension plastic strain
d_c	Compression damage parameter
d_t	Tension damage parameter
$\bar{\sigma}_c\left(\tilde{\varepsilon}_c^{pl}\right)$	Effective compressive cohesion stress
$\bar{\sigma}_t\left(\tilde{\varepsilon}_t^{pl}\right)$	Effective tensile cohesion stress
σ_{bo}	Initial equibiaxial compressive yield stress
σ_{co}	Initial uniaxial compressive yield stress
$\bar{q}$	Mises equivalent stress
J_2	Second deviatoric stress invariant
$\bar{p}$	Effective hydrostatic pressure stress
I_1	First stress invariant
f_{cm}	Mean compressive stress at 28 days
f_{ck}	Characteristic cylindrical compressive strength of concrete at 28 days
ε_{c1}	Strain at peak stress
γ	Eccentricity
Ψ	Dilation angle
u_t^{cr}	Crack-opening displacement
u^{pl}	Plastic displacement
K	Stiffness matrix
F^{nr}	Internal load vector
μ	Viscosity parameter
ε_v^{pl}	Viscoplastic strain

CHAPTER ONE

INTRODUCTION

1.1. Background of the Study

Horizontally curved reinforced concrete beams are extensively used in many fields, such as in the construction of modern highway bridges, circular balconies, the rounded corners of buildings, stadium construction. In these cases, large depths are needed for curved beams in order to resist high loads and to fulfill some aesthetic purposes. The analysis of such members is very complex due to the fact that those members are subjected to combined action of bending, shear and torsion. Furthermore, non-homogeneous nature of the materials involved contributes to the complexity of the problem. Therefore, it becomes necessary to employ numerical analysis procedures using finite element method, to satisfy the safety and the economy requirements (Ammar Y.A., etal; 2010).

Beams with large depths in relation to spans are considered as deep beams. Simply-supported beam is classified as deep when the ratio of its effective span L to overall depth D is less than 2 and Continuous beams are considered as deep when the ratio L/D is less than 2.5 (IS 456,2000). The effective span is defined as the centre-to-centre distance between the supports or 1.15 times the clear span whichever is less. They are structural elements loaded as simple beams in which a significant amount of the load is carried to the supports by a compression force combining the load and the reaction. As a result, the strain distribution is no longer considered linear, and the shear deformations become significant when compared to pure flexure. Because of their proportions deep beams are likely to have strength controlled by shear rather than flexure. On the other hand, their shear strength is expected to be significantly greater than predicted by the usual equations, because of a special capacity to redistribute internal forces before failure and to develop mechanisms of force transfer quite different from beams of common proportions. Deep beams are widely used as transfer girders in offshore structures and foundations, walls of bunkers, load bearing walls in buildings, plate elements in folded plates, pile caps, raft beam wall of rectangular tank, hopper, floor diaphragm and shear walls. With the strong growth of construction work in many developing countries, deep beam will be designed and its behavior prediction is a subject of considerable relevance. Traditional design assumptions, especially

regarding plane section remain plane after bending for shallow beams; do not apply to deep beams. Beams with clear span to effective depth ratio less than 5 are considered as deep beams (ACI 318-99). Beams with span to total depth less than or equal to 3 are considered as deep beam (EBCS EN 1992, 2013). However, it should be noted that the design of these structural elements are not adequately covered by existing codes of practices. Failure behavior of deep beams is significantly different from that of shallow beams because of geometry and load transfer mechanism. Thus serviceability and failure pattern of these structural elements is not reported extensively due to the lack of clear procedure for prediction of their behavior.

A horizontally curved deep beam, loaded transversely to its plane, is subjected to torsion in addition to bending and shear. Therefore, special features of analysis and design for horizontally curved deep beams is necessary to include the effect of above mentioned factors. However, till yet studies concerning reinforced concrete horizontally curved deep beams are rare. One of the most effective numerical methods utilized for analyzing reinforced concrete members is the finite element method (Ammar Y.A., etal; 2010). Using this method, many aspects of the phenomenological behavior of reinforced concrete structures can be modeled rationally. These aspects include the tension-stiffening, non-linear multi-axial material properties, modeling of cracking and crushing, and many other properties related to the behavior of reinforced concrete members under stresses. An important utilization of the finite element method is the modeling of the degradation of concrete compressive strength in the presence of transverse tensile straining as happens in members subjected dominantly to torsion or shear stresses. Therefore, the present study has been adopted a three dimensional finite element model to investigate the torsional effect and the load carrying capacity of reinforced concrete horizontally curved deep beams.

1.2. Statement of the Problem

Currently, complex construction industry is drastically growing in the world especially in urban areas. In this progress the demand of constructing different types of structure are increasing. Among these, deep beam is one type structure that can be constructed in different arrangement in order to increase its resistance to torsion, shear, bending moment, fire, and temperature and additionally to increase the beauty and to fit the geometric pattern of the building structure.

The deep beam can be straight and horizontally curved. Horizontally curved deep beams are used in the rounded corners of buildings, stadium construction, modern highway bridges etc. The demands of horizontally curved reinforced concrete deep beam in different building structure are increasing because of its high resistance capacity. Therefore, detail studying of shear, moment and torsional behavior of horizontally curved reinforced concrete deep beam is crucial in order to provide safe and economic deep beam structure (Ammar Y.A., etal; 2010). Horizontally curved deep beams are mostly acted by transverse action that is perpendicular to its plane of curvature. These arises the need for more elaborate investigations to be done for better understanding and design of horizontally curved reinforced concrete deep beams.

The difficulty for structural engineer in the world with load carrying capacity and torsional behavior on horizontally curved deep reinforced concrete beam, initiated to study on this area. There is unclear understanding on the torsional behaviour and effect. Most of the design works in practice are more of ignorant for torsional consideration, even though its effect is disastrous. The study gives more discussion on load carrying capacity and torsional behavior to set possible recommendation on measure to be taken relating to its effect. On other hand, the load carrying capacity and torsional behavior analysis for horizontally reinforced concrete deep beam is incomplete, needs further research. Therefore, the study of this paper gives deep understanding and solution to those questions. In general, it needs for every structural engineer to be easy access to horizontally curved reinforced concrete deep beam in order to satisfy with the required condition, to increase the appearance of the structure.

1.3. Research Questions

The research questions that addressed were as follows:

- How L/R and L/D ratio affect the deflection and twisting angle of horizontally curved reinforced concrete deep beam?
- How L/R and L/D ratio affect the load resistance of horizontally curved reinforced concrete deep beam?
- How the torsion related to the flexural resistance of horizontally curved reinforced concrete deep beam?

1.4. Objectives of the study

1.4.1 General objective

- To investigate the load carrying capacity and torsional behavior of horizontally curved reinforced concrete deep beam

1.4.2. Specific objective

- To investigate the effect of L/R and L/D ratio on the deflection and twisting angle of horizontally curved reinforced concrete deep beam.
- To study the effect of L/R and L/D ratio on the load resistance of horizontally curved reinforced concrete deep beam.
- To evaluate the effect of torsion on the load resistance of horizontally curved reinforced concrete deep beam.

1.5. Significance of the Study

Recently, horizontally curved reinforced concrete deep beam become a popular in the construction of rounded corners of the building, modern highway bridges, and stadium construction which is used to carry huge concentrated load that come from column that does not start from ground and others. In building structure, huge concentrated transverse load and the dead load from slab are carried by beams. In order to increase the appearance and fit the geometric shape of the construction, civil engineers are interested in constructing horizontally curved reinforced concrete deep beam. This paper makes every civil engineers easy access to horizontally curved reinforced beam by identifying the effect of torsion to construct the most safest and economic section.

1.6. Scope and Limitation of the Study

The research mainly focused on the study of torsional behavior of horizontally curved reinforced concrete deep beam having constant length of 1200mm, L/R ratio of 1.57, 1.31, 1.05, 0.79, 0.52, and 0.26, length to depth ratio of 3, 2.67, 2.4, width of 100mm, concrete grade of 25Mpa, and steel with yield strength of 568Mpa, 596Mpa, and 643Mpa. Three straight deep beams were also considered as control group. Single span fixed type support was used. When the length and depth

changed with the same factor for practical application, the compressional, tension and longitudinal distribution reinforcement should be increased by using the cross sectional ratio of deep beam. Additionally, lateral reinforcement can be rearranged based on length ratio.

CHAPTER TWO

LITERATURE REVIEW

2.1. General

Horizontally curved deep beam is a horizontal structure that is mainly used to resist bending moment, torsional moment and shear force which is transversely applied its longitudinal axis. It can be made from different material like steel, reinforced concrete, composite (steel structure and concrete) based on requirement. Reinforced concrete deep beam is made from the combination of concrete and steel wherein the steel reinforcement provides the tensile strength lacking in the concrete (Macgregor, 1997).

2.2. Concrete

Reinforced concrete is a composite material consisting of steel reinforcement and concrete. These two materials had vastly different properties. The required mechanical properties of reinforcing steel are generally known. However, those for concrete are more difficult to define depending upon the particular condition of mixing, placing, curing, nature, rate of loading and environmental influences. Concrete contains a large number of micro-cracks, especially at interfaces between coarse aggregate and mortar, even before any load has been applied. This property is decisive for the mechanical behavior of concrete. The propagation of these micro-cracks during loading contributes to the nonlinear behavior of concrete at low stress level and cause volume expansion at failure.

2.2.1. Uniaxial Compression Behavior for Concrete

A typical stress-strain behavior for concrete under uniaxial compression is shown in Figure 2.1. It is nearly linear up to about (0.3-0.5) times the ultimate strength of concrete (f_c').

The stress-strain curve shows a gradual increase in curvature that occurs up to a stress level of $0.75f_c'$ to $0.9f_c'$, after which the stress-strain curve bends sharply and approaches the peak point at (f_c') (Chen, 1982, Chen and Saleeb, 1981). Then, the stress-strain curve descends until failure occurs due to the crushing of concrete at the ultimate strain (ε_u).

The shape of the stress-strain curve is similar for concrete of low, normal, and high strengths. High strength concrete behaves in a linear fashion to a relatively higher stress level than the low strength concrete. The strain at the maximum stress is approximately (0.002) (although high strength concretes have somewhat a little higher strain at peak stresses). On the descending portion of the stress-strain curve, higher strength concretes tend to behave in a more brittle manner, with the stress dropping off more sharply than it does for concrete with lower strength (Wischers, 1978).

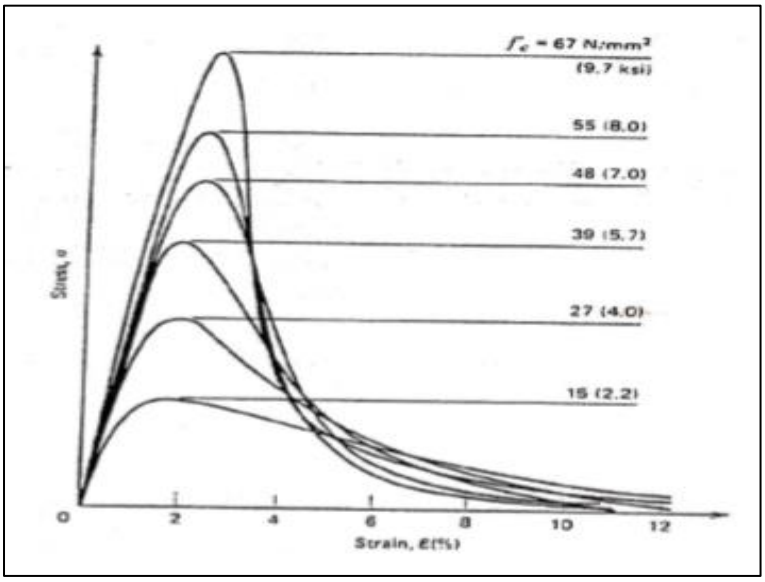

Figure 2.1: Uniaxial Compressive Strain curve for concrete with different strength (Wischers, 1978)

The modulus of elasticity of concrete E_c is generally taken to be a function of the compressive strength f'_c .The Poison's ratio v for concrete under uniaxial compression ranges from 0.15 to 0.22 which remains constant up to about $0.8f'_c$(Chen, 1982, Mackava and Okamura, 1983).

2.2.2. Tensile Behavior of Concrete

The general mechanical behavior of concrete under uniaxial tensile loading shows many similarities to the behavior observed in uniaxial compression. Typical stress – strain curves for concrete in uniaxial tension are shown in Figure 2.2. In general, at a stress less than 60 % of the tensile strength, the creation of new micro-cracks is negligible. So, this stress level will

correspond to a limit of elasticity. Above this level of stress, the bond micro-cracks start to grow (Hughes and Chapman, 1966). The direction of crack propagation for uniaxial tension is transverse (normal) to the stress direction. The growth of every new crack will reduce the available load - stress capacity and this reduction causes an increase in the stresses at critical crack tips. The failure in tension is caused by a few connected cracks rather than by numerous cracks, as it is for compressive states of stress.

The ratio between uniaxial tensile strength f_t and compressive strength f_c' may vary considerably but usually ranges from 0.05 to 0.1. The modulus of elasticity under uniaxial tension is somewhat higher and Poisson's ratio somewhat lower than in uniaxial compression.

The direct tensile strength of concrete is difficult to measure and is normally taken as $(0.3 - 0.4)\sqrt{f_c'}$. Many times, either the modulus of rupture $f_t$or the split cylinder strength f_t is used to approximate the tensile strength of concrete. The value of the modulus of rupture of concrete varies quite widely but is normally taken as $0.65\sqrt{f_c'}$ (ACI Committee 318M, 2011) and $0.3fck^{2/3}$(Eurocode2, 2004).The split cylinder tensile strength is usually somewhat lower, at approximately $(0.45 - 0.55)\sqrt{f_c'}$ in MPa (Chen, 1982).

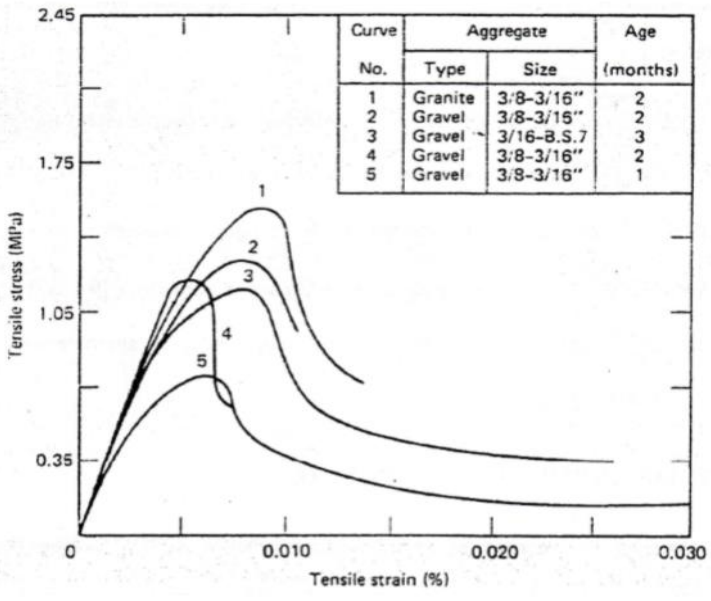

Figure 2.2: Typical Tensile Stress-Strain Curve for Concrete (Hughes, B. P. and Chapman, 1966)

2.2.3. Biaxial Stress Behavior Concrete

(Kupfer and Grestle, 1973) had performed extensive experimental tests on concrete plates made with three different concrete strengths (19, 31 and 58 Mpa) and loaded in orthogonal directions. The ultimate strength data were reported in terms of a biaxial stress envelope as shown inFigure2.3. Under biaxial compression, the compressive strength increases approximately 25 % over that of the uniaxial strength at the stress ratio of ($\sigma_2 = 0.5\sigma_1$) and this is reduced to about 16 % at an equal biaxial compression state ($\sigma_2 = \sigma_1$). Under biaxial tension - compression, the compressive strength is decreased almost linearly as the applied tensile stress is increased. Under biaxial tension, the concrete strength is almost the same as that of the uniaxial tensile strength.

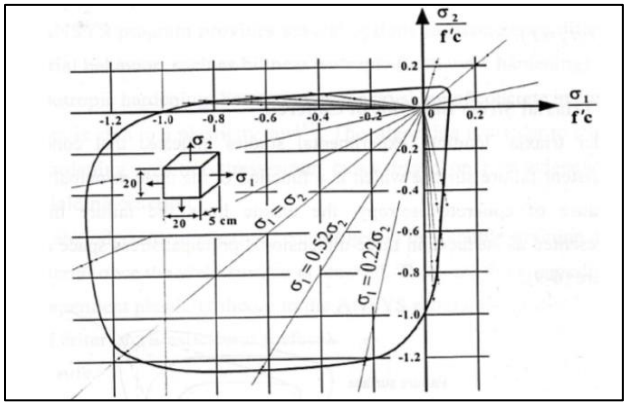

Figure 2.3: Biaxial State of Loading (Kupfer and Grestle, 1973)

2.2.4. Tri-axial Stress Behavior of Concrete

Under tri-axial loading, experimental studies indicated that concrete has a consistent failure surface which is a function of the three principal stresses (Chen and Saleeb, 1981). Because of concrete isotropy, the elastic limit and failure limit can be represented as surfaces in three dimensional principal stress space shown in Figure 2.4.

For increasing hydrostatic compressions along the ($\sigma_1 = \sigma_2 = \sigma_3$)axis, the deviatoric sections (planes perpendicular to the axis ($\sigma_1 = \sigma_2 = \sigma_3$)) of the failure surface are more or less circular, which indicates that the failure in this region is independent of the third stress invariant. For smaller hydrostatic pressure, these deviatoric cross sections are convex and noncircular. The failure surface can be represented by three stress invariants.

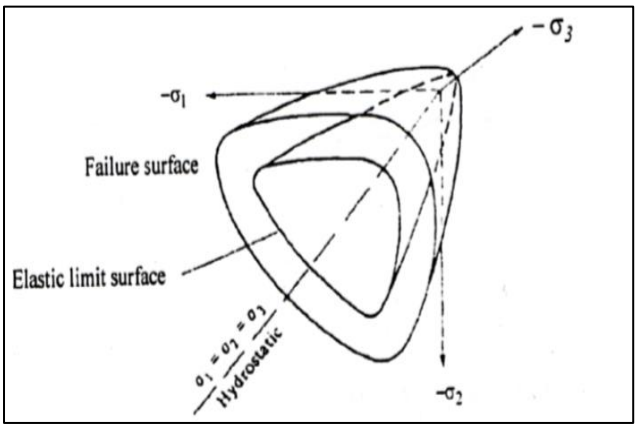

Figure 2.4: Failure Surface of Concrete in 3-D Stress Space (Chen and Saleeb, 1981)

2.3. Steel reinforcement

Since the reinforcing bars are normally long and relatively slender, they can generally be assumed to be capable of transmitting axial forces only. The useful strength of ordinary reinforcing steels in tension as well as compression (yield strength) is about 15 times the compressive strength of common structural concrete and well over 100 times its tensile strength. Steel reinforcement is a high cost material compared with concrete. It also used to resist compressive force in addition to tension force. The most common types of reinforcement are hot-rolled round deformed bars. The closely spaced rib shaped surface deformations of the reinforcing bars provide a high degree of interlocking of the two materials. The typical stress-strain curve for steel reinforcement is shown in Figure 2.5.

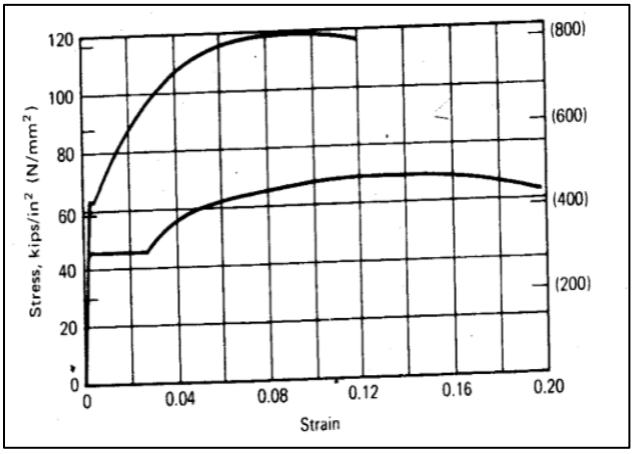

Figure 2.5: Typical stress-strain curves for steel reinforcement (Park andPaulay, 1974)

2.4. Reinforced concrete structure

Reinforced concrete is used as building construction materials in every country. The universal nature of reinforced concrete construction stems from the wide availability of reinforcing bars and of the constituents of concrete (gravel or crushed rock, sand, water, and cement), from the relatively simple skills required in concrete construction, and from the economy of reinforced concrete compared with other forms of construction (Macgregor, J. G, 2012).

2.5. Reinforced concrete deep beam analysis

2.5.1. Strut-and-Tie method

The strut-and-tie models have been widely used as an effective tool for designing reinforced concrete deep beam structures (Hamed, 2009). The principle of the strut-and-tie method is to design a truss where all the stresses are condensed into compression members and tension members connected by nodes (Maxwell, 1996). The concrete is considered to transfer only compressive forces, while reinforcing steel transfers the tension forces. The designer needs to have experience to choose optimum trusses (Hamed, 2009). Designing a member using the strut-and-tie method should begin with determining the stress distribution in the member caused by the loading and support condition. The distribution of the stresses in the member depends on the shape and place of the openings, type of loads and support conditions of the structure.

Each discontinuity (change in shape, the presence of opening) in these members will cause a distortion in the stress flow in the structure. SeeFigure 2.6 for some examples (Nelson, 2004). Defining the disturbed region or the discontinuity region (D-region) and the Bending region (B-region) is needed because the design of each region differs from the other. The plane sections of the B-region are considered to remain plane. These regions can be designed by analyzing the sectional forces using traditional methods. The strut-and-tie method is effective for designing D-regions.

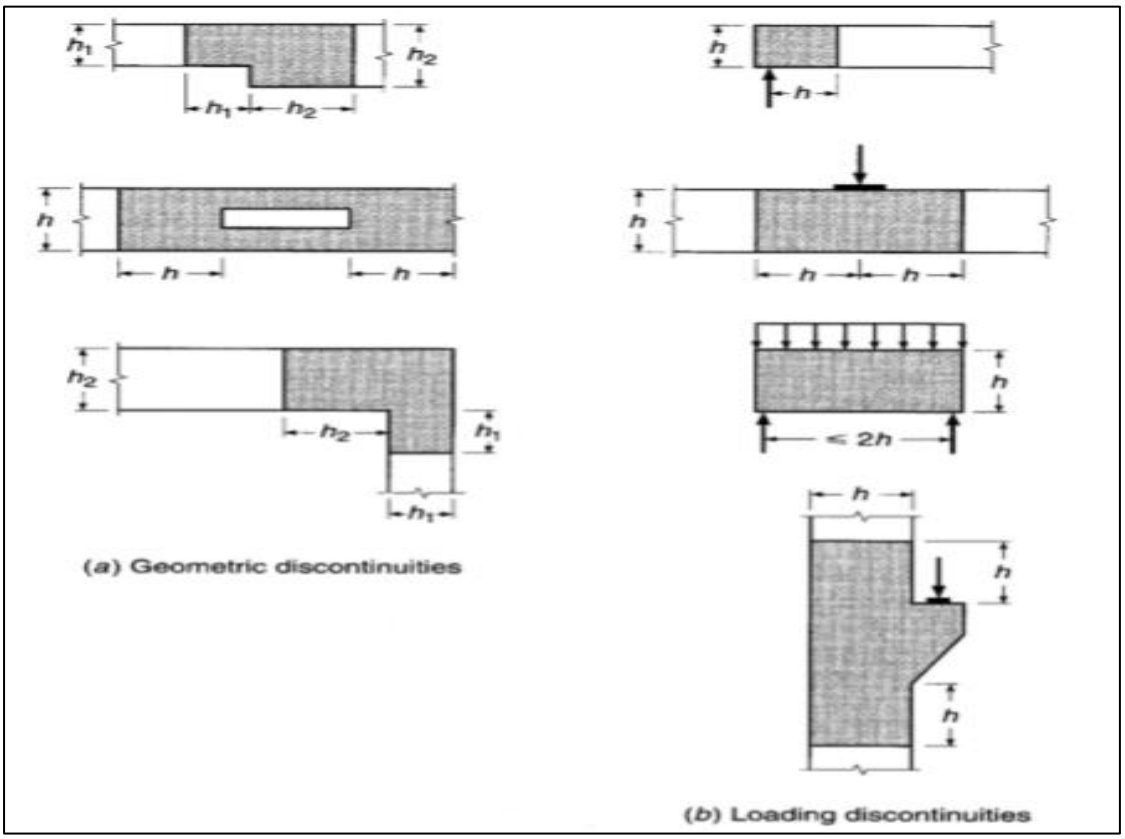

Figure 2.6: Geometric and load discontinuities for D-regions (Nelson, 2004)

This model is emerging as a code worthy methodology for the design of all types of D-regions in structural concrete. The most familiar types of D-regions, such as deep beams, corbels, beam-column joints, and pile caps can be analyzed and designed by strut and tie model. In the STM, the complex flow of internal forces in the region under consideration is idealized as a truss carrying the imposed loading through the region to its supports. Like a real truss, a strut and tie model consists of strut and ties interconnected at nodes called nodal zones or nodal regions. Figure 2.7 shows a deep beam with strut, tie and nodal zone as a simple example. Struts are the compression members of a strut and tie model and represent concrete stress fields whose principal compressive stresses are predominantly along the centerline of the strut and ties are the tension members of a strut and tie model. (Macgregor, J. G., 2012).

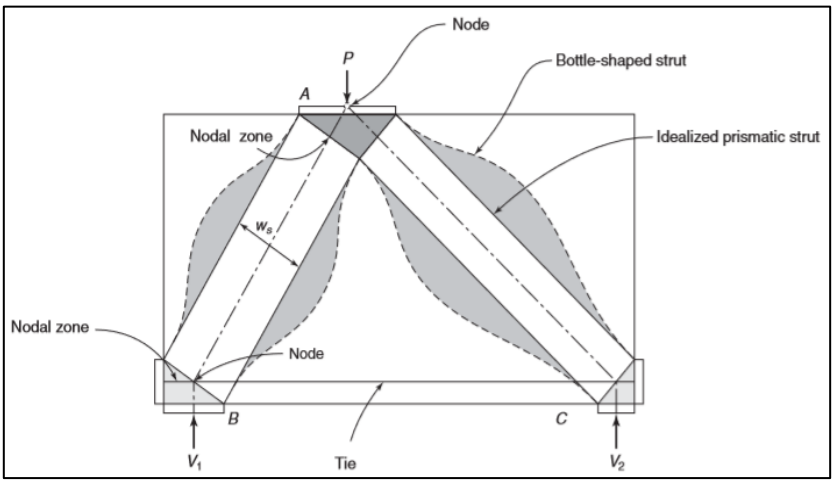

Figure 2.7: Strut-and-tie model of a deep beam (Macgregor, J. G., 2009)

If the structural member presents a complex or unfamiliar stress distribution, finite element analysis can be used to give the designer an idea of the flow of forces within the un-cracked member (Hamed, 2009).

2.5.2. Finite element method

The concept of the finite element method was originally introduced for structural analysis by (Turner et al, 1956) and (Argyris and Kelsey, 1955) in the mid-50. The name "finite element" was originally coined in a paper by (Clough, 1960) in 1960, in which the technique was presented for plane stress analysis. Since then general progress has been so rapid that the method is now one of the most powerful tools available in structural analysis. It has also been recognized as a general numerical method for approximately solving various systems of partial differential equations with known boundary conditions. Thus its application covers a wider range of physical problems other than structural. For instance, problem arising in such fields as fluid mechanics, magneto- and electro-dynamics, and temperature fields can be solved.

(Zienkiewicz, 1977) covers the mainstream of these developments and includes a wide bibliography of the publications reflecting these activities. The method is a general discretization procedure for solving continuum problems defined by certain classes of mathematical statements. The continuum is subdivided into finite regions termed "elements", each of which possess a finite number of unknown parameters which approximate the values of the field

variables which define the problem. These field variables may be scalars, vectors, or high order tensors. These elements connect with each other through common points existing on their boundaries at which continuity and compatibility of the field variables are enforced. These common points are termed "nodes". A set of functions are chosen to define the variation of the required field variable within each element in terms of the unknown nodal values.

In structural mechanics problems, the unknown field variables can be displacements, stresses, or both. This gives rise to the displacement (stiffness) method, the force (flexibility) method, or the hybrid method respectively. The displacement method is the most widely used because of its relative ease of formulation compared to the other methods, although advocates of the hybrid method claim that it is as easy to formulate, and perhaps more accurate (Spilker,1979).

2.6. Finite Element Analysis Software (ABAQUS)

There are many commercially available software packages that are used for finite element analysis of reinforced concrete structures. Some of which includes: ADINA (Automatic Dynamic Incremental Nonlinear Analysis) developed by ADINA R&D Inc., and is mainly used for modeling fluid structure interactions, heat transfer and also linear and nonlinear structural analysis (ADINA R&D, 2015), DIANA (Displacement Analyzer) developed by TNO DIANA, which employs the displacement method and mainly used for structural and geotechnical analysis (TNO DIANA BV, 2015), and ANSYS developed by ANSYS Company, is used for simulation in different technologies including structural mechanics, fluid mechanics, and electromagnetic (ANSYS, 2015). However, ABAQUS is the finite element software that was selected for the simulation performed in this study (DSS, 2014).

ABAQUS was developed by Hibbitt, Karlsson and Sorensen, Inc. which was established in 1978. This company was then acquired by Dassault Systemes Simulia Corp. (DSS) located in Providence, Rhode Island USA, in 2005. ABAQUS is a very powerful finite element analysis tool due to its broad selection of materials and elements and its capacity to model one, two, and three-dimensional projects. The ABAQUS program suite includes three major products: ABAQUS/CAE, ABAQUS/Standard, and ABAQUS/Explicit. The first product refers to Complete ABAQUS Environment, and is used to create, analyze, and visualize model output all in one environment using graphical user interface (GUI). ABAQUS/CAE gives the option of

creating the model geometries using the software drawing tools, or importing CAD models that have been prepared by another compatible products. Users can then submit the assembled and meshed model parts for analysis. The results are reviewed and graphed by the help of the available comprehensive visualization tools. ABAQUS/Standard is generally used for finite element simulations of structures that are subjected to static and low-speed dynamic effects. ABAQUS/Explicit on the other hand is more suitable for transient dynamic and highly nonlinear simulations. However, ABAQUS/CAE supports both Standard and Explicit version for pre-processing and post-processing simulations (DSS, 2014).

2.7. Constitutive Models of Concrete in ABAQUS

There are three concrete constitutive models supported by ABAQUS, and their application depends on the type of structural loading and cracking analysis. These models include: Smeared Crack Model (SCM), Brittle Cracking Model (BCM), and Concrete Damaged Plasticity Model (CDPM). The three models are fully capable of modeling a variety of concrete structures such as beams, trusses, shells, and solids. Although, these models can be used for plain concrete or other quasi-brittle materials, they are mainly utilized to model reinforced concrete structures (Stoner, 2015).

The Smeared Crack Model (SCM) can be employed in ABAQUS/Standard and is primarily used for concrete structures subjected to monotonic loadings at low confining pressure. Cracking of concrete is one of the most crucial aspects in any structural analysis, and thus it is imperative to implement the cracking and post-cracking behavior of concrete in the modelling. A smeared crack approach is usually used to reflect the discontinuous brittle response of cracked concrete. However, this technique does not track the formation of macro cracks; instead it updates the stress and stiffness material properties to account for the crack effect.

The Brittle Cracking Model (BCM) is usually implemented in ABAQUS/Explicit and is intended for applications in which tensile cracking of materials is dominant. This approach is suitable for ceramics, brittle rocks, and plain concrete. In this model, the concrete compressive behavior is assumed to be linear-elastic which is an enormous simplification of the actual response. Thus, the BCM is only practical in applications where tensile behavior overshadows

the assumption of linear-elastic compression model. The BCM only represents the brittle aspects of concrete behavior (i.e. when micro-cracks merge to form discrete macro-cracks resulting in a highly localized deformation).

On the other hand, the Concrete Damaged Plasticity Model (CDPM) can be utilized in both ABAQUS/Standard and ABAQUS/Explicit. It is usually used to analyze plain concrete and other quasi-brittle materials. The CDPM can be implemented for the analysis of concrete structures under monotonic, cyclic, and dynamic loading under low confining pressure. It is proven that Concrete Damaged Plasticity Model is highly flexible in modelling concrete under different loading conditions. Therefore, the CDPM model was selected for the analysis of concrete materials in this study, and will be reviewed in broader details in the following section.

2.8. Concrete Damaged Plasticity Model

In most recent numerical studies of concrete materials, including this research work, plasticity and damage evolution of concrete parts are considered in the basic finite element modelling. The typical damaged plasticity model uses the concepts of isotropic tensile and compressive plasticity to represent the inelastic behavior of concrete. These concepts are reflected by the assumption of two failure mechanisms: tensile cracking and compressive crushing of concrete composites. Hardening variables correspond to the extent of damage in concrete, and stiffness degradation parameter is used to characterize the uniaxial tensile and compressive stress-strain relationships under applied loads. The hardening variables are then used in cooperation with the yield surface to identify the failure mechanisms under tensile and compressive loading. In concrete modelling, a non-associated plastic flow potential is implemented using the Drunker Pager hyperbolic function to represent flow potential. Furthermore, a Viscoplastic regularization of the constitutive models is sometimes used to improve the convergence rate in the concrete softening and stiffness regimes. The following sections give more details on the available constitutive models which are used for the concrete plasticity concepts.

2.8.1 Concrete Compression Model

The general stress-strain response of the concrete under uniaxial compression is illustrated in Figure 2.8. It is observed that concrete behaves linearly within the elastic region until the initial

yield, σ_{co}. After reaching the initial yield point, concrete starts behaving in a plastic fashion and exhibits some work-hardening up to the ultimate stress, σ_{cu}, followed by strain-softening.

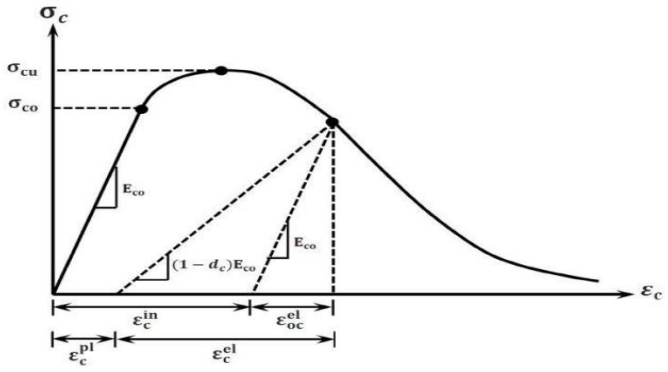

Figure 2.8: Compressive stress-strain response of concrete (DSS, 2014)

The elastic compression behavior of concrete can be modeled by calculating the initial undamaged modulus of elasticity, E_{co}. For the inelastic response, compressive stresses are provided in a tabular form as a function of the inelastic strain, ε_c^{in} which can be calculated by the following equation:

$$\varepsilon_c^{in} = \varepsilon_c - \varepsilon_{oc}^{el} = \varepsilon_c - \frac{\sigma_c}{E_{co}} \tag{2.1}$$

Where ε_c^{in} the inelastic strain, ε_c is the total compressive strain, ε_{oc}^{el} is the elastic compressive strain corresponding to the undamaged material, σ_c is the compressive stress, and E_{co} is the initial undamaged modulus of elasticity. The inelastic strain data are inputted in the material definition section of ABAQUS model as positive values, starting at zero value corresponding to the initial yield point.

2.8.2 Concrete Tension Model

Figure 2.9 illustrates the general stress-strain response of a concrete member under uniaxial tensile loading. It can be seen that the stress-strain response is linear elastic until the peak stress σ_{ot}. The onset of micro-cracks occurs when the tensile stress reaches the peak point, which leads to strain localization. The latter impacts the crack growth and may result in the unloading of regions beyond strain localization which in turn induces strain-softening post-peak response.

In a typical reinforced concrete beam, the concrete (a quasi-brittle material) is bonded to the reinforcement. When cracking initiates in the member, concrete continues to resist some tensile stresses between the cracks. This characteristic is referred to as "tension stiffening", and it helps improve the control of the deformation of an RC member and the growth of crack widths.

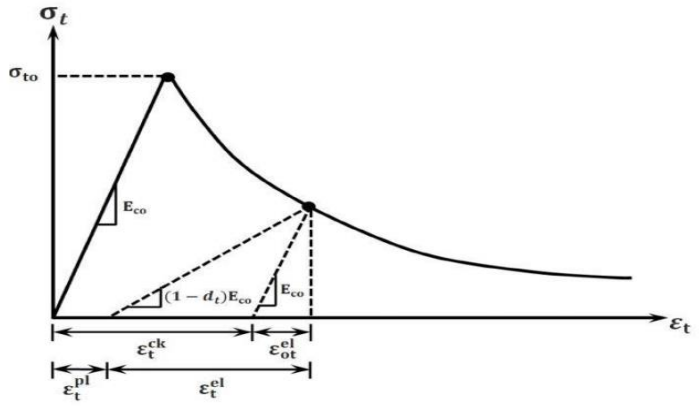

Figure 2.9: Tensile stress-strain response of concrete (DSS, 2014)

In ABAQUS, the user is required to define the post-peak tensile response of concrete in order to account for the interaction between the concrete and the reinforcing bars. The Concrete Damaged Plasticity Model in ABAQUS provides three different methods that can be used to characterize the post-peak response of concrete in tension:

1. The tensile stress in concrete can be entered in a tabular form as a function of the corresponding cracking strain, ε_t^{cr}.
2. The tensile stress can be entered in a tabular form as a function of the crack opening displacement, w.
3. The value of concrete fracture energy, G_f, can be simply inputted into the model.

In the first method, the user can plot a stress-strain curve similar to that illustrated in Figure 3.3. The post-peak response can be determined in a procedure similar to the one described in the concrete compression model. The cracking "inelastic" strain, ε_t^{ck}, can be calculated using the following expression:

$$\varepsilon_t^{ck} = \varepsilon_t - \varepsilon_{ot}^{el} = \varepsilon_t - \frac{\sigma_t}{E_{co}} \tag{2.2}$$

Where ε_t^{ck} is the cracking strain, ε_t is the total tensile strain, ε_{ot}^{el} is the elastic tensile strain corresponding to the undamaged material, σ_t is the tensile stress, and E_{co} is the initial undamaged modulus of elasticity. Similarly, the cracking strain data are entered in the Concrete Damaged Plasticity Model of ABAQUS model in a positively increasing manner. The first value is set as zero corresponding to the initial yield stress.

In the second method, the post-peak tensile behavior of concrete is defined in a way that the user has to input the tensile stress as a function of the crack-opening-displacement, w. Hillerborg et al. (1976) has proposed the concept of using fracture energy, Gf, in this method. This fracture energy of a brittle material corresponds to the energy required to open a crack of unit area. Therefore, the post-peak behavior of concrete in idealized by a stress-displacement response rather than a stress-strain response as in the first method. The user has the liberty to modify the tension stiffening response of the concrete member by selecting one of the proposed examples of stress-displacement curves as shown in Figure 2.10.

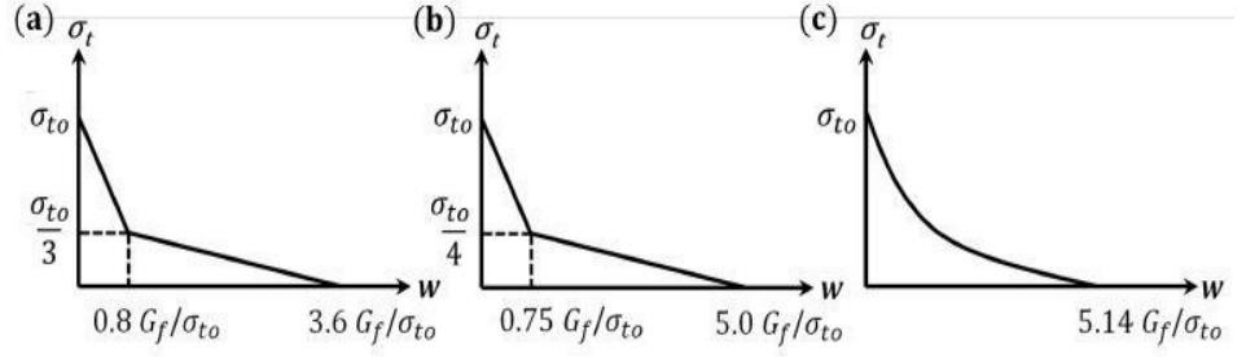

Figure 2.10: Various examples of stress-displacement curves (Stoner, 2015)

It is worth mentioning that the area under these curves represents the fracture energy of the material. Therefore, this method has the advantage of allowing the user to define the rate of strength loss after cracking and also the material's fracture energy (Stoner, 2015).

Finally, the third method allows the user to simply define the tensile peak stress, σ_{to}, and the value of the fracture energy,G_f.As it can be seen in Figure 2.11, this method assumes a linear stress-displacement post-failure response.

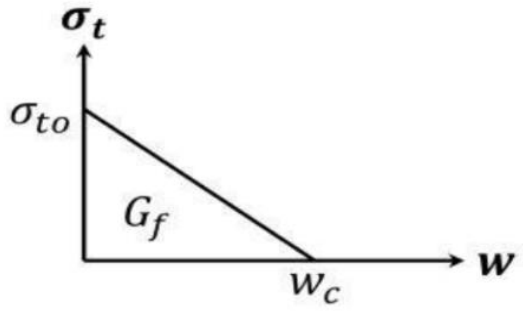

Figure 2.11: Linear stress-displacement curve (Stoner, 2015)

The user is expected to identify the value of the peak stress and the area under the linear curve (i.e. the calculated fracture energy). Then after, the maximum crack displacement corresponding to a complete loss of strength, wc, is computed by the equation:

$$w_c = \frac{2G_f}{\sigma_{to}} \tag{2.3}$$

2.8.3 Damage Modelling

Sometimes, unloading of the concrete member can occur within the post-peak region of the compression and tension stress-strain curves. In such case, the unloading response becomes weaker and degraded, and modulus of elasticity is utilized to account for this degradation as expressed in Figure 2.8 and Figure 2.9. This degradation during the unloading phase is identified by two damage variables, d_c and d_t for member subjected to compression and tension, respectively. The damage parameters are functions of the plastic strains ε_c^{pl} and ε_t^{pl}, temperature θ, and other predefined filed variables f_i, as can be seen in the next equations.

It is noted that the values of the damage parameters ranges from zero (corresponding to the undamaged material) to one (for the material with complete loss of strength).

$$d_c = d_c\left(\varepsilon_c^{pl}, \theta, f_i\right) 0 \le d_c \le 1.0 \tag{2.4}$$

$$d_t = d_t\left(\varepsilon_t^{pl}, \theta, f_i\right) 0 \le d_t \le 1.0 \quad (2.5)$$

As it has been mentioned previously, the damage parameters are functions of plastic strains, and hence, ABAQUS will automatically generate the plastic strains from the user-defined inelastic or cracking strain. The plastic strain in compression is obtained by converting the inelastic strain εcin, and damage parameters, dc as expressed below:

$$\varepsilon_c^{pl} = \varepsilon_c^{in} - \frac{d_c}{1-d_c}\frac{\sigma_c}{E_{co}} \quad (2.6)$$

Where: E_{co}:is the initial undamaged modulus of elasticity However, the calculation of plastic strain in tension depends on the method used to define the tensile post-peak response of concrete. If the first method was used, damage parameters are provided as functions of the cracking strains, ε_t^{cr}, which are converted to plastic strains as shown below:

$$\varepsilon_t^{pl} = \varepsilon_t^{cr} - \frac{d_t}{1-d_t}\frac{\sigma_t}{E_{co}} \quad (2.7)$$

However, if method two or three was used to define the tensile post-peak curve of the concrete member, damage parameter values are considered as functions of the crack-opening displacement, u_t^{cr} (also referred to as w). The plastic displacements are then obtained by the equation:

$$u_t^{pl} = u_t^{cr} - \frac{d_t}{1-d_t}\frac{\sigma_t l_o}{E_{co}} \quad (2.8)$$

and the term l_o corresponds to the specimen length which is assumed to be equal to 1.0. Furthermore, the value of the damage parameter ought to be controlled within the range of 0-0.99 to avoid severe damage, and thus possible convergence issues (Stoner, 2015). When the initial undamaged modulus of elasticity E_{co} is identified, the stress-strain response of the concrete under tension and compression with consideration of the degradation of the elastic stiffness can be represented by:

$$\sigma_c = (1-d_c)E_{co}\left(\varepsilon_c - \varepsilon_c^{pl}\right) \quad (2.9)$$

$$\sigma_t = (1-d_t)E_{co}\left(\varepsilon_t - \varepsilon_t^{pl}\right) \quad (2.10)$$

It should, however, be mentioned that a concrete structure subjected to uniaxial load will exhibit crack initiation and propagation. Therefore, a reduction in the expected load carrying area is expected which in turn increases the concrete effective stresses. ABAQUS accounts for that phenomenon by calculating these effective compressive and tensile stresses, $\bar{\sigma}_c$ and $\bar{\sigma}_t$, respectively. These terms are expressed in the following equation:

$$\bar{\sigma}_c = \frac{\sigma_c}{1-d_c} E_{co}\left(\varepsilon_c - \varepsilon_c^{pl}\right) \quad (2.11)$$

$$\bar{\sigma}_t = \frac{\sigma_t}{1-d_t} E_{co}\left(\varepsilon_t - \varepsilon_t^{pl}\right) \quad (2.12)$$

2.8.4 Yield Function

The Concrete Damaged Plasticity Model in ABAQUS implements a yield function proposed by Lubliner et al. (1989), and incorporates modifications presented by Lee and Fenves (1998) to account for different modes of strength evolution. The yield function can be expressed as follows:

$$F(\bar{\sigma}, \tilde{\varepsilon}^{pl}) = \frac{1}{1-\alpha}\left[\bar{q} - 3\alpha\bar{p} + \beta(\tilde{\varepsilon}^{pl})(\hat{\sigma}_{max}) - \gamma(-\hat{\sigma}_{max})\right] - \bar{\sigma}_c(\tilde{\varepsilon}^{pl}) = 0 \quad (2.13)$$

$$\alpha = \frac{(\sigma_{bo}/\sigma_{co})-1}{2(\sigma_{bo}/\sigma_{co})-1} \quad (2.14)$$

$$\beta = \frac{\bar{\sigma}_c\left(\tilde{\varepsilon}_c^{pl}\right)}{\bar{\sigma}_t\left(\tilde{\varepsilon}_t^{pl}\right)}(1-\alpha) - (1+\alpha) \quad (2.15)$$

$$\gamma = \frac{3(1-k_c)}{2k_c-1} \quad (2.16)$$

Where:

$\bar{\sigma}_c\left(\tilde{\varepsilon}_c^{pl}\right)$ *and* $\bar{\sigma}_t\left(\tilde{\varepsilon}_t^{pl}\right)$ are the effective compressive and tensile cohesion stress, respectively;

σ_{bo} :is the initial equibiaxial compressive yield stress;

σ_{co} : is the initial uniaxial compressive yield stress;

$\bar{q}$: is the Mises equivalent stress, where $\bar{q} = \sqrt{3J_2}$, J_2 is the second deviatoric stress invariant;

$\bar{p}$: is the effective hydrostatic pressure stress, where $\bar{p} = \frac{-I_1}{3}$; and I_1 is the first stress invariant;

$\hat{\sigma}_{max}$: is the maximum principal effective stress.

The two terms , and experimental data put this ratio between 1.10 and 1.16, resulting in values of between 0.09 and 0.12 (Lubliner, et al., 1989). The default value of ($\sigma bo/\sigma c0$) adopted by ABAQUS is 1.16 based on a parametric study performed by Kupfer et al. (1969). On the other side, the term γ corresponds to the state of tri-axial compression where $\sigma max < 0$, and is a function of the parameter Kc. The latter is defined as a ratio of the second stress invariant on the tensile meridian (T.M.) to the second stress invariant on the compression meridian (C.M.) at initial yield for any given pressure invariant value. The value of Kc governs the shape of the failure surface within the deviatoric plane (see Figure 2.12). In the case of Kc= 1.0, the failure surface within the deviatoric plane takes the shape of a circle, which sets well with the classical Drucker-Prager theory. Moreover, the original model suggested by Lubliner et al (1989) indicates that constant values of Kcvarying from 0.64 to 0.80 are acceptable. However, the Concrete Damaged Plasticity Model in ABAQUS recommends a default value of 2/3 for Kc, and limits the permissible value to 0.5 <Kc≤ 1.0 (Stoner, 2015).

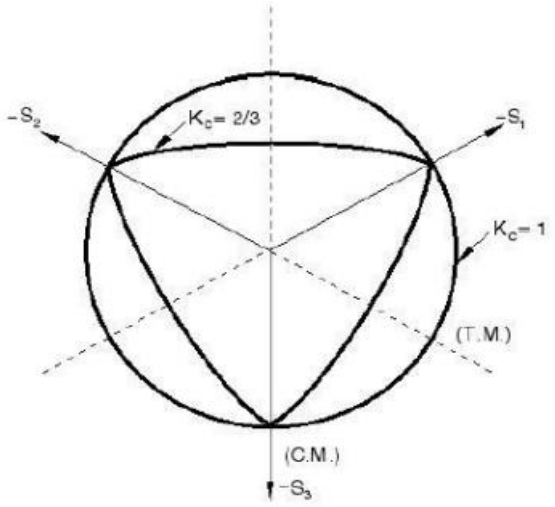

Figure 2.12: Yield surfaces in plane stress (DSS, 2014)

2.8.5 Hardening Variables

Lubliner et al. (1989) have recommended the use of isotropic hardening in their plasticity model. Though this hardening rule is effective in modelling members under monotonic loading, it has been proven inappropriate for cyclic response of concrete structures. When cyclic load is applied, the progress of on strength (compression or tension) does not affect the progress of the other strength. Consequently, in the modifications proposed by Lee and Fenves (1998) included two-variable hardening rule; one variable to control compression and the other to control tension. In another word, the hardening of the material occurs in an independent manner in both compression and tension. Nonetheless, the evolution of yield and loading surface, in the Plasticity model of concrete, is governed by two hardening variables, $\tilde{\varepsilon}_c^{pl}$ and $\tilde{\varepsilon}_t^{pl}$which refer to the tensile and compressive equivalent strains, respectively.

2.8.6 Flow Rule

Several studies have shown that the application of the associated rule for concrete is not adequate for full range of the concrete response spectrum, and thus results in large inconsistencies between the experimental and theoretical predictions (Hu & Schnobrich, 1989). Concrete is proven to be a material that undergoes large volumetric changes under loading. Therefore, a non-associated flow rule is appropriate to control the dilatancy in the modelling (Lee & Fenves, 1998). The Concrete Damaged Plasticity Model in ABAQUS uses a non-associated plastic potential flow rule, which can be expressed in the effective stress space as follows:

$$\dot{\varepsilon^{pl}} = \frac{\dot{\lambda}(\partial G(\bar{\sigma}))}{\partial \bar{\sigma}} \quad (2.17)$$

Where $\dot{\varepsilon^{pl}}$: is the plastic strain rate, G: is the flow potential function and $\dot{\lambda}$: is a non-negative scalar hardening parameter. The flow potential function, G, used in this study is a hyperbolic Drucker-Prager function and is expressed in the $p-q$ plane (meridional plane) using the following equation:

$$G = \sqrt{\in \sigma_{to} tan\psi + \bar{q}^2} - \bar{p} tan\psi \quad (2.18)$$

where ψ is the dilation angle, σ_{to} is the user-defined uniaxial tensile stress of concrete at failure, and ϵ is the plastic potential eccentricity.

The flow potential curve helps establish a connection between the plastic flow direction and the plastic strain rate. This curve is continuous and smooth to ensure that the flow direction is always clearly defined. Figure 2.13 defines the flow potential curve within the $p - q$ plane.

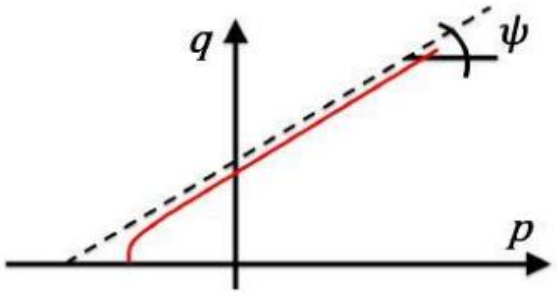

Figure 2.13: Hyperbolic Drucker-Prager flow potential function (DSS, 2014)

The function asymptotically approaches the linear Drucker-Prager flow potential as the confining pressure increases, and intersects the hydrostatic pressure axis at 90°. The shape of the hyperbola is modified by the use of the eccentricity parameter, ϵ. This parameter is taken as a small positive quantity that defines the rate in which the plastic potential function approaches the asymptote. ABAQUS recommends a default value of 0.1 for this parameter which implies that the material has a relatively constant dilation angle over a wide range of confining pressure. However, trials have shown that using an eccentricity value that is considerably different from the default value might lead to convergence issues when modelling low confining pressure. This can be attributed to the tight curvature of the function at the intersection with the p- axis (Stoner, 2015).

Moreover, the flow potential function depends on the dilation angle, ψ. This angle is defined as a material property which is used to measure the inclination of the flow potential function within the meridional plane relative to the hydrostatic pressure axis at high confining pressures (see Figure 2.14). When a small value is assumed for this angle, a brittle behavior is expected. On the contrary, higher value of eccentricity angle leads to more ductile response (Malm, 2009).

2.8.7 Viscoplastic Regularization

The softening behavior and stiffness degradation that occur in some materials upon loading often result in in tension due to the significant change in slope of the tensile stress-strain curve at peak stress. One of the common techniques used to resolve this issue is to implement Viscoplastic regularization of the constitutive models. The Concrete Damaged Plasticity Model in ABAQUS uses a generalization of the Devaut-Lions approach which allows the stresses to pass the yield surface. To incorporate the Viscoplastic regularization in the ABAQUS model, the user can enter a small value of viscosity parameter, instead of the default value of zero. When a viscosity parameter is greater than zero, the Viscoplastic strain $\dot{\varepsilon}_v^{pl}$ is defined by the following equation:

$$\dot{\varepsilon}_v^{pl} = \frac{1}{\mu}\left(\varepsilon^{pl} - \varepsilon_v^{pl}\right) \tag{2.19}$$

where μ is the viscosity parameter which represents the relaxation time of the Viscoplastic system, ε^{pl} is the plastic strain evaluated in the in viscid solution (i.e. no viscoplastic regularization is assumed), and ε_v^{pl} is the viscoplastic strain. Moreover, when the viscoplastic strain is used, the viscous stiffness damage variable $\dot{d}_v$ is introduced and expressed below:

$$\dot{d_v} = \frac{1}{\mu}(d - d_v) \tag{2.20}$$

Where: d is the damage variable of the in viscid solution. It has to be noted that when Viscoplastic regularization is used, model output will be based on plastic strain and elastic stiffness degradation values, ε_v^{pl} and d_v, respectively. In conclusion, the use of a small value for the viscosity parameter will yield a significant improvement in the solution convergence rate without affecting the accuracy of the results (Stoner, 2015). When the value of μ approaches zero, the solution becomes a plastic response. Conversely, as the μ parameter is taken significantly larger than the iteration time increment, the solution tends to be elastic solution.

2.9. Non-linear finite element analysis

In any three-dimensional finite element analysis, the performance of any structural member under load depends on the behavior of the type of material used to construct the member. In

concrete members which are made of different materials, concrete and reinforcing bars are brought together to behave as a composite system. The steel can be considered as a homogeneous material that exhibits a similar stress-strain relationship in tension and compression. While, the behavior of concrete is monitored to have grossly heterogeneous internal structure because it is dependent on the properties of each of its components; namely, cement mortar, aggregates and air voids. One of the main objectives of the finite element analysis of structures is to determine the response of the structure under loading. A typical load deformation response for a monotonically loaded member is essentially linear up to a certain limit of load. Beyond this limit a nonlinear load deformation response occurs. Such response is due to a combination of nonlinear material behavior (material nonlinearities), large deformation in the structure (geometric nonlinearities), and interface nonlinearity for composite members (changing status) (Dawlat, 2007). In the analysis of reinforced concrete structures, at nonlinear stage of behavior, it is not possible to solve the governing equilibrium equations directly; therefore, resort has to be made to more sophisticated solution strategies.

A nonlinear structural problem must obey the basic laws of continuum mechanics, i. e. equilibrium, compatibility, and the constitutive relations of the material. Displacement compatibility is automatically satisfied in the displacement finite element technique. Common nodes between elements ensure continuity and compatibility of displacements along internal element boundaries (including the nodes) and polynomial shape functions ensure continuity and single valued displacements internally. Therefore it becomes only necessary to enforce that the nonlinear constitutive relations are correctly satisfied whilst at the same time preserving the equilibrium of the structure.

In general for a particular load level, a number of successive linear solutions are required to remove the residual forces to a desired degree of accuracy. The method is obviously iterative in nature and the final results will depend on the factors associated with the iterative process, for example the increment size, accuracy required, the exact type of solution process employed etc. Clearly it is impossible to obtain a unique solution to a particular problem because of these many factors.

There can be several causes of nonlinear behavior in a structure, which can be divided into two classes**:**

a. Nonlinear material behavior,
b. Geometric changes (i. e. large deformations) in the structure, including changing boundary conditions.

Stress-strain relations are a major source of nonlinearity. These can vary from short-term nonlinear relationships between stress and strain such as plasticity, cracking, nonlinear elasticity, etc., to time-dependent effects such as creep, viscoelastic behavior, shrinkage, etc.

In concrete, cracks even exist before any external loading has been applied ((Mindess, 1981), (Neville, 1981)). This is due to effects such as segregation, water gain, and bond cracks at the matrix-aggregate interface. The second source of nonlinearity is when deflections are sufficiently large that the equilibrium equations based on the original geometry are no longer valid and need to be modified to account for the new geometry. This affects the force-displacement equations, because additional internal forces are generated due to the deflected geometry. Also if the large displacements cause large strains, then additional higher order terms must be included in the mathematical definition of strain. This results in nonlinear strain-displacement equations. ((Desai, 1972), (Cook, 1981)).

Changes in the external boundary conditions are, in a sense, another source of geometric nonlinearity. For example, beams on elastic foundations in which the size and location of contact zones between beam and foundation depends on the nature of the applied force. In certain circumstances, reinforced concrete structures present another example where boundary conditions change with varying load. Cracking and crushing cause separation of adjacent parts of the structure, which can be interpreted as a new geometric configuration, and this interpretation can be included in analytical procedures, such as the spring element method of (Ngo, 1970).

2.9.1. Numerical integration

In most finite element analyses, the element stiffness matrix [Ke] cannot be obtained analytically. Thus, to perform the integration required to evaluate the element stiffness matrix, a suitable scheme of numerical integration has to be used. In this study numerical integration is required because analytical integration is impossible. For this purpose Gauss-Legendre quadrature rules have been used extensively because of their higher efficiency over other forms of quadrature. They can integrate exactly a polynomial $f(\xi)$ of degree (2n-1), where n is the number of sampling points. Also they are suitable for isoparametric elements because the

range of these integration rules are ±1 which coincides with the local coordinate system of limits ±1 on element boundaries.

The application of the three-dimensional finite element analysis in connection with the nonlinear behavior of structures needs a large amount of computation time due to frequent evaluation of the stiffness matrix. Therefore, it is necessary to choose a suitable integration rule that minimizes the computation time but with sufficient accuracy.

Hence, the equations of the stiffness matrix element in one, two and three dimensions can be expressed as equation (a, b, c) respectively (Zienkiewicz, 2005):

$$I = \int_{-1}^{1} f(\xi) d\xi \approx \sum_{j=1}^{m} W_i f(\xi_i) \quad (2.21)$$

$$I = \int_{-1}^{1} \int_{-1}^{1} f(\xi, \eta) d\xi \, d\eta \approx \sum_{i=1}^{n} \sum_{j=1}^{m} W_i W_j f\left(\xi_i, \eta_j\right) \quad (2.22)$$

$$I = \int_{-1}^{1} \int_{-1}^{1} \int_{-1}^{1} f(\xi, \eta, \zeta) d\xi \, d\eta \, d\zeta \approx \sum_{i=1}^{n} \sum_{j=1}^{m} \sum_{k=1}^{l} W_i W_j W_k f\left(\xi_i, \eta_j, \zeta_k\right) \quad (2.23)$$

Where: n, m, l Total number of integration points.

ξ_i, η_j, ζ_k Coordinate of the ith, jth and kth integration point.

W_i, W_j, W_k The ith, jth and kth weighting factor

2.9.2. Techniques for Solving Non-Linear analysis

The finite element discrimination process yields a set of simultaneous equations:

$$[F^a] = [K][U] \quad (2.24)$$

Where: [K]: is the stiffness matrix

[U]: is the vector of nodal displacements

$[F^a]$: is the vector of applied loads.

The solutions of nonlinear problems by the finite element method are usually attempted by one of three basic techniques(Zienkiewicz, 2005):

- Incremental (step-wise procedure).
- Iterative (Newton method).
- Incremental-iterative (mixed procedure).

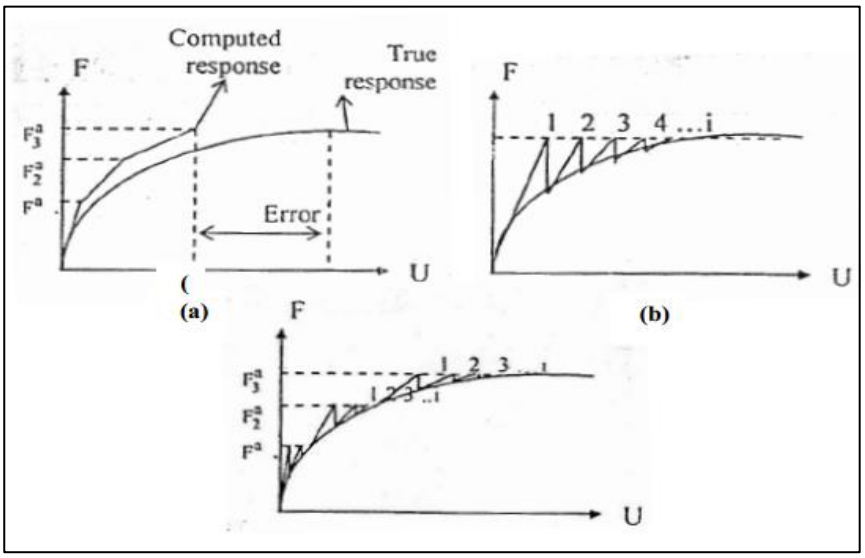

Figure 2.14: Basic Technique for Solving the Nonlinear Equation (a) Incremental (b) Iterative (c) Incremental–Iterative (Maurizio et al, 2002)

A. **Incremental method**

The basis of the incremental method is the subdivision of the total applied load vector into smaller load increments, which do not necessarily need to be equal. During each load increment the equation (2.24) is assumed to be linear, i. e. a fixed value of [K] is assumed using material data existing at the end of the previous increment. Nodal displacements can then be obtained for each increment and these are added to the previously accumulated displacements. The process is repeated until the total load is reached.

The accuracy of this procedure depends on the increment size; the smaller the increments the better the accuracy, but at the same time the more computational effort required. A modification of this method is the "midpoint Runge-Kutta" method (Bhavikatti, 2005). In this, the first step is to apply half the load increment and to calculate new stiffness's corresponding to the total stresses at this value. These stiffness's are then utilized to compute an approximation for the full load increment.

The incremental method in its original and modified form do not account for force redistribution during the application of the incremental load (i. e. No iteration process exists to restore equilibrium).

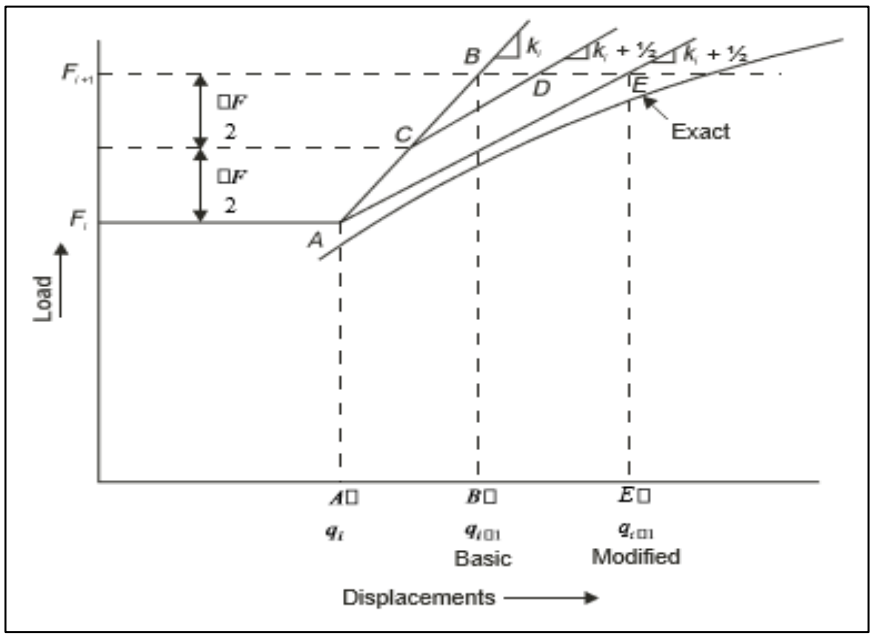

Figure 2.15: Midpoint Runge-Kuttaincremental procedures (Bhavikatti, 2005)

B. **Iteration method**

In the iteration method, the full load is applied in one increment. Stresses are evaluated at that load according to the material law. This gives equivalent forces which may not be equal to the external applied forces, i. e. equilibrium is not necessarily satisfied. Then, the portion of the total loading that is not balanced is calculated as the difference between the total applied load vector and internal nodal forces. These are the unbalanced nodal forces [F] which are then used to compute an additional increment of displacements, and hence new stresses, which give a new set of equivalent nodal forces. This process is repeated until equilibrium is approximated to a certain degree of accuracy. When this stage is reached the total displacement is calculated by summing the displacements from each iteration.

This process can be written as:

$$[K_i^T][\Delta U_i] = [F^a] - [F^{nr}] \quad (2.25)$$

$$[\Delta U_{i+1}] = [U_i] + [\Delta U_i] \quad (2.26)$$

Where: [K]: is the stiffness matrix

(i): is the subscript representing the current equilibrium iteration and

F^{nr}: is the internal load vector.

This procedure fails to produce information about the intermediate stage of loading. For structural analysis including path-dependent nonlinearities increments are in equilibrium in order to correctly follow the load path. This can be achieved by using the combined incremental iterative method.

C. **Incremental-iterative method**

In this method a combination of the incremental and iterative process is used. The load is applied in increments and the solution at that load is obtained iteratively until equilibrium is obtained.

When Full Newton-Raphson procedure is applied the stiffness matrix is formed at every iteration. The advantage of this procedure may give more accurate result. The disadvantage of this procedure is that a large amount of computational effort may be required to form and decompose the stiffness matrix, as shown in Figure 2.16.

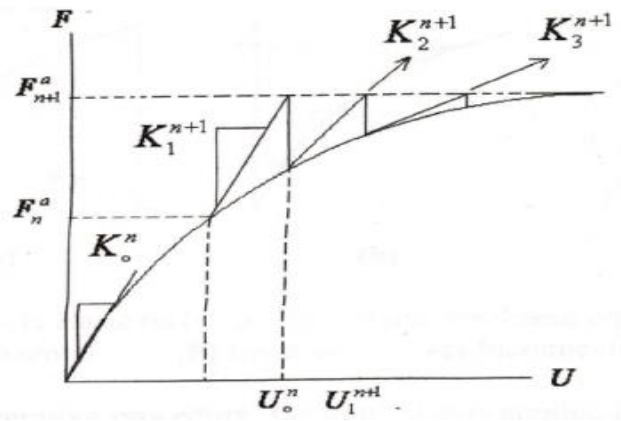

Figure 2.16: Incremental-Iterative Procedures Full Newton-Raphson procedure (Maurizio et al, 2002)

2.9.3. Convergence criteria

If a solution strategy based on iterative methods is to be effective, realistic criteria should be used for the termination of the iteration. At the end of each iteration, the solution obtained should be checked to see a convergence. If the convergence tolerances are too loose, inaccurate results are obtained, and if the tolerances are too tight, much computational effort is spent to obtain needless accuracy. For every incremental load the iteration continues until convergence is

achieved. The convergence criterion for the nonlinear analysis of structural problems can be classified as: force criterion, displacement criterion and stress criterion.

In displacement criterion, the incremental displacements at iteration i^{th} and the total displacements are determined. The solution is considered to be converged when the norm of the incremental displacements is within a given tolerance of the norm of the total displacements; infinite norm is used and takes the form:

$$\|\{\Delta U_i\}\| = (max|\Delta U_i|) \leq T_n(max|\Delta U_i|) \quad (2.27)$$

Where: U may equal u, v, w or θz.

For force criteria the norm of the residual forces at the end of each iteration are checked against the norm of the current applied forces as:

$$\|\{R\}\| = (\sum R_i^2)^{0.5} \leq T_n(\sum F_i^2)^{0.5} \quad (2.28)$$

Where {R} is the residual vector:

$$\{R\} = \{F^a\} - \{F^{nr}\} \quad (2.29)$$

The main function of convergence criteria is to control the number of iterations in an increment. The control is exercised by the user through the choice of convergence tolerances and the type of norm. In most cases the user will also specify a maximum number of iterations allowed, irrespective of the state of convergence. The number of iterations will influence the predicted shape of the load- deformation curve and ultimate load, e. g. too few might give an over stiff response.

Hence it is of paramount importance that the user understands the factors influencing convergence behavior and redistribution of forces. Very little information on these aspects exist in published literature, but it is clear that more is required if unreliable results are to be avoided. Fine tolerances are theoretically desirable but can be very expensive to obtain because they quite often require a lot of iterations.

They can be particularly difficult to achieve when discontinuous material laws (such as tension cracking) form part of the nonlinear behavior. Steep discontinuities in material laws can cause large residuals and these residuals need to be redistributed. However, this redistribution will cause more discontinuities and hence residuals in other parts in subsequent iterations. In such cases the rate of accumulation of residuals can be higher than the rate of distributing them. Another situation is when residuals are nearly redistributed and another discontinuity occurs

which increases the residuals again and requires more iterations. These effects cause a high number of iterations which will continue until a stable crack situation is reached. In practice the initiation of particular cracks is subject to some variation, and it is arguable whether it is necessary to wait until a completely stable.

2.10. Reviewed related literatures

(Chu and Thelen, 1963) preformed a plastic analysis for balcony girders of circular curved beam with a subtended angle of not more than 180 degree, with a constant cross section, fixed at both ends and subjected to uniform load perpendicular to the plane of the curved beam. In this analysis, as in any other plastic analysis, to determine the ultimate load the following conditions must be satisfied: static equilibrium, yield condition, flow law, and mechanism and compatibility conditions. A yield surface for combined bending and torsion, at a section where a plastic hinge was formed, and had been represented by:

$$m_o^2 + t_o^2 = 1 \tag{2.30}$$

Fulfillment of the flow law requirement was achieved through the relationship:

$$tan\gamma_o = \frac{t_o}{\alpha_o . m_o} \tag{2.31}$$

$$m_o = \frac{M}{M_P} \tag{2.32}$$

$$t_o = \frac{T}{T_P} \tag{2.33}$$

$$\alpha_o = \frac{T_P}{M_P} \tag{2.34}$$

Where: M: applied bending moment at cross section.

T: applied torsional moment at cross section.

M_p: plastic bending capacity of cross section.

T_p: plastic torsional capacity of cross section.

γ_o: angle between the axis of rotation at the plastic hinge and the vector radius

Figure 2.18 shows the yield surface for combined bending and torsion, at a section where a plastic hinge was formed. The general method of analysis was examined, the various

mechanisms of failure were investigated, and the results of the load capacity of curved beams were presented in a chart to facilitate their application.

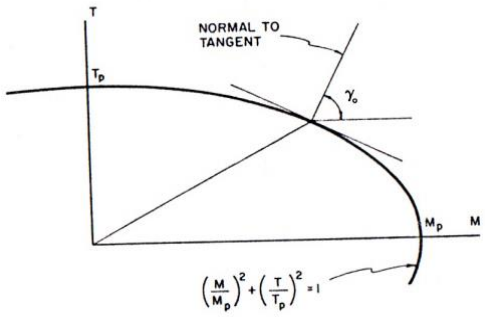

Figure 2.17: Yield surfaces for combined bending and torsion, at a section where a plastic hinge was formed (Chu and Thelen, 1963)

(Jordaan et al., 1974) developed plastic methods of analysis for the determination of collapse load for reinforced concrete curved beams with subtended a central angle less than 180 degree. In this study, the plastic analyses for the cases of a single point load besides uniformly distributed loads were extended to take into account two concentrated loads placed at any point on the beam. A plastic hinge was predicted at a particular cross section of the curved beam if the internal moments at that cross section satisfy the same yield criterion and flow law mentioned in eq. (2.31) and eq. (2.32) respectively. In the experimental part of this study, four curved and six straight reinforced concrete beams were tested. All the beams had constant moment and torque capacities at any section. The beams were completely fixed at the supports. Each curved beam had a radius of 2.21m and a subtended angle of 86^o degree as shown in Figure 2-19. According to amount of reinforcement, the curved beams were divided into two groups. One curved beam from each group was tested under single point load and the other curved beams were tested under two concentrated loads.

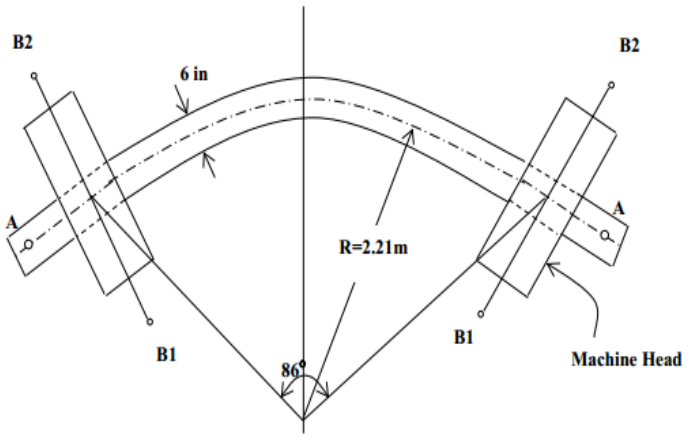

Figure2.18: Geometry of Test Specimens (Jordaan, 1974)

(Sadjad, A. H. 2014) investigated both analytically and experimentally on the behavior and performance of reinforced concrete horizontally curved beams with and without openings, unstrengthens and strengthened externally by CFRP laminates or internally by steel reinforcement. An experimental work performed on fourteen horizontally curved reinforced concrete beams dividing into two groups. The first group included ten of semicircular beams (one without opening and nine with openings), while the second group consisted of four full circular reinforced concrete beams (one without opening and three with openings). The variables considered in the experimental program included: geometry of circular beam, location of opening through profile of beam, presence of internal strengthening by reinforcing steel (stirrups) and external strengthening by CFRP laminates for beam around openings. The beams then tested under effect of point loads at top edge of each mid span. Experimentally proved that, the presence of opening at region of maximum bending moment and shear force caused a significant decrease in ultimate load capacity by about 35% for semi-circular beams and 50% for full circular (ring) beams compared with control beams without opening associated with beam shear mode failure. The use of steel reinforcement as internal strengthening and CFRP laminates as external confinement around openings improved the ultimate load capacity of the semi-circular beam by a ratio of (3% to 30%) and (11% to 40%), respectively. While for full circular (ring) beam the increasing in ultimate load reached about 60% and 75% for internal and external strengthening, respectively. Also, both types of strengthening around opening (internally by steel reinforcement or externally by CFRP laminates) enhanced crack patterns, post cracking torsional

and flexural stiffness's. Additionally, numerical work performed on three-dimensional nonlinear finite element model using the computer program ANSYS version 12.1 for the analysis of the tested reinforced concrete horizontally curved beams with or without openings and unstrengthen or strengthened by(CFRP laminates or reinforcing steel) under incremental loading. Full bond was assumed between the CFRP and concrete surface and between the steel reinforcement and concrete. A rectified reasonable agreement between the finite element solutions and experimental results has been obtained concerning estimated load-deflection response, mode of failure, cracking and ultimate loads with average difference about 4.1% and 16% for ultimate load and deflection respectively. The numerical results for the analyzed beams show that the ultimate load decreased about 12% when the length increased by 50% and it increased by 14% when the lengthof opening decreased by 50%. Moreover, an increment in ultimate load about 41% was found for circular opening instead of rectangular opening with the same area.

(Thomas et al, 1978)studied the behavior of reinforced concrete horizontally curved beams. Test was performed on seven horizontally curved reinforced concrete beams fixed at both ends. The beams were subjected to a concentrated load at mid-span. The results showed, for theconventional design of horizontally curved reinforced concrete beams, it is suitable to calculate the flexural moments, torsion moments and the shear forces by an elastic analysis using the un-cracked cross section. Since moment redistribution occurs after cracking, design of curved beams using cracked section is then recommended particularly near supports where torsional moment changes rapidly along the length. For beams designed by this method, the longitudinal steel yields, almost simultaneously at the supports and at mid-span. Torsional moments in a horizontally curved beam are primary moments required by equilibrium. They cannot be reduced or neglected.

(Mansur and Hasnat, 1979) tested twenty-two reinforced concrete beams with small openings under torsion. The beams were divided into three groups according to nominal concrete strengths. In the first and the third groups, investigations were made for a 76mm hole size, whereas in the second group four different hole sizes of 51mm, 76mm, 102mm, and 127mm in diameter were used to study the effect of opening size. All beams were provided with both longitudinal and transverse reinforcement. Torsion load was applied in increments. After application of each load increment the load, rotation, and strains were recorded and cracks, if

any, were marked. The theoretical predictions with ACI Code 318-77 are found to be in close agreement with the available test results.

(Ali, A.Y., 2010) studied the analysis of reinforced concrete horizontally curved deep beams, loaded transversely to its plane, using a three dimensional nonlinear finite element model in the pre and post cracking levels and up to the ultimate load. The 20-node isoperimetric brick element with sixty degrees of freedom was of ANSYS Program employed to model the concrete, while the reinforcing bars are modeled as axial members embedded within the concrete brick element. Perfect bond between the concrete and the reinforcing bars was assumed. The effects of some important numerical in addition to material parameters had been investigated to study their influence on the predicted load-deflection curves and the ultimate load capacity. The numerical study was carried out to investigate the effect of the central subtended angle, boundary conditions, amount of transverse reinforcement, and using additional longitudinal bars (horizontal shear reinforcement) on the behavior of reinforced concrete horizontally curved beams with different shear length to effective depth ratios (a/d). It was found that decreasing the central subtended angle causes an increase in the ultimate load resisted by curved beams. Also, it was found that the effect of the internal torsion and the amount of transverse reinforcement on the ultimate load resisted by curved beams was decrease as (a/d) ratio decrease, while the effect of the flexural moment and using additional longitudinal bars as a horizontal shear reinforcement was increase when (a/d) ratio decrease.

(Adel, A. A., etal, 2011) performed the linear elastic behavior of curved deep beams resting on elastic foundations with both compressional and frictional resistances. Timoshenko's deep beam theory is extended to include the effect of curvature and the externally distributed moments under static conditions. As an application to the distributed moment generations, the problems of deep beams resting on elastic foundations with both compressional and frictional restraints have been investigated in detail. The finite difference method was used to represent curved deep beams and the results were compared with other methods to check the accuracy of the developed analysis. Several important parameters are incorporated in the analysis, namely, the vertical sub grade reaction, horizontal sub grade reaction, beam width, and also the effect of beam thickness to radius ratio on the deflections, bending moments and shear.

(Ammar, Y. A., etal, 2015) presented experimental and theoretical investigation of the overall shear behavior of reinforced concrete deep beams made from hybrid concrete strength : Normal strength concrete (NSC) in tension zone and high strength concrete (HSC) in compression zone. The experimental work included testing of nine models of hybrid reinforced concrete deep beams under the effect of two point loads. One of the beams was tested as pilot and the other eight beams were divided into two groups namely group (A) and group (B) to study the effects of the following parameters: (HSC) the layer thickness, the effect of presence of web reinforcement and method of casting (i.e. monolithically or at different times), on the ultimate shear strength, the cracking load, the cracking pattern, the deflection, the ductility and failure modes. The experimental test results obtained from the adopted hybridization technique of (HSC) and (NSC) have shown that for beams made from (HSC) (about 45MPa) with a layer in compression zone of thickness (25 - 50) % of total beam depth, the ultimate shear strength was increased about (11.2 - 19.5) % for beams without web reinforcement and (16.75 - 22.25) % for beams with minimum web reinforcement. It has also shown that, the first cracking load was increased about (32.8 - 48) % and (43.4 - 57.9) % for beams without and with web reinforcement, respectively. The hybrid concrete beams that cast monolithically, have exhibited an increase in ductility about (13.3- 22.6) % and (17.3 - 26.3) % for specimens without and with web reinforcement, respectively. While, the hybrid concrete beams with construction joint and epoxy resin layer of thickness about (1mm), have exhibited larger increasing in ductility about (28.7%) and (30.2%) for specimens without and with web reinforcement, respectively. On the other hand, a non-linear three dimensional finite elements simulation using ANSYS computer program was adopted to trace the load-deflection response, cracking pattern and ultimate shear strength of the tested reinforced hybrid concrete beams with or without construction joint. Afterward, a parametric study has been conducted to investigate the effects of many important variables (compression strength for (HSC) layer, thickness of (HSC) layer, and shear span to effective depth ratio (L/D), thickness of resin bond layer). Comparison between the analytical and experimental results has shown a reasonable agreement of the load-deflection response, where, the average of the maximum difference in first cracking and ultimate loads was (13) % and (9.6) %, respectively.

CHAPTER THREE

RESEARCH METHODOLOGY

3.1.General

Nonlinear finite element analysis helps researchers to conduct more detailed investigations on the behavior of reinforced concrete structural elements. The implementation of nonlinear material law in finite element analysis codes is generally tackled by the software development industry in one or more ways. A number of powerful finite element software packages have been becoming commercially available. They include ANSYS, ABAQUS, COSMOSM, MARC and LUSAS.

In recent years, using ABAQUS finite element software, many research works have been performed successfully to simulate the behavior of reinforced concrete elements (beams, walls, columns and other structures).

In order to meet the objectives of this research, horizontally curved reinforced concrete deep beam was modeled using ABAQUS 6.13 software program. This chapter explains the process to build the model and the process to run the nonlinear analysis. The research significantly reveals the torsional behavior of horizontally curved reinforced concrete deep beam with respect to different center of curvature and length to deep ratio.

3.2. Finite element modeling

Finite Element (FE) Method is commonly used in evaluating and determining nonlinear load-displacement and cracking behavior of reinforced concrete structural members and systems. The plastic behavior of steel and concrete is quite complicated and hard to analytically model. Lumped and distributed plasticity models as well as continuum mechanics-based models were developed for inelastic modeling of concrete. Most realistic simulations can be carried out by the finite element analysis of 3D models. Many finite element packages are available to consider for the analysis of reinforced concrete systems. Each package can have its own strengths and weaknesses, i.e., some can report crack locations and/or widths while others allow easy embedding of reinforcing bars, etc. Steel rebar's can be modeled as smeared within a finite

element or can be taken account discretely. Discrete steel rebar's can be embedded inside concrete solid elements quite easily through embedding constraint which does not consider slip of reinforcement. The reinforcement interaction with concrete can be taken into account by introducing tension stiffening in the definition of material model. Two-node truss and eight-node solid finite elements are usually preferred in modeling steel reinforcement and concrete, respectively. When embedding constraint is used, the truss elements of reinforcement are joined to concrete solid elements. This option constrains the translational degrees of freedom of the embedded truss nodes to the interpolated values of the corresponding degrees of freedom of the concrete solid element.

Therefore, the reinforcement was assumed to be fully bonded to the concrete solid elements. For concrete material, there are two modeling options in ABAQUS. One is "Smeared crack concrete model" and the other is "Concrete Damaged Plasticity Model (CDPM)". Smeared crack concrete model is preferred for applications where concrete is subjected to monotonic straining. CDPM can be used with monotonic, cyclic, and/or dynamic loading conditions.

For this particular research, concrete damaged plasticity model was used. The CDPM required concrete compressive and tensile constitutive relationship, cracking and crushing damage parameters and special parameters such as dilation angle, eccentricity, biaxial loading ratio, the coefficient K and viscosity parameter.

3.3. Material properties

3.3.1. Concrete

A. Stress-Strain Relationship for Concrete in Compression

The stress-strain data for concrete in compression and tension is crucial for analysis utilizing concrete damaged plasticity model. However, this was not reported as part of the experimental results, only the ultimate compressive strength of the concrete at 28 days was recorded in experimental test. The curves were created using mathematical models found in literature. The compressive stress strain of concrete data was generated using Eurocode 2 (Eurocode, 2004) mathematical model for this research paper as shown in Figure 3.1.

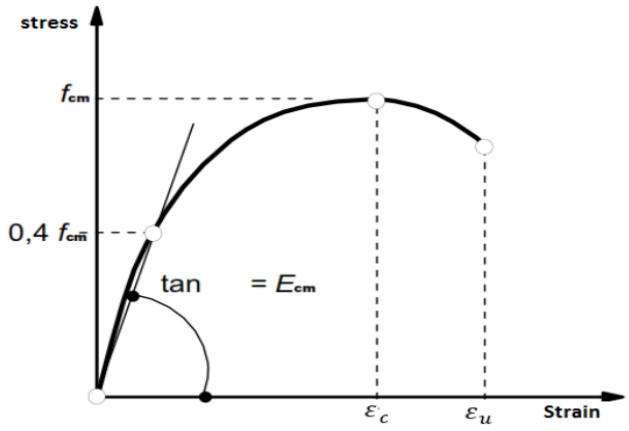

Figure 3.1: Stress-strain model for concrete in compression [Eurocode, 2004]

$$\frac{\sigma_c}{f_{cm}} = \frac{k\eta - \eta^2}{1+(k-2)\eta} \quad (3.1)$$

The parameters in Equation (3.1) are expressed as follows:

$$\eta = \frac{\varepsilon_i}{\varepsilon_{c1}} \quad (3.2)$$

$$\varepsilon_{c1} = 0.7 f_{cm}^{0.31} < 2.8 \quad (3.3)$$

$$\varepsilon_{cu} = 0.0035 \quad (3.4)$$

$$k = 1.05 E_{cm} \left({}^{\varepsilon_{c1}}/_{f_{cm}} \right) \quad (3.5)$$

$$f_{cm} = f_{ck} + 8\ (N/mm^2) \quad (3.6)$$

Where:

fck: is the characteristic cylindrical compressive strength of concrete at 28 days

ε_{c1}: is the strain at peak stress

ε_u: is the ultimate strain

The modulus of elasticity of concrete (Young's modulus) was computed using the simplified relationship provided by (Eurocode 2,2004):

$E_{cm} = 22[f_{cm}/10]^{0.3}$(3.7)

Equations 3.1 up to 3.7 were applied to generate the compressive behavior of concrete damage plasticity data shown in table 3.2.

B. Tensile stress Behaviour of Concrete

The tensile strength of concrete under uniaxial stress is seldom determined through a direct tension test because of the difficulties involved in its execution and the large scatter of the results. Indirect methods, such as sample splitting or beam bending, tend to be used (Eurocode 2, 2004):

$$f_{ctm} = 0.30 f_{ck}^{2/3} \quad (3.8)$$

The term cracking strain $\tilde{\varepsilon}_t^{ck}$ is used in CDP model numerical analyses. The aim is to take into account the phenomenon called tension stiffening. Concrete under tension is not regarded as a brittle-elastic body and such phenomena as aggregate interlocking in a crack and concrete-to-steel adhesion between cracks are taken into account. This assumption is valid when the pattern of cracks is fuzzy. Then stress in the tensioned zone does not decrease sharply but gradually. The strain after cracking is defined as the difference between the total strain and the elastic strain for the undamaged material:

$\tilde{\varepsilon}_t^{ck} = \varepsilon_t - \varepsilon_{ot}^{el}$(3.9)

$\varepsilon_{ot}^{el} = {}^{\varepsilon_t}/_{E_c}$(3.10)

In order to plot curve $\sigma_t - \varepsilon_t$ one should define the form of the weakening function. According to the ABAQUS user's manual, stress can be linearly reduced to zero, starting from the moment of reaching the tensile strength for the total strain ten times higher than at the moment of reaching f_{ctm}. But to accurately describe this function the model needs to be calibrated with the results predicted for a specific analyzed case.

The proper relation was proposed by, among others, (Wang and Hsu, 2001):

$$\sigma_t = E_c \varepsilon_t \ \ if\ \varepsilon_t \leq \varepsilon_{cr} \quad (3.11)$$

$$\sigma_t = f_{ctm}\left({}^{\varepsilon_{cr}}/_{\varepsilon_t}\right)^{0.4} if\ \varepsilon_t \geq \varepsilon_{cr} \quad (3.12)$$

The tensile strength of concrete beyond the cracking is often ignored in design standards. Nevertheless, in reality concrete is capable of carrying some tensile stresses between cracks when there is sufficient bond between the concrete and the internal reinforcement. This phenomenon is known as "tension stiffening', and can be modeled using a descending post peak tensile response (see Figure 3.2).

Equations 3.8 up to 3.13 were applied to generate the tensile behavior of concrete damage plasticity data shown in table 3.3.

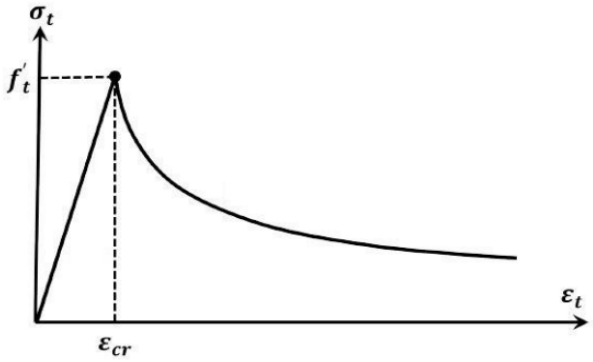

Figure 3.2: Idealized uniaxial stress-strain curve of concrete under tension (Stoner, 2015)

C. Selection of concrete damage parameters

Since the calculations for these parameters involve complex mathematical derivations and assumptions using the yield surface of the concrete damage plasticity model, the proposed values in other researchers' work have been used here, and the verification of the model is performed by comparing the numerical results with published experimental data.

Dilation angle – A parametric study carried out by Malm et al. (2006) suggested that there is no significant difference between 20° and 40° dilation angle if a reinforced concrete beam is subjected to bending. The best agreement with experimental data was reached for a dilation angle between 30° and 40°. Lee and Fenves (1998) also performed a verification of this material model with experimental data from Kupfer et al. (1969), where a dilation angle of 31° was

adjusted for uniaxial tensile and compressive failures, whereas a value of 25° was used for biaxial compressive failure. Hence, the dilation angle is selected as 31° in this work.

Flow potential eccentricity –The flow potential eccentricity is a small positive number, which defines the rate at which the hyperbolic flow potential approaches its asymptote (Abaqus Analysis User's Manual 2014). In the finite element simulation done by Ren et al. (2014), the default value of 0.1 was used, which fitted the experimental test.

Ratio of biaxial to uniaxial compressive yield stress –The biaxial stress ratio and the tensile-to-compressive meridian ratio were assumed to be equal to 1.16 and 0.667, respectively, based on recommendations of Chen and Han (1995).

Viscosity parameter –Since nonlinear material models with stiffness degradation often have convergence issues in ABAQUS, applying the technique of Viscoplastic regularization is a common method to overcome this difficulty, which for sufficiently small amount of time increments, causes the consistent tangent stiffness of the softening material to become positive (Abaqus Analysis User's Manual 2014). However, as suggested by Lapczyk et al. (2007), the selection of the value for the viscosity parameter affects the stiffness model, and a low value of the viscosity parameter should be selected (small compared to the characteristic time increment). The authors also performed parametric studies, and they found that the specimens with a viscosity parameter ranging from 0.00025 to 0.001 had good agreement with experimental results. The concrete damaged parameters used for this study has been summarized in table 3.1 based on good agreement with the experimental results.

Table 3.1 Summary of concrete damage parameters

Concrete		Concrete Damage Parameter	
Grade	C25	Eccentricity (γ)	0.1
Density	2.40E-09	Dilation angle (ψ)	31
Modulus of elasticity	28960	K	0.667
Poisson's ratio	0.18	σ_{bo}/σ_{co}	1.16
		Viscosity parameter	0.001

Table 3.2: Compressive behavior of concrete damage plasticity

Compressive behaviour		Compressive damage	
σ_c	e_{in}	d_c	e_{in}
10.20	0	0	0
13.44	8.6831E-05	0	8.6831E-05
18.46	0.0002244	0	0.0002244
22.90	0.0005023	0	0.0005023
24.83	0.00086645	0	0.00086645
25.00	0.00103674	0.00	0.00103674
24.66	0.00130338	0.0134837	0.00130338
22.70	0.00180231	0.09217729	0.00180231
19.19	0.00235449	0.23254493	0.00235449
14.34	0.00295272	0.42626595	0.00295272
13.67	0.00302771	0.45290305	0.00302771

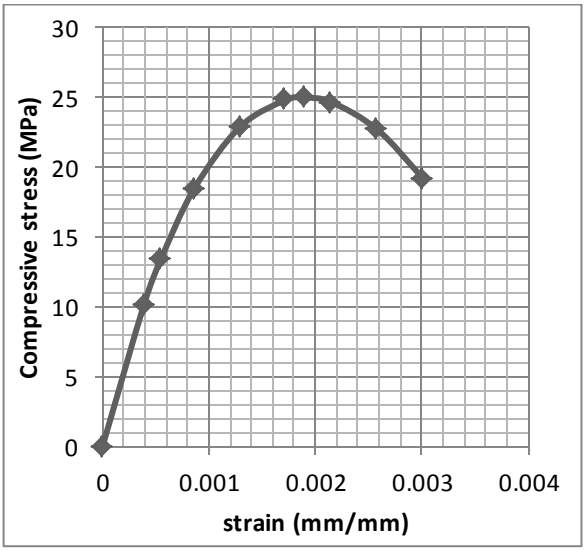

Figure 3.3: Compressivestress versus inelastic strain

Table 3.3: Tensile behavior of concrete damage plasticity

Tensile stress		Tension damage	
f_t(Mpa)	c_r(mm/mm)	d_t	c_r
1.983	0.000000	0.00	0.000000
1.503	0.000085	0.24	0.000085
0.813	0.000609	0.59	0.000609
0.557	0.001618	0.72	0.001618
0.353	0.005125	0.82	0.005125
0.318	0.006626	0.84	0.006626
0.254	0.011628	0.87	0.011628
0.226	0.015629	0.89	0.015629

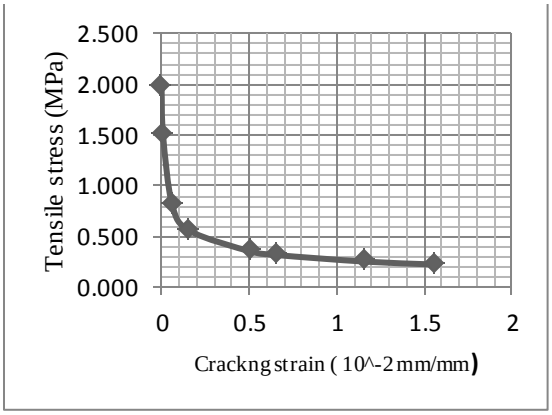

Figure 3.4: Tensile versus cracking strain

3.4.2. Steel reinforcement

The steel for the finite element models has been assumed to be an elasto-plastic material and identical in tension and compression. It is based on a linear elastic response up to yielding and a constant stress from the point of yielding to the ultimate strain. For this particular study,the steel reinforcement having Poisson's ratio of 0.3 and Elastic modulus of 200,000 Mpa has been used.

In a nonlinear analysis, ABAQUS requires the input of the steel stress-strain curves in the form of true stress versus true plastic strain. The true stress (σ_{true}) and true strain (ϵ_{true}) were converted from the engineering stresses (σ) and engineering strains ($\in$) as equation (3.13 and 3.14) (Phama & Hancockb, 2010):

$$\sigma_{true} = \sigma(1+\epsilon) \tag{3.13}$$

$$\epsilon_{true} = \ln(1+\epsilon) - {}^{\sigma_{true}}/_{E} \tag{3.14}$$

Table 3.4: Steel reinforcement properties used in the model

		$\emptyset 4mm\ bar$		$\emptyset 10mm\ bar$		$\emptyset 12mm\ bar$	
Density(tone/mm3)		7.85E-09		7.85E-09		7.85E-09	
Elastic properties	E	200000 Mpa		200000 Mpa		200000 Mpa	
	v	0.3		0.3		0.3	
Plastic properties		σ_{true} (MPa)	ϵ_{true}	σ_{true} (MPa)	ϵ_{true}	σ_{true} (MPa)	ϵ_{true}
		568	0	596	0	643	0
		597.2	0.0472	626.7	0.0471	676.2	0.0469
		624.8	0.0922	655.6	0.0920	707.3	0.0918
		681.6	0.1789	715.2	0.1788	771.6	0.1785

3.4. Geometry

Geometry is the important factor that determines the behavior of reinforced concrete deep beam. In this research paper twenty one (21) different reinforced concrete deep beams were modeled to evaluate the torsional behavior with respect to increasing load. Among those, three deep beams are horizontally straight, which are used as control beam. Eighteen deep beams are horizontally curved with different center of curvature and length to depth ratio. The designation and dimension of each deep beam have been presented in table 3.5. All are modeled using ABAQUS 6.13 software program.

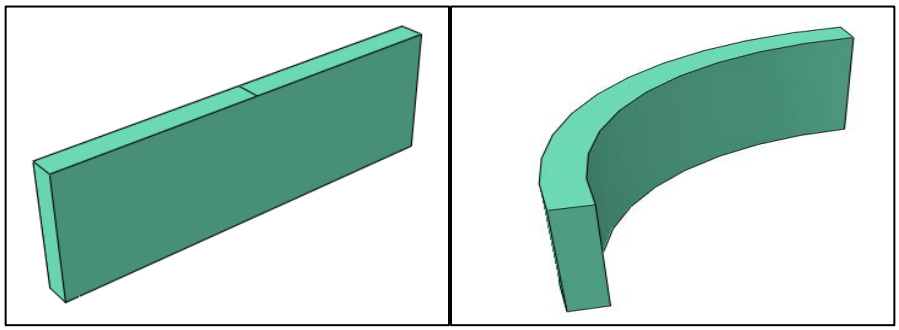

Figure 3.5: Sample of straight and horizontally curved deep beam geometry

Geometry of the reinforcement bars are greatly influence deep beam geometry for analysis. The reinforcement bars have a circular cross section and hence, they are modeled with a circular cross-section. Detail reinforcents of the models are shown in figure 3.6 for both sample straight and curved deep beam.

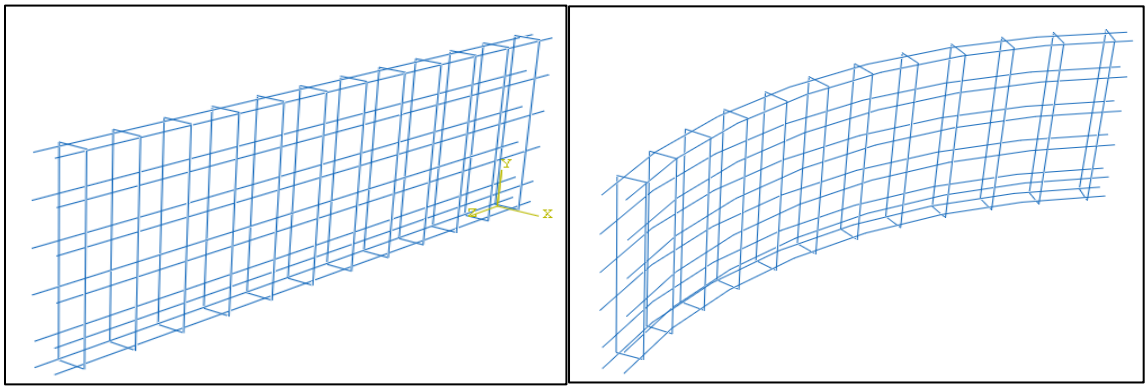

Figure 3.6: Geometrical descriptions of longitudinal rebar and stirrup

Table 3.5: The case under study and dimension of the deep beam model

No	Designated By:	Length (mm)	Depth(mm)	Width (mm)	L/R ratio	L/D ratio	Long. bar size(mm)	Stirrup size(mm)
1	AA10	1200	400	100	….	3	4ϕ4 , 2ϕ10 & 4ϕ12	12ϕ4
2	AA11	1200	400	100	1.57	3	4ϕ4 , 2ϕ10 & 4ϕ12	12ϕ4
3	AA12	1200	400	100	1.31	3	4ϕ4 , 2ϕ10 & 4ϕ12	12ϕ4
4	AA13	1200	400	100	1.05	3	4ϕ4 , 2ϕ10 & 4ϕ12	12ϕ4
5	AA14	1200	400	100	0.75	3	4ϕ4 , 2ϕ10 & 4ϕ12	12ϕ4
6	AA15	1200	400	100	0.52	3	4ϕ4 , 2ϕ10 & 4ϕ12	12ϕ4
7	AA16	1200	400	100	0.26	3	4ϕ4 , 2ϕ10 & 4ϕ12	12ϕ4
8	BB20	1200	450	100	……	2.67	6ϕ4 , 2ϕ10 & 4ϕ12	12ϕ4
9	BB21	1200	450	100	1.57	2.67	6ϕ4 , 2ϕ10 & 4ϕ12	12ϕ4
10	BB22	1200	450	100	1.31	2.67	6ϕ4 , 2ϕ10 & 4ϕ12	12ϕ4
11	BB23	1200	450	100	1.05	2.67	6ϕ4 , 2ϕ10 & 4ϕ12	12ϕ4
12	BB24	1200	450	100	0.75	2.67	6ϕ4 , 2ϕ10 & 4ϕ12	12ϕ4
13	BB25	1200	450	100	0.52	2.67	6ϕ4 , 2ϕ10 & 4ϕ12	12ϕ4
14	BB26	1200	450	100	0.26	2.67	6ϕ4 , 2ϕ10 & 4ϕ12	12ϕ4
15	CC30	1200	500	100	……	2.4	6ϕ4 , 2ϕ10 & 4ϕ12	12Y4
16	CC31	1200	500	100	1.57	2.4	6ϕ4 , 2ϕ10 & 4ϕ12	12ϕ4
17	CC32	1200	500	100	1.31	2.4	6ϕ4 , 2ϕ10 & 4ϕ12	12ϕ4
18	CC33	1200	500	100	1.05	2.4	6ϕ4 , 2ϕ10 & 4ϕ12	12ϕ4
19	CC34	1200	500	100	0.75	2.4	6ϕ4 , 2ϕ10 & 4ϕ12	12ϕ4
20	CC35	1200	500	100	0.52	2.4	6ϕ4 , 2ϕ10 & 4ϕ12	12ϕ4
21	CC36	1200	500	100	0.26	2.4	6ϕ4 , 2ϕ10 & 4ϕ12	12ϕ4

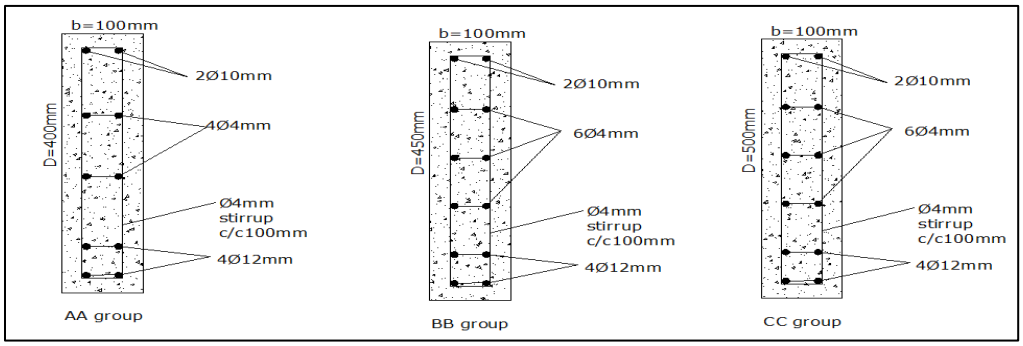

Figure 3.7: Cross-sectional view of each group of deep beam

3.5. Element types

The general procedure of modeling any structure in ABAQUS is to assemble meshed sets of finite elements into one global assembly, and then evaluate its overall response under loading. ABAQUS provides an extensive library of elements that can be effectively used to model a variety of materials. The geometry and the type of an element is characterized by several parameters including: family, degree of freedom, number of nodes, formulation, and integration. Each element in ABAQUS has a unique name which is derived from the five aspects mentioned previously. Figure 3.1 illustrates some of the most commonly used elements.

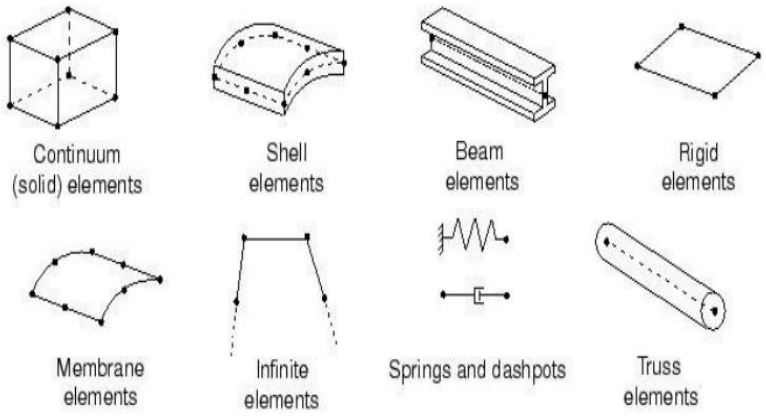

Figure 3.8: Various elements types (DSS, 2014)

In a standard stress analysis, the degrees of freedom of interest are the translations of the element nodes. In order to evaluate the field variables (usually displacements) at all nodes within the element domain, interpolation of these nodal values is performed. The number of nodes per elements determines the order of the interpolation (e.g. linear, quadratic, cubic, etc.). The 8-node continuum brick element, shown in Figure 3.8, uses linear interpolation and is referred to as a first-order element. On the other hand, a 20-node continuum element utilizes quadratic interpolation and known as a second-order element. In theory, second-order elements provide more accurate results than first-order elements, if they were used in adequately small applications. However, the use of higher-order elements has some of drawbacks associated with convergence issues, especially when used in highly nonlinear analyses. For that reason, it is

imperative to select the appropriate type of elements to achieve a sound numerical analysis. Although first-order elements are a quite practical choice for a large number of applications, they happen to exhibit a phenomenon called "shear locking". This phenomenon can be seen as a constrained distortion which may lead to drastic convergence issues. For example, when the two-dimensional block illustrated in Figure 3.9(a) is subjected to pure bending, the entire element will deform in the manner shown in Figure 3.9(b). However, if a two-dimensional, 4-noded, quadrilateral, linear element with four integration points is used to model that block, the material is expected to deform as seen in Figure 3.9(c).

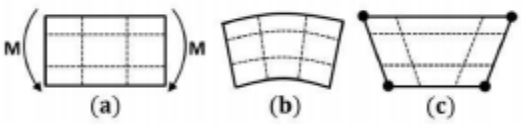

Figure 3.9: Shear locking of first-order elements (DSS, 2014)

In Figure 3.9(c), the dashed lines are no longer perpendicular at each integration point which implies that the shear is not zero at these points. This development contradicts the assumption that materials under pure bending do not exhibit shear stresses. This is attributed to the inability of linear elements to have curved edges. Consequently, strain energy is generating shearing deformation as opposed to the expected bending deformation, which results in a stiffer elements. However, one of the effective resolutions to this issue is to reduce the number of integration points per element so the excessive restraint is prevented (check Figure 3.10)

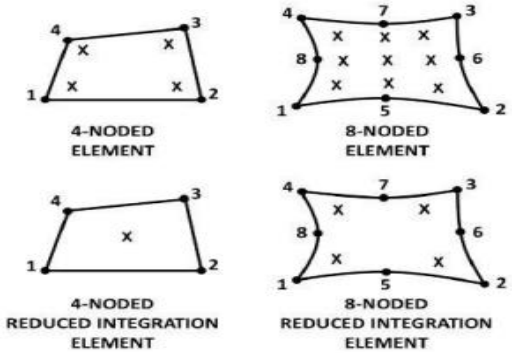

Figure 3.10: The reduction of integration points (DSS, 2014)

The reduced integration method is considered rather advantageous in modelling three dimensional problem as it decreases the time of analysis. Within the environment of ABAQUS, the user can choose the type of integration to be performed on the elements. A solid element such C3D8 is an 8-node continuum element with 8 integration points refers to full integration option. While a C3D8R is the same element with the exception of having only one reduced integration point (reduced integration option). Although, this practice is effective in eliminating shear locking, it may also result in a phenomenon named "hour glassing". The quadrilateral element in Figure 3.11 has only one integration point (reduced from a fully integrated element with 4 integration points). When this element is subjected to pure bending, the length of the two dashed lines and the angle between then remain unchanged. This implies that all the components of stress at the element's single point of integration are equal to zero. In another word, the strain energy in the element is assumed to be zero, and thus the element will not resist this type of deformation as it has no stiffness under this loading. As a result, the occurrence of hour glassing may cause significant uncontrolled distortions in the mesh (Stoner, 2015). However, ABAQUS offers elements with hourglass control to overcome this issue.

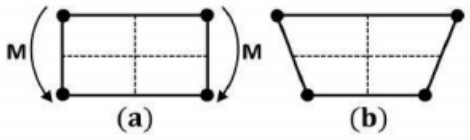

Figure 3.11: Hour glassing in reduced integration point (DSS, 2014)

For this particular paper, Solid 3D elements 8-node bricks (C3D8R) were used to model ordinary concrete and two node linear 3D truss element (T3D2) were used to model the reinforcement steel.

3.6. Meshing

As an initial step, the finite element analysis requires meshing of the model. Hence, the model is divided into a number of small elements. After the application of the load, the stress and the strain are calculated at integration points of these elements. An important step in finite element modelling is the selection of the mesh density. A convergence of results is obtained when an

adequate number of elements are used in a model. This is achieved when an increase in the mesh density has a negligible effect on the result. Therefore, it is very important to study the mesh convergence to determine an appropriate mesh density.

For this particular research, the models are meshed with 25mm size of elements as shown in figure3.12.

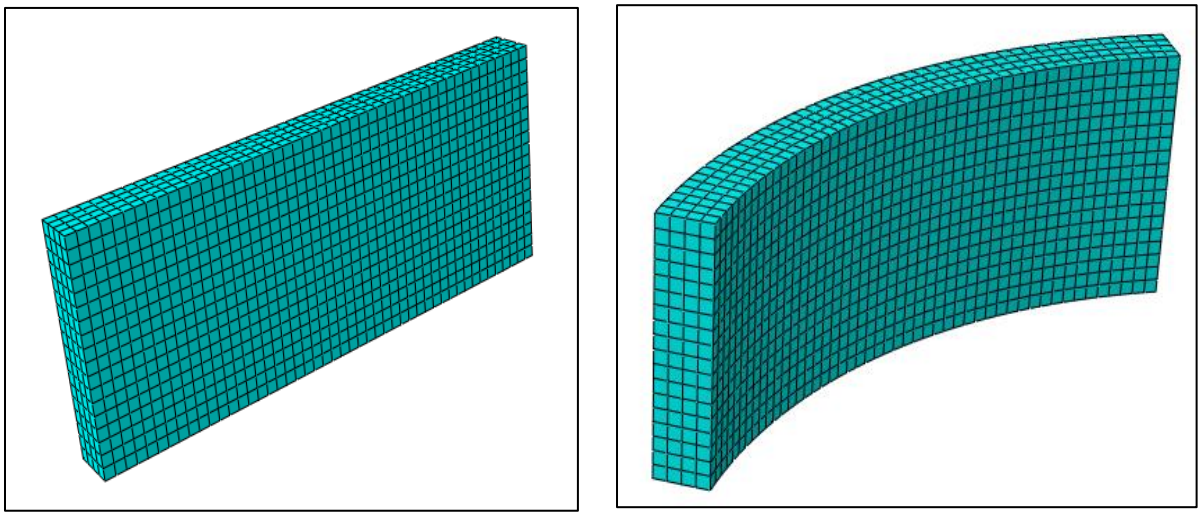

Figure 3.12: Meshing of beam model

3.7. Loading and Boundary condition

Displacement of boundary conditions is used to constrain all reinforced concrete beam models for the purpose of getting a unique solution. Those models constrained from both rotation and translation in all direction $(Uz = Uy = Ux = \theta x = \theta y = \theta z = 0)$means fixed support was applied at both ends as illustrated in figure 3.13.

The load was applied in small increments to overcome numerical instability difficulties that could be occurred when a large load had been applied suddenly. A concentrated load is applied incrementally at mid span (figure 3.13) of deep beam until its failure.In addition discrete plate was used to apply concentrated load at the center of span of deep beam as shown in figure3.13.

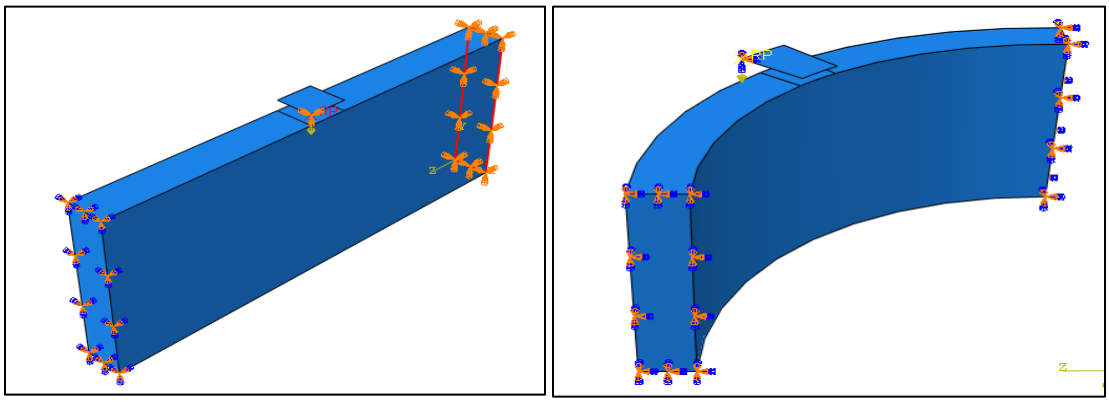

Figure 3.13: loading and boundary condition

3.8. Method for non-linear solution

There are different methods available in Abaqus for finding the solution of non-linear equations such as the linear method, the Newton Raphson method and the modified Newton Raphson method. In this study the modified Newton Raphson method has been used for solving the simultaneous equations and finding incremental equilibrium. This is an iterative process of solving the non-linear equations.

One approach of non-linear solution is to break the load into a series of load increments. The load increments can be applied either over several loads or over several load steps within a load step. At the completion of each incremental solution, the program adjusts the stiffness matrix to reflect the non-linear changes in structural stiffness before proceeding to the next load increment. The ABAQUS program overcomes this difficulty by using the Full Newton Raphson method, or the modified Newton Raphson method, which drives the solution to equilibrium convergence at the end of each load increment. In the Full Newton Raphson method, it uses the following set of non-linear equations:

$K(p)\Delta p = q - f(p)$(3.15)

Where is the vector of total applied joint loads is the vector of internal joint force, is the deformation increment due to loading increment, are the deformations of the structure prior to the load increment and is the stiffness matrix, relating loading increments to deformation increments.

Figure 3.14 illustrates the use of the Newton Raphson equilibrium iterations in non-linear analysis. Before each solution, the Newton Raphson method evaluates the out of balance load vector, which is the difference between restoring forces (the load corresponding to the element stress) and the applied load. The program then performs a linear solution using the out of balance loads and checks for convergence. If convergence criteria are not satisfied the out of balance load vector is re-evaluated and the stiffness matrix is updated then a new solution is obtained. This iterative procedure continues until the problem converges to within defined criteria.

Sometimes the most time consuming part of the Full Newton Raphson method solution is the recalculation of the stiffness matrix at each iteration. In many cases this is not necessary and we can use the matrix from the first iteration of the step. This is the basic idea of the so called Modified Newton Raphson method. It produces very significant time savings. But on the other hand it also exhibits a slower convergence of the solution procedure. The simplification adopted in the Modified Newton Raphson method can be mathematically expressed by:

$$\boldsymbol{K(p_i - 1) = K(p_o)}(3.16)$$

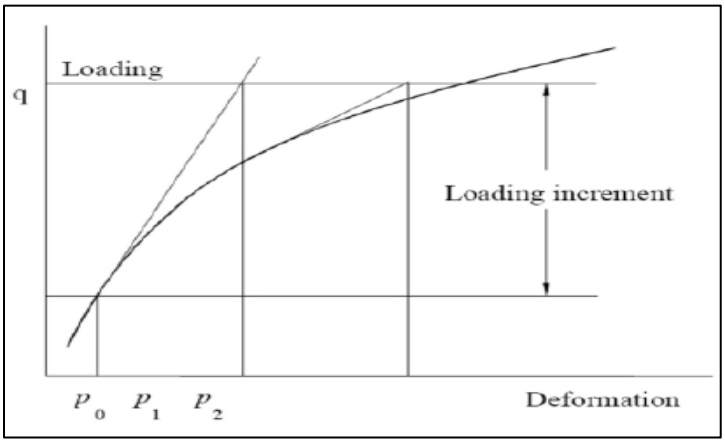

Figure 3.14: Full Newton Raphson Method

The modified Newton Raphson method which was used in this study is as shown, which when compared to the Full Newton Raphson method it shows that the Modified Newton Raphson method converges more slowly than the original Full Newton Raphson method.

On the other hand a single iteration costs less computing time because it is necessary to assemble and invert the stiffness matrix only once. In practice a careful balance of the two methods is usually adopted in order to produce the best performance for any particular case. Usually it is recommended to start a solution with the original Newton Raphson method and later i.e. near extreme points switch to the modified procedure to avoid divergence.

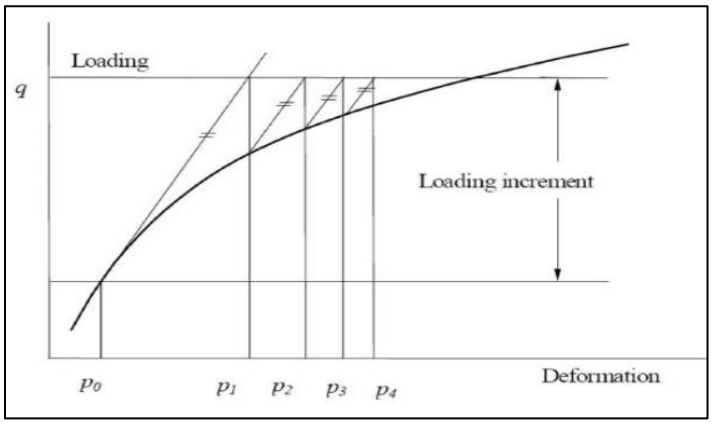

Figure 3.15: Modified Newton-Raphson Method

3.9. Load stepping and failure definition for finite element method

For the nonlinear analysis, automatic time stepping in the Abaqus program predicts andcontrols load step size. Based on the previous solution history and the physics of the models,if the convergence behavior is smooth, automatic time stepping will increase the loadincrement up to a selected maximum load step size. If the convergence behavior is abrupt,then the automatic time stepping will bisect the load increment until it is equal to a selectedminimum load step size. The maximum and the minimum load step sizes are required for theautomatic time stepping.

In this particular study the time period, the maximum number of increments, the initial increment, minimum increment size and maximum increment size were set to 1, 10000, 0.001, 1E-020 and 1 respectively.

3.10. Flowchart of the finite element analysis

Figure 3.16 shows the procedure followed to analysis the deep beam in ABAQUS 6.13 software package program.

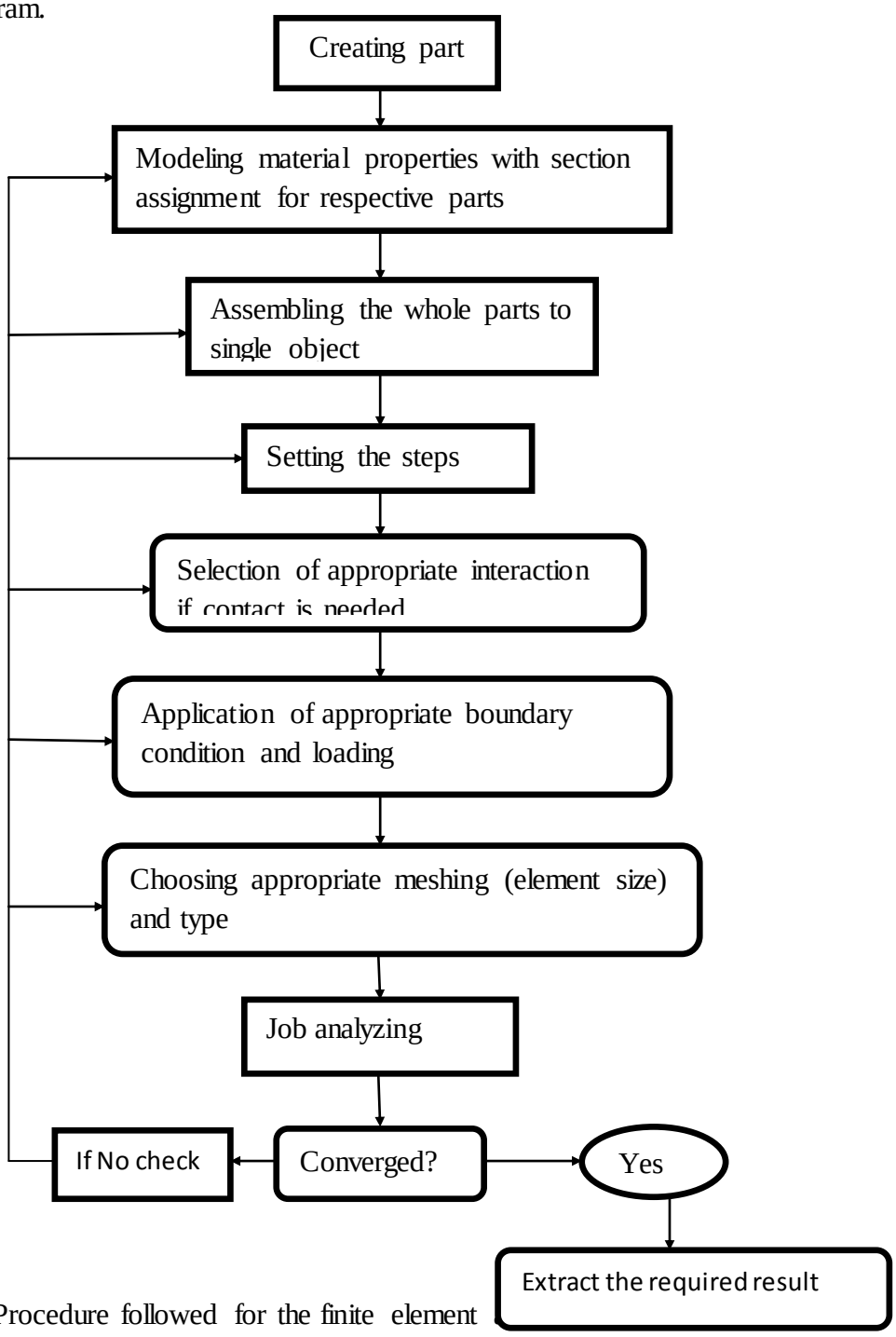

Figure 3.16: Procedure followed for the finite element

3.11.Validation

The validity of the proposed analytical model is checked through extensive comparisons between analytical and experimental results of RC deep beam under concentrated load. The load deflection curve has been presented experimentally under two concentrated load applied at one third span length of deep beam with simply supported condition. The theoretical results from finite element analysis showed in general a good agreement with the experimental values.

3.11.1 General description on the genesis of data used in experiment

a. Material Properties

Concrete

The concrete is defined as an isotropic material in the modeling, and should be deliberately expressed in verification genesis.

Table 3.6: Concrete properties of validity parameters (Ammar, 2015)

Concrete properties	Magnitude
Elastic Modulus	28960 Mpa
Poisson's Ratio	0.2
Compressive strength	25 Mpa
Tensile strength	1.923 Mpa

Reinforcement steel

Steel reinforcement with different diameter and yield strength were used in the experimental setup of the reinforced deep beam. The yield strength of steel fy used in the model for bar diameters $(12\ mm, 10\ mm,\ 4\ mm)$was$(643, 596,\ 568\ MPa)$ respectively with modulus of elasticity $200\ GPa$. The properties of steel reinforcement are summarized in table 3.7.

Table 3.7: Steel properties of validity parameters (Ammar, 2015)

Steel properties	Diameter of bar		
	ϕ4mm	ϕ10mm	ϕ12mm
Elastic Modulus	200000 Mpa	200000 Mpa	200000 Mpa
Poisson's Ratio	0.3	0.3	0.3
Yield Strength	568	596	643

b. Geometry

Test specimens having a total length $(l = 1400mm)$, span length $(ln = 1200mm)$, overall depth $(h = 450mm)$, effective depth $(d = 400mm)$ and width $(b = 100mm)$ with shear span to effective depth ratio (a/d) about 1.0 to ensure that tied-arch action of deep beam would be developed. Four $(ø12mm)$diameters of deformed bars were provided as longitudinal tension reinforcement with about 1.13% and $2ø10mm$ to be used as compressive bars. Additionally horizontal and vertical reinforcement were provided as shown in figure 3.16.

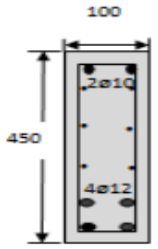

Figure 3.16: The cross section of deep beam under experimental set up (Ammar, 2015)

c. Test set up and loading

The hydraulic universal testing machine with capacity $(2000KN)$was used to test the beam. The deep beam was loaded under a monotonically increasing two concentrated load acting at one third span length until collapse. The loading and the mid span deflection readings were recorded at some interval of load increments. The loading and test setup is shown in Figure 3.17 and figure 3.18 respectively.

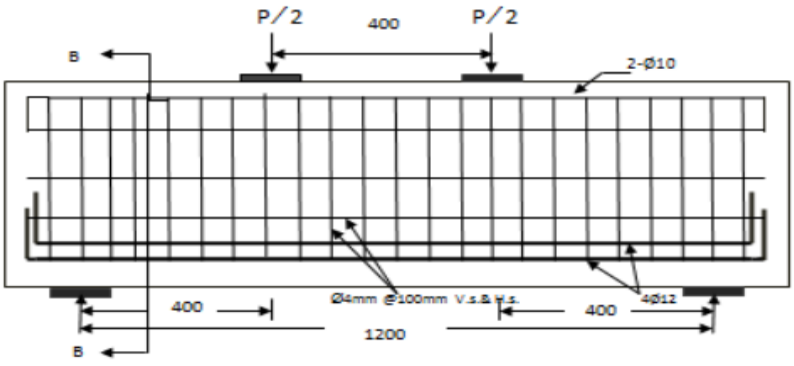

Figure 3.17: Loading condition of test setup (Ammar, 2015)

Figure 3.18: Experimental set up (Ammar, 2015)

3.11.2 Comparison of the Results

The results obtained from laboratory test were used to comparewith the results obtained from the finite element analysis. Hence, the finite element model was implemented based on the parameters and conditions used in the laboratory test. The load deflection curve for both experimental and finite element analysis (ABAQUS Software package) has been presented in figure 3.19. The comparison showed a good agreement between experimental and finite element result.

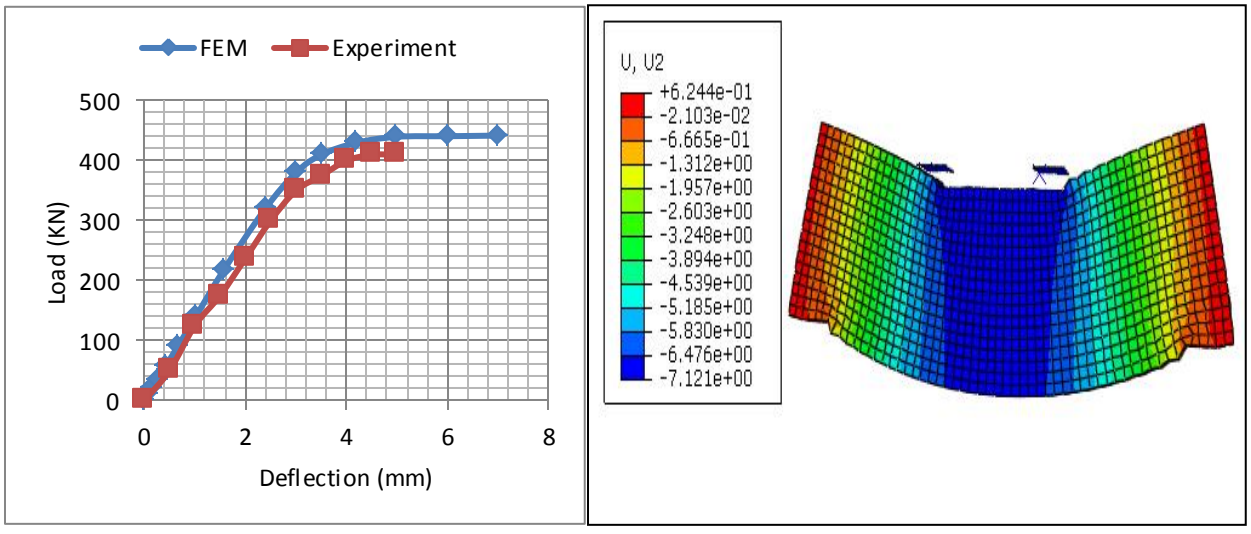

Figure 3.19: Comparison of experimental(Ammar, 2015) and finite element result

CHAPTER FOUR

RESULTS AND DISCUSSION

4.1 General

This chapter presents the results of the torsional behaviors and it effect on the loading capacity (flexural capacity) of reinforced deep beam. The study was undertaken by considering the effect of different (L/D) and (L/R) ratio on flexural (load carrying capacity) and torsional behaviour.

4.2 The Results of Finite Element Analysis

The concentrated load was assigned at the mid-span of deep beam to study the load carrying capacity and torsional behaviour with its effects. All deep beams were modeled and analyzed in ABAQUS software package in order to determine the ultimate load to be resisted. Table 4.1 shows the ultimate load that resisted by each deep beams obtained from finite element analysis. As load carrying capacity increases the flexural capacity also increases.

Table 4.1: The reduction in ultimate load resisting capacity

Designation	Ultimate load(KN)	Designation	Ultimate load(KN)	Designation	Ultimate load(KN)
AA10	421.90	BB10	587.86	CC10	808.37
AA11	414.10	BB11	578.46	CC11	791.55
AA12	407.30	BB12	567.56	CC12	775.76
AA13	398.50	BB13	554.16	CC13	757.01
AA14	386.70	BB14	537.76	CC14	737.31
AA15	370.90	BB15	516.86	CC15	705.68
AA16	349.92	BB16	489.88	CC16	680.14

The reduction of load carrying capacity of reinforced concrete deep beam with the same depth, width, length and steel reinforcement is due to the variation of center of curvature (aspect ratio) as shown in table 4.1 (considering only one deep beam). The reduction came from the development of torsional moment.The development of internal torsion is caused from center of

curvature (aspect ratio) the deep beam.Figure 4.1 shows the effect of aspect ratio on ultimate by considering different depth.

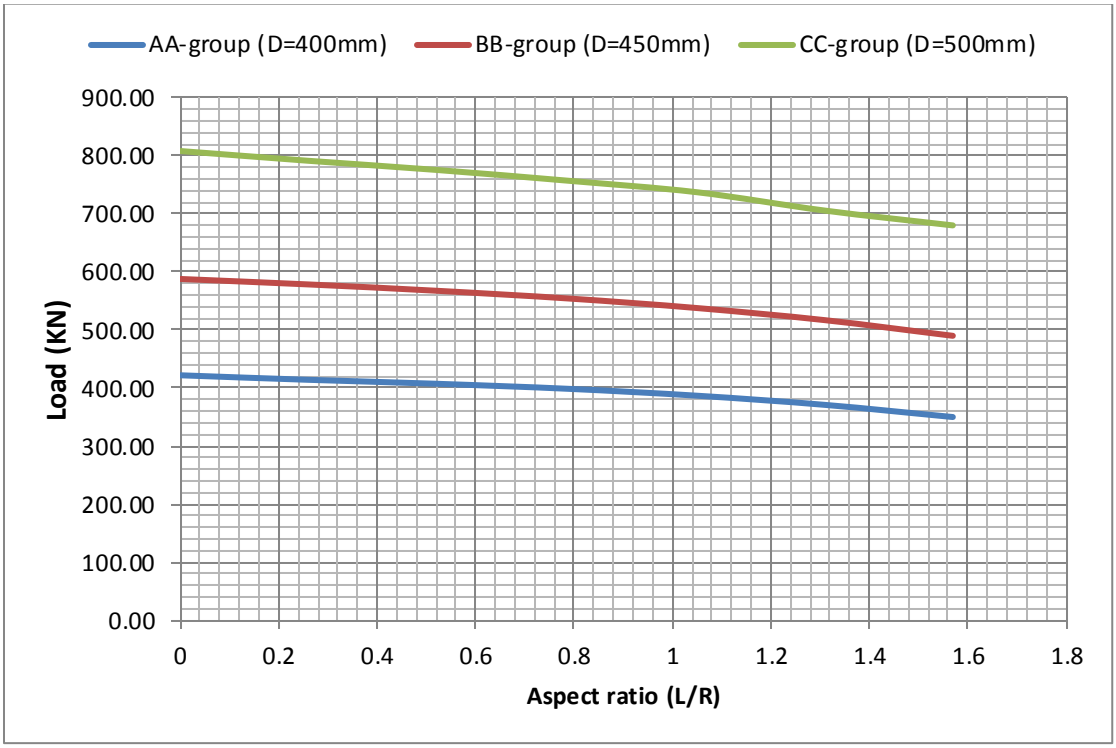

Figure 4.1: Load carrying capacity versus aspect ratio curve considering different depth

4.3. Parametric studies

4.3.1. Effect of L/R ratio on deflection versus load

The effect of L/R ratio on load deflection curve of horizontally curved reinforced concrete deep beams had been studied. A figure (4.2), (4.3) and (4.4) shows the numerical results of the finite element analyses of load deflection of curved deep beams. These figures reveal that, the load carrying capacity (flexural resistance) decreases as length to radius ratio (aspect ratio) increase. Each figure shows, the load versus deflection result of deep beam with the same depth, length, width, steel reinforcents and concrete grade with different aspect (L/R) ratio. The decrease in load carrying capacity is due to the development of torsion which increases as aspect ratio increase.

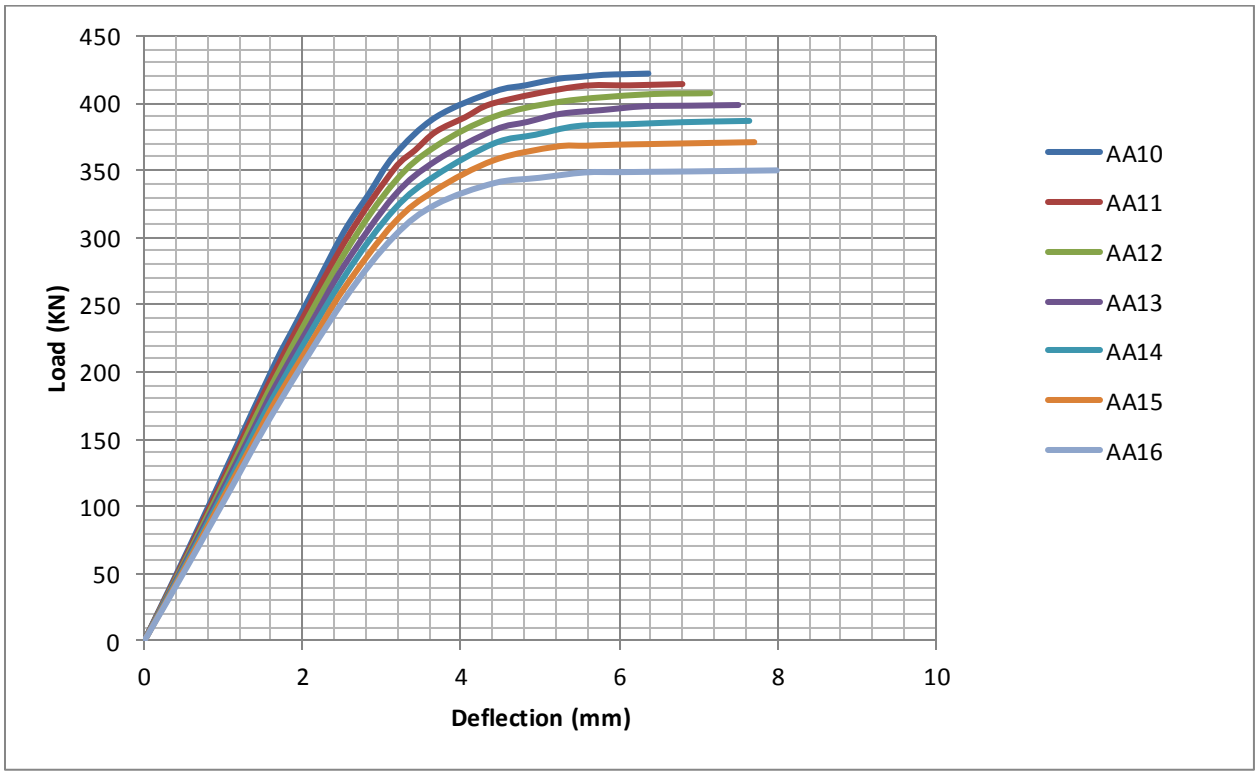

Figure 4.2: Load versus deflection for deep beam group AA10 up to AA16

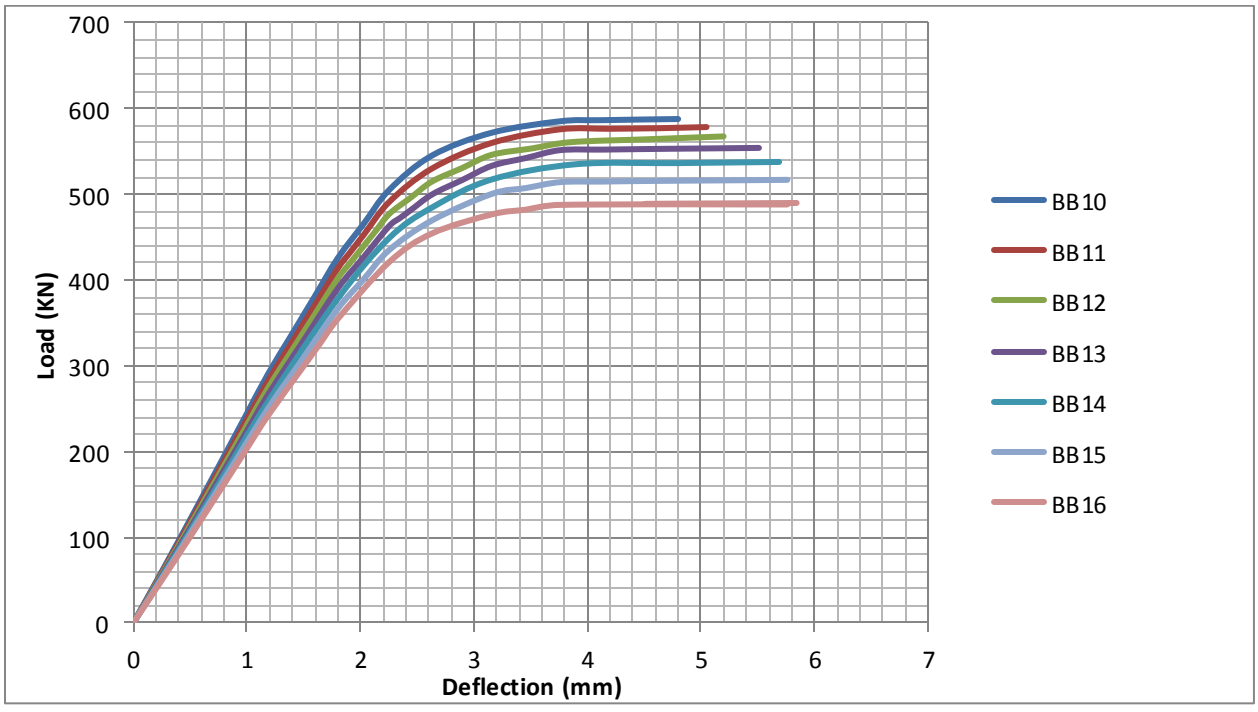

Figure 4.3: Load versus deflection for deep beam BB10 up to BB16

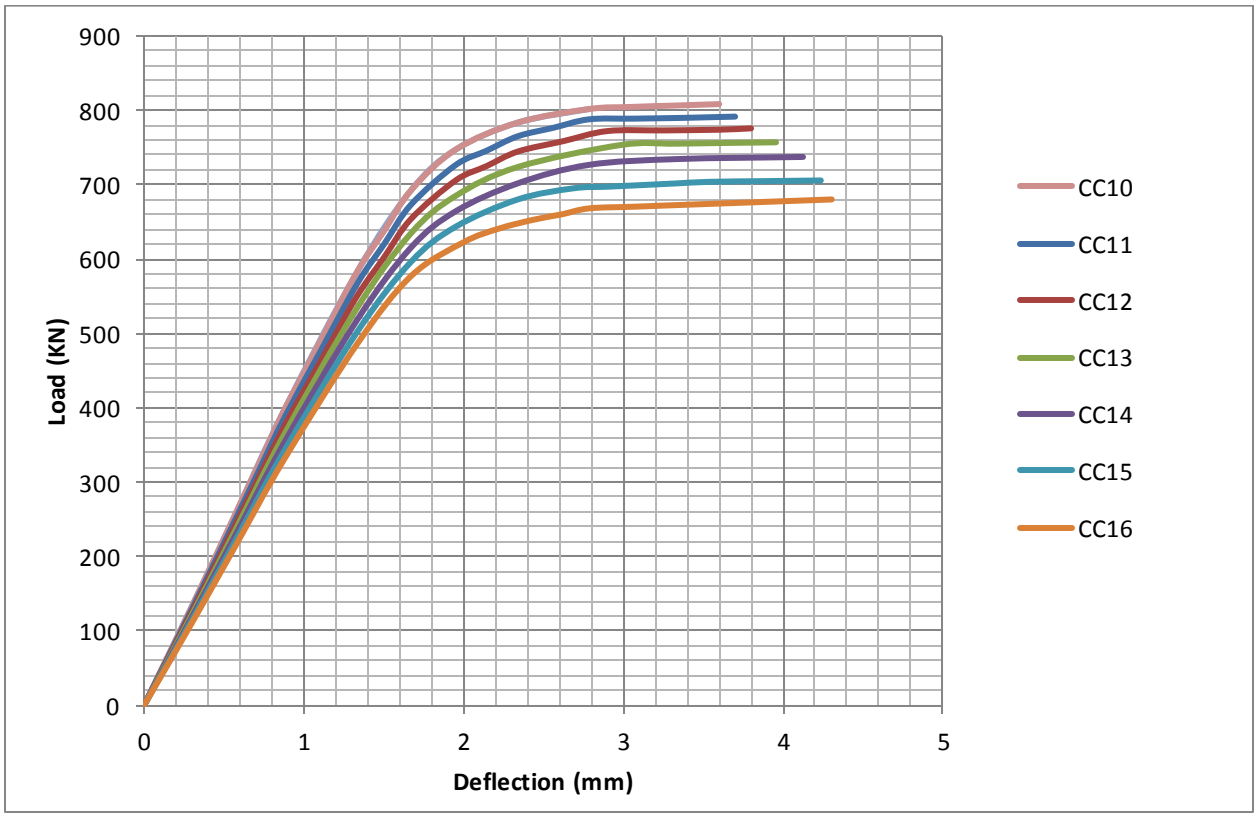

Figure 4.4: Load versus deflection for deep beam group CC

4.3.2. Effect of L/D ratio on deflection versus load

The effect of L/D ratio on load deflection curve of horizontally curved reinforced concrete deep beams had been also studied. Figure 4.5 shows the numerical results of the finite element analyses of load deflection curve of horizontally curved deep beam by considering different Length to depth (L/D) ratio with the same center of curvature (aspect ratio). These figures reveal that, the load carrying capacity (flexural resistance) decreases as length to depth (L/D) ratio increase. Each figure 4.5(a), (b), (c), (d), (e), (f) and (g) shows, the load versus deflection result of deep beam with the same aspect ratio (L/R) and different length to depth (L/D) ratio. The ultimate load resisted by the curved beam is decreased, as length to depth (L/D) ratio increased, when the aspect ratio (L/R) kept constant. However, the effect of length to depth (L/D) ratio is more than aspect ratio (L/R) on the load deflection of the deep beam.

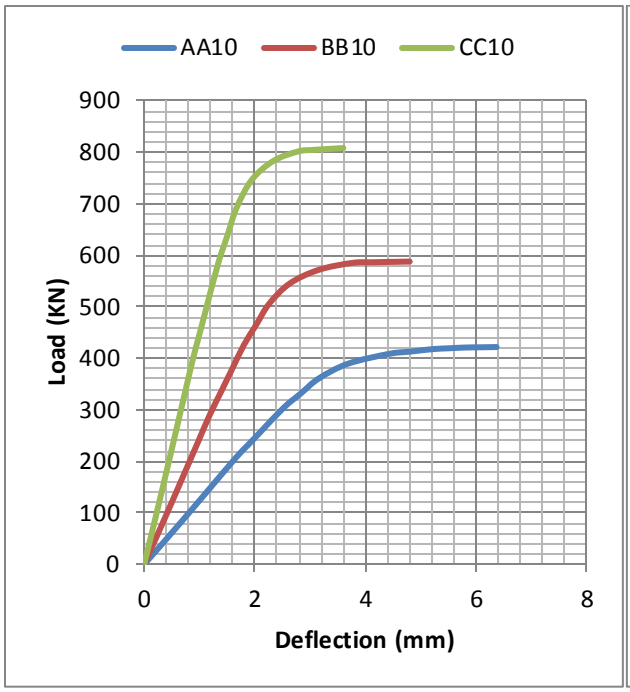
AA10
BB10
CC10
Load (KN)
Deflection (mm)
0
100
200
300
400
500
600
700
800
900
0
2
4
6
8

(a)

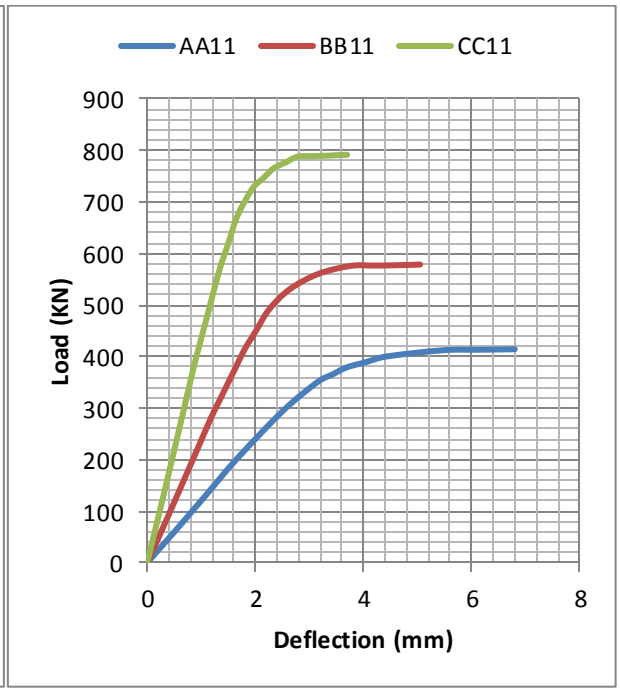
AA11
BB11
CC11
Load (KN)
Deflection (mm)
0
100
200
300
400
500
600
700
800
900
0
2
4
6
8

(b)

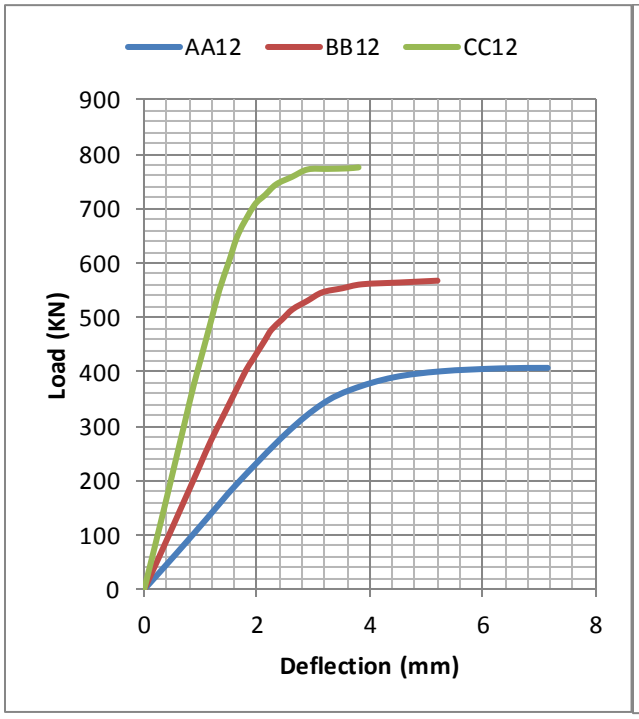
AA12
BB12
CC12
Load (KN)
Deflection (mm)
0
100
200
300
400
500
600
700
800
900
0
2
4
6
8

(c)

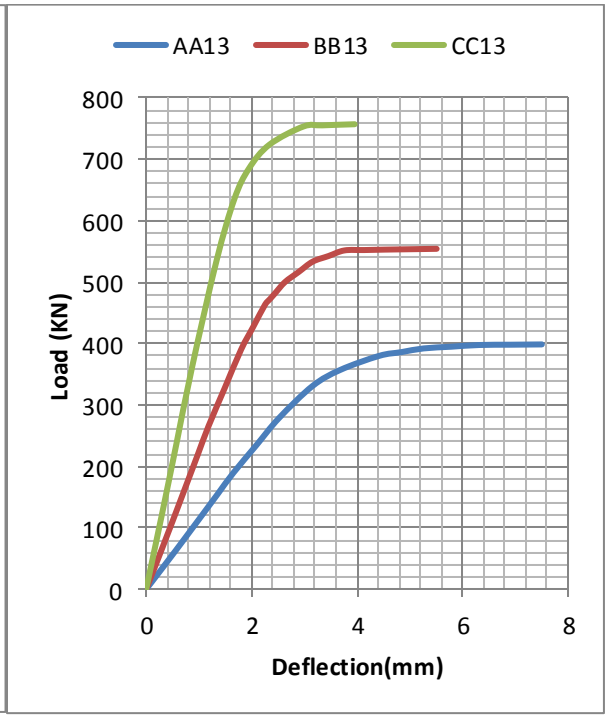
AA13
BB13
CC13
Load (KN)
Deflection(mm)
0
100
200
300
400
500
600
700
800
0
2
4
6
8

(d)

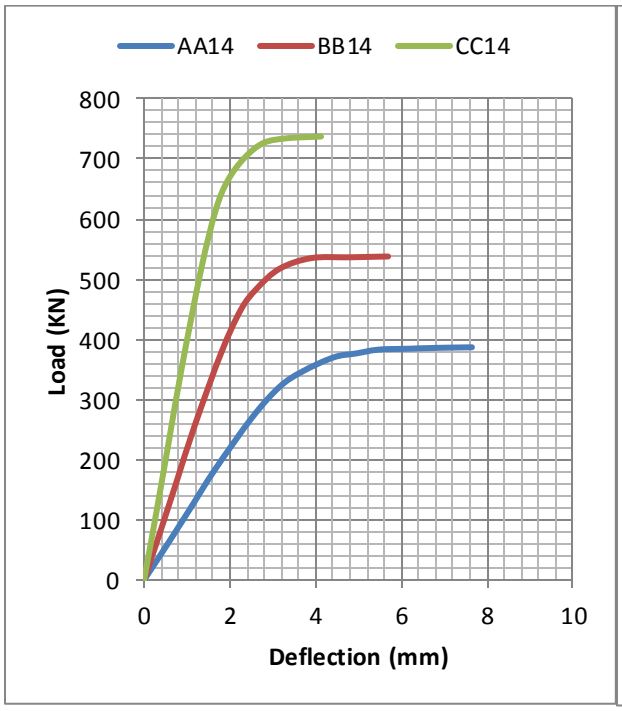

(e)

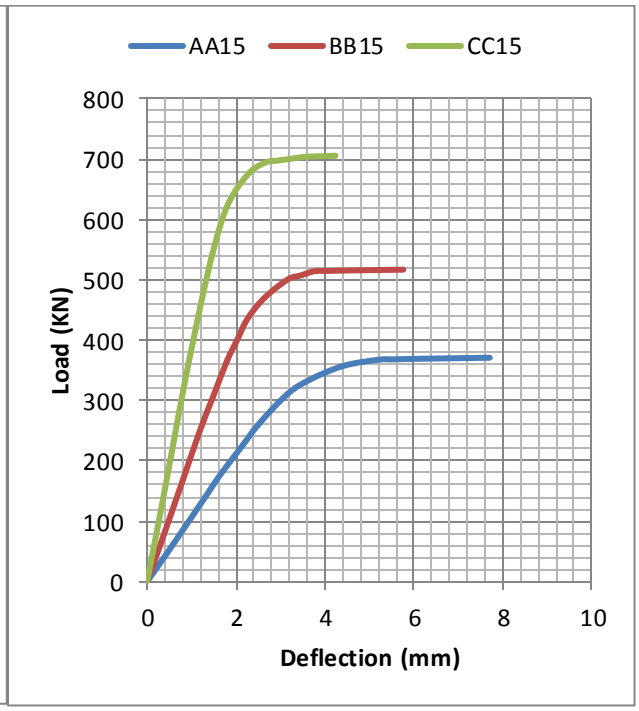

(f)

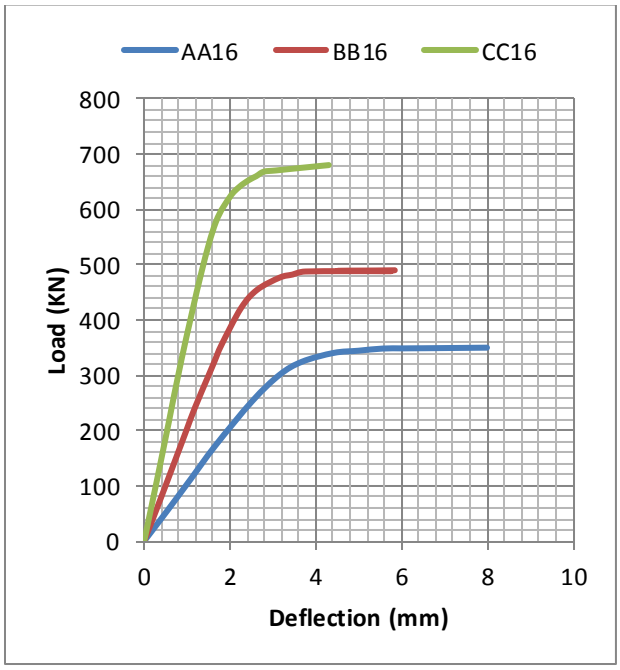

(g)

Figure 4.5: Effect of L/D ratio on load versus deflection

4.3.3. Effect of L/R ratio on twisting angle versus load

In addition to load deflection curve, the load twisting angle curve had been determined using finite element analysis. Figures (4.6), (4.7),and (4.8) shows the numerical results of the finite element analyses of load twisting angle of horizontally curved deep beam under the same depth, width, length, steel reinforcement, concrete grade and different center of curvature. The figures showed that, at the same load, load twisting angle response become greater as length to radius (L/R) ratio increases. This implies as center of curvature or aspect ratio increased, the internal torsion is also increased. The increase in internal torsion resulted in the decrease in load carrying capacity of the deep beam.

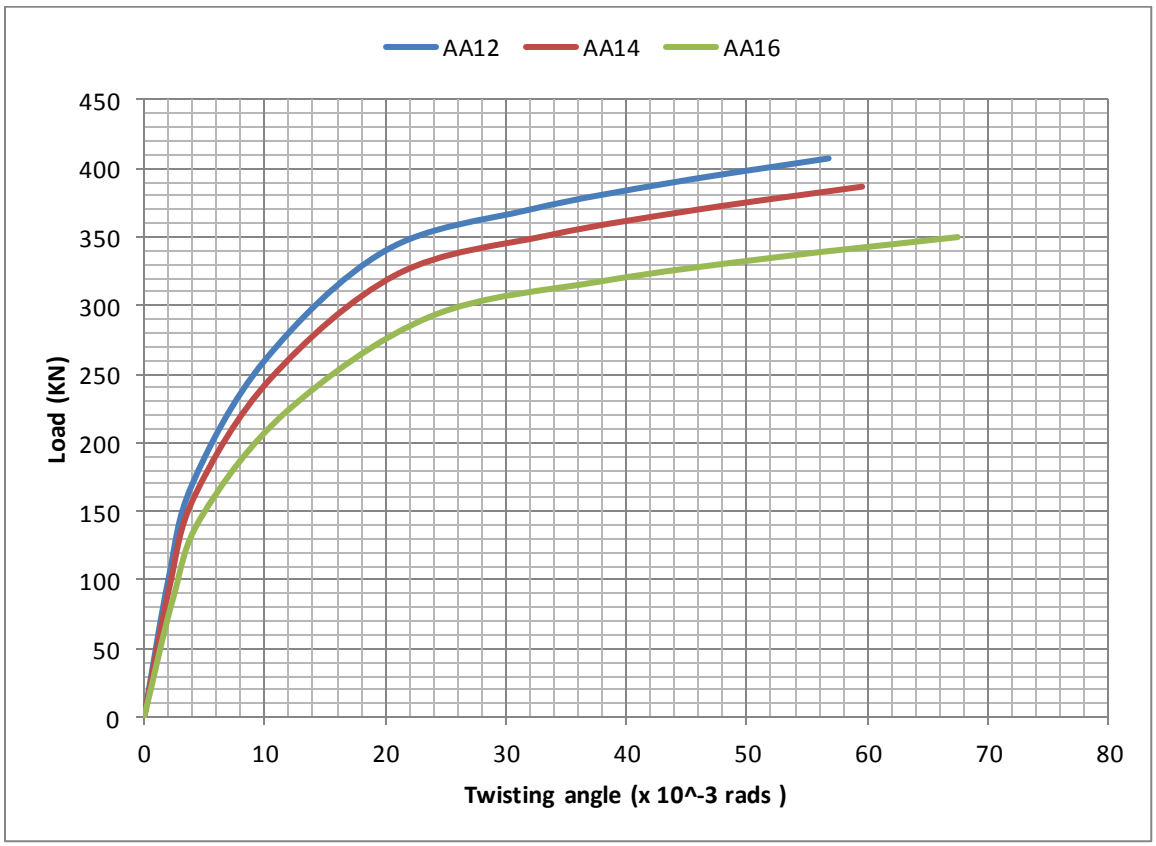

Figure 4.6 Load versus twisting angle for AA12, AA14 and AA16

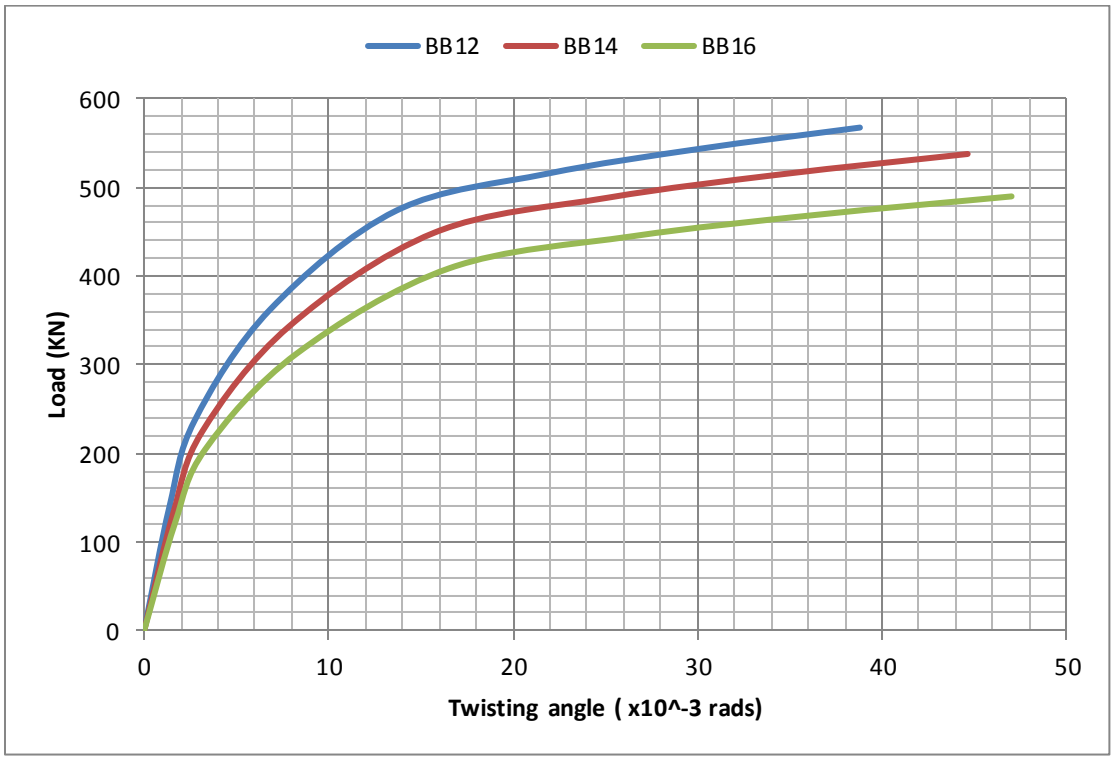

Figure 4.7: Load versus twisting angle for BB12, BB14 and BB16

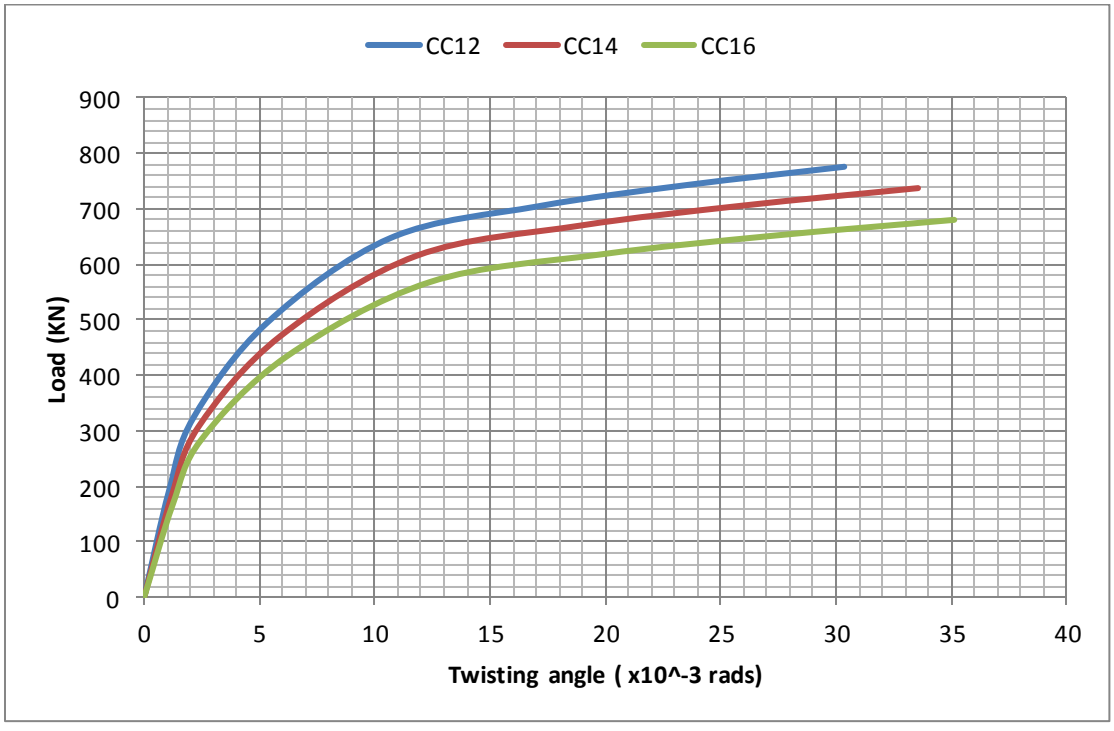

Figure 4.8: Load versus twisting angle for CC12, CC14 and CC16

4.3.3. Effect of L/D ratio on twisting angle versus load

The effect of L/D ratio on load twisting angle curve of horizontally curved reinforced concrete deep beams had been also studied. Figure 4.9, 4.10 and 4.11 shows the numerical results of the finite element analyses of load twisting curve of horizontally curved deep beam by considering different length to depth (L/D) ratio with the same center of curvature (aspect ratio). These figures reveal that, the effect of internal torsion is increased as length to depth (L/D) ratio increased. This implies that, under the same load application, the twisting angle is increased as length to depth ratio increased. Each figure shows, the load versus twisting angle result of deep beam with the same aspect ratio (L/R) and different length to depth (L/D) ratio. However, length to depth (L/D) ratio has more effect on load twisting angle curve than aspect ratio.

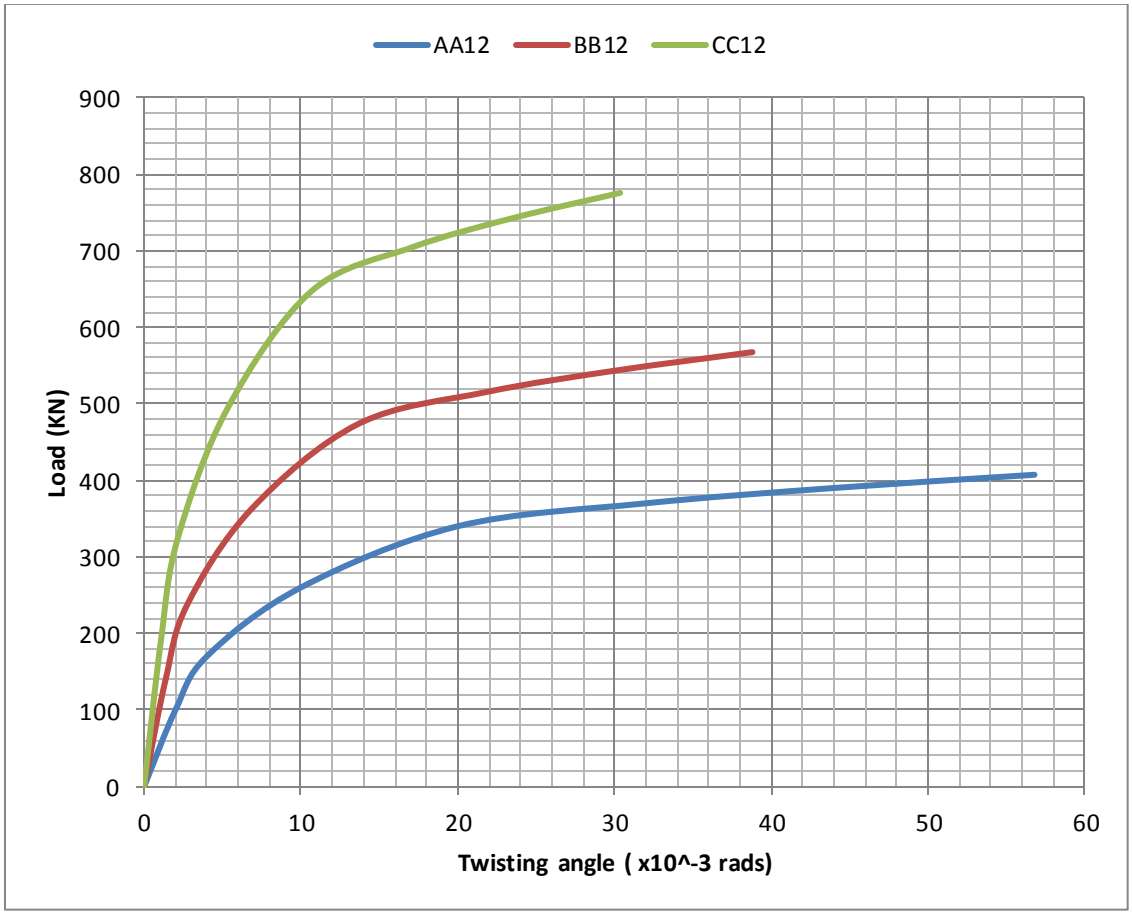

Figure 4.9: load versus twisting angle for AA12, BB12 and CC12

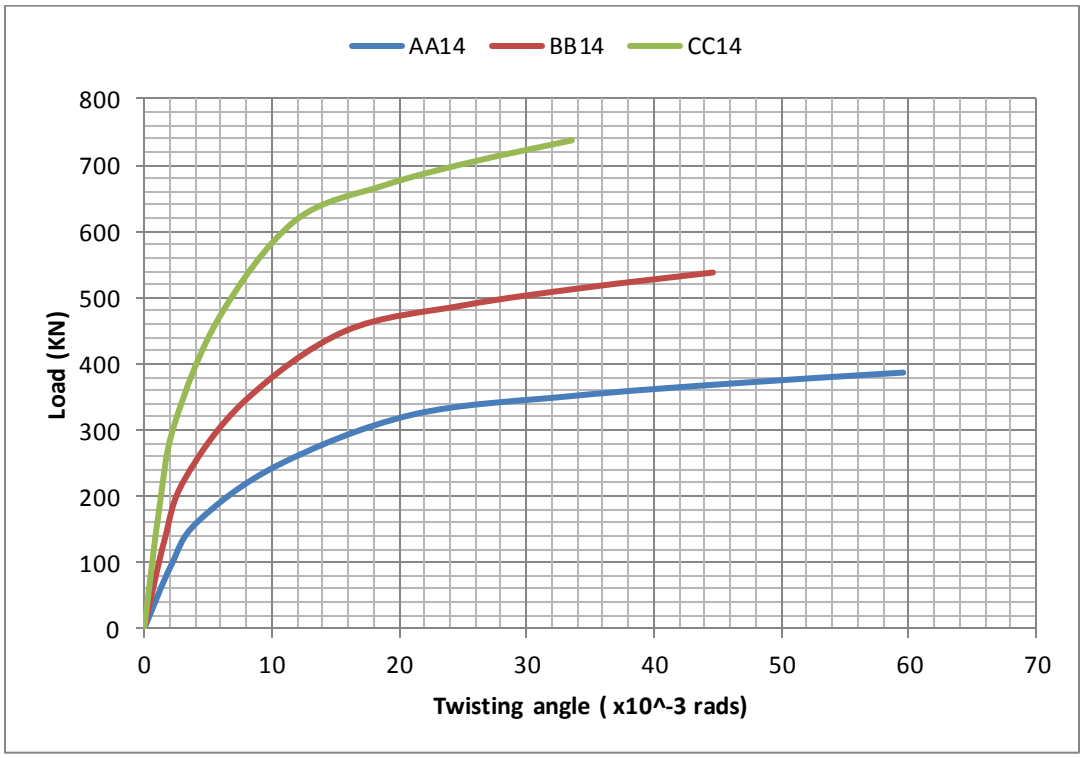

Figure 4.10: load versus twisting angle for AA14, BB14 and CC14

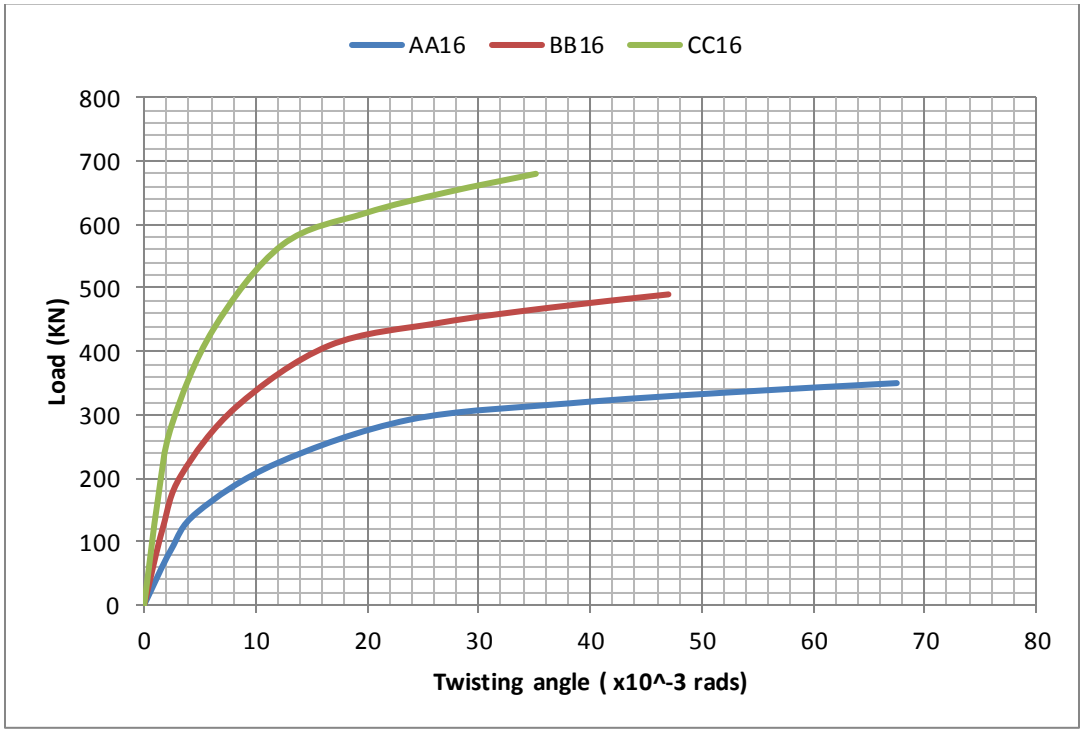

Figure 4.11: load versus twisting angle for AA16, BB16 and CC16

CHAPTER FIVE

CONCLUSIONS AND RECOMMENDATION

The main objective of this research is to study the load carrying capacity and torsional behavior of horizontally reinforced concrete curved deep beams with different length to depth (L/D) and length to radius (L/R) ratio. This research included a nonlinear finite element analysis by (ABAQUS Software package) in order to predict the load carrying capacity, load deflection curve and load twisting angle curve of horizontally curved reinforced concrete deep beam specimen presented in chapter three.

In this chapter, conclusion based on analytical evidences as well as some recommendations for future extension of the work has been presented.

5.1. Conclusion

The main conclusions observed from each phase of investigation (finite element analysis) for horizontally reinforced concrete curved deep beam with different L/D and L/R ratio is presented in this section which represents the summary and benefit of this research:

1. The load carrying capacity of horizontally curved reinforced deep beam increased as length to depth (L/D) decreased.As L/D ratio increased from 2.4 to 2.67 and 2.4 to 3 the ultimate load resisted were reduced by27.97% and 48.6% respectively with respect the load carrying capacity of L/D ratio equal to 2.4.
2. Varying the center of curvature L/R (aspect ratio) of curved deep beams, keeping cross section, concrete grade and steel reinforcement constant, load carrying capacity is affected. Increasing the central subtended angle (L/R ratio) is found to cause, a decrease of the ultimate load resisted by curved deep beams. As L/R ratio increased from 0 to 1.57 the ultimate load resisted was reduced by to 17.06%, 16.67% and 15.86% for L/D ratio 3, 2.67 and 2.4 respectively with respect the load carrying capacity of horizontally straight deep beam.
3. The load deflection and load twisting angle response become steeper, as both length to depth (L/D) and aspect ratio (L/R) decreased. Additionally, at ultimate load, as L/D ratio increased from 2.4 to 3 the maximum deflection was increased by 1.89 times (increased

by 89.3%) & the twisting angle was increased up to 1.921 times (increased by 92.1%) and as L/R ratio increased from 0.52 to 1.57 the twisting angle was increased up to 21.2%.

4. The internal torsion increased as the aspect ratio (L/R) of curved deep beams increased. The increase of internal torsion resulted, the decrease of the ultimate load resisted by the beam.
5. The three-dimensional nonlinear finite element model, adopted in the present work, is suitable to predict the torsional behavior of the reinforced concrete curved deep beams. The numerical results are in good agreement with available experimental load-deflection results throughout the entire range of behavior.

5.2. Recommendations for Further Works

- Investigate the torsional behavior of horizontally curved reinforced concrete deep beams with opening.
- Studying the behavior of horizontally curved reinforced concrete deep beams with and without opening subjected to dynamic and impact loading.
- Experimentally determining the torsional behavior of horizontally curved reinforced concrete deep beams with and without openings.
- Studying the shear and flexural resistance horizontally curved reinforced concrete deep beams with openings.

REFERENCE

ABAQUS (2014). ABAQUS 6.14: Documentation, Dassault Systemes Simulia Corp., Providence, RI, USA.

Ammar, Y. A., etal (2015). Experimental Investigation and Nonlinear Analysis of Hybrid Reinforced Concrete Deep Beams. *Al-Qadisiyah Journal for Engineering Sciences.* 8(2):

Page 99-119

ACI Committee 318,(2011). Building Code Requirements for Structural Concrete (ACI318M.11) and Commentary. American Concrete Institute, Farmington Hills, Michigan, USA.

ADINA R&D. (2015).ADINA. Watertown, MA, USA.

ANSYS.(2015). ANSYS. Pittsburgh, PA, USA.

Al-Temeemi, M.A. (2002). Nonlinear Analysis of Reinforced Concrete Horizontally Curved Beams on Elastic Foundation, M.Sc. Thesis, University of Babylon.

Adel, A. A., Ali, S. S. (2011). Finite difference analysis of curved deep beams on winkler foundation, *ARPN Journal of Engineering and Applied Sciences*.6 (3): Page 42-48.

Ali, A.Y., (2010). Three-Dimensional Nonlinear Finite Element Analysis of Reinforced Concrete Horizontally Curved Deep Beams, *Journal of Babylon University*. 18(1).

Argyris, J. H., Kelsey, G. (1960).Energy theorems and structural analysis.Butterworth.

Bhavikatti, (2005). Finite Element Analysis.

Badawy, H. E. I, Jordan, I. J., McMullen, A. E. (1977).Effect of Shear on Collapse of Curved Beams, Journal of the Structural Division, ASCE. 103(9) :Page 1849-1866.

Chen, W. F., Han, D. J. (2012). Plasticity for structural engineers.Springer Science & Business Media.

Cook, R. D. (1981). Concepts and applications of finite element analysis.Wiley. 2nd ed.

Chu, K., Thelen, A. (1963). Plastic Analysis of Circular Balcony Girders, Journal of Structural Division, ASCE. 89(6): Page 159-185.

Clough, R. W. (1960).The finite element method in plane stress analysis.Proc.2nd Conf.on Electronic Computation, ASCE, New York.

Chen, W. F., Saleeb, A. F. (1981). Constitutive Equations for Engineering Materials. West Lafayette. Indiana.

Chen, W. F. (1982).Plasticity in Reinforced Concrete. McGraw-Hill, pp. 471.

DSS, D. S. (2014).ABAQUS (6.14-2). Providence, RI, USA.

Dawlat, D. A., (2007). Experimental and Theoretical Investigation of the Behavior of Reinforced Concrete Beams Strengthened by Fiber Reinforced Polymer. Ph. D. Thesis, University of Baghdad/College of Engineering.

Desai, C.S., Abel, J.F. (1972). Introduction to the finite element method. Van Nostrand.

Eurocode 2 (2004). Design of concrete structures - Part 1-1: General.

EBCS EN 1992, (2013).Ethiopian Building Code Standard.

Hu, H., Schnobrich, W. (1989). Constitutive modeling of concrete by using non-associated

Plasticity, Journal of Materials in Civil Engineering. 1(4): Page 199-216.

Hamzah, B.A. (2012). Behavior of RC Curved Beams with Openings and Strengthened by CFRP Laminates ,P.hd. Thesis, University of Basrah.

Hillerborg, A., Modeer, M., Petersson, P. (1976). Analysis of crack formation and crack

growth in concrete by means of fracture mechanics and finite elements. Cement and

Concrete Research. 6(6): Page 773-782

Hamed M. S., (2004). The Micro Truss Model: An Innovative Rational Design Approach for Reinforced Concrete, Journal of Advanced Concrete Technology. Vol. 2.

Hughes, B. P., Chapman, G. P., (1966). The Complete Stress-Strain Curve for Concrete in Direct Tension, Bulletin RILEM. No. 30: Page 95-97.

Jordaan, I. J., et al (1974).Collapse of Curved Reinforced Concrete Beams, Proceedings, ASCE. 100(11): Page 2255-2269.

Kupfer, H., Grestle, K., (1973).Behavior of Concrete under Biaxial Stress.ASCE-Journal of Engineering Mechanics. 104(4)

Kupfer, H., Hilsdorf, H. K., Rusch, H. (1969). Behaviour of concrete under biaxial stresses, Int. ACI Journal proceedings.66 (8).

Kupfer, H., Hilsdorf, H., Rusch, H. (1969). Behaviour of concrete under biaxial stresses, ACI Journal Proceedings. 66(8): Page 656-666.

Lee, J., Fenves, G. (1998). Plastic-damage model for cyclic loading of concrete structures, Journal of Engineering Mechanics. 124(8): Page 892-900.

Lee, J., Fenves, G. (1998). Plastic-damage model for cyclic loading of concrete structures, Journal of Engineering Mechanics. 124(8): Page 892-900.

Lubliner, J., Oliver, J., Oller, S., Onate, E. (1989). A plastic-damage model for concrete,

International Journal of Solids and Structures. 25(3): Page 299-326.

Malm, R., James, G., Sundquist, H. (2006). Monitoring and evaluation of shear crack initiation and propagation in webs of concrete box-girder sections. In International Conference on Bridge Engineering-Challenges in the 21st Century, Hong Kong. Civil Division, The Hong Kong Institution of Engineers.

Maurizio, G., Kypros, P., Peter, W., (2002). Shear Performance of FRP Reinforced Concrete Beam, Journal of Reinforced Plastics and Composites. No. 22.

Mindess, S., Young, F. J. (1981).Concrete, Prentice-Hall.

Malm, R. (2009). Predicting shear type crack initiation and growth in concrete with nonlinear finite element method". Stockholm, Sweden: Royal Institute of Technology.

Mansur, M.A., Hasnat, A. (1979). Concrete Beams with Small Openings under Torsion, Journal of the Structural Division, ASCE. 105(11): Page. 2433-2447.

Mansur, M.A., Tan, K.H., Lee S.L. (1985). Design Method for Reinforced Concrete Beams with Large Openings, ACI Structural Journal. 82(4): Page 517-524.

Maxwell, B. S. (1996).An experimental study of a structural concrete deep beam with a large opening using the strut-and-tie model.

Mackava, K., Okamura, H., (1983). The Deformation Behavior and Constitutive Equation of Concrete Using the Elasto-Plastic and Fracture Model, Journal of Faculty of Engineering.University of Tokyo.

Macgregor, J. (2009). Reinforced Concrete Mechanics and Design.5th ed. Newjersy.Prentice hall.

Macgregor, J. (2012).Reinforced Concrete Mechanics and Design.6th Ed.

Ngo, D., Franklin, H. A., Scordelis, A. C. (1970). Finite element study of reinforced concrete beams with diagonal tension cracks.University of California.

Neville, A. M., (1981). Properties of concrete.Pitman, 3rded.

Neff, C., Schnellenbach-Held, M., Daus, S. (2002). RC Beams with one Large Rectangular Opening-Experimental Investigations. Vol.17.

Nelson, H., etal (2004). Design of concrete structures. 4thed.

Park, R., Paulay, T., (1974).Reinforced concrete structures. Christ church, Newzeland.

Phama, C., Hancockb, G. (2010). Numerical simulation of high strength cold-formed purlins in combined bending and shear, Journal of Constructional Steel Research. 66:1205-1217.

Ren, W., et al (2014). Numerical Simulation of Prestressed Precast
Concrete Bridge Deck Panels Using Damage Plasticity Model, International Journal of Concrete Structures and Materials. Page 1-10.

Stoner, J. G. (2015).Finite element modelling of GFRP reinforced concrete beams.Master's Thesis, University of Waterloo, Waterloo, Canada.

Sadjad, A. H. (2014). Behavior of R.C. Horizontally Curved Beams with Openings Strengthened by CFRP Laminates. Thesis, University of Babylon, Iraq.

Spilker, R. L., Pian, T. H. (1979). Hybrid-stress models for elastic-plastic analysis by the initial-stress approach. International Journal Numerical Method of Engineering. Vol. 14: 359-378.

TNO DIANA BV. (2015). DIANA. Deft, The Netherlands.

Thannon, A. Y. (1993). Nonlinear three dimensional finite element analysis of reinforced concrete curved beams, Al-Rafidain Engineering. 1(2): Page 2-16.

Thomas, T. C., Leonard, F. Mehmet, J. (1978). Behaviors of reinforced concrete horizontally curved beams, ACI. 75(4): Page 112-123.

Turner, M. J., et al (1956).Stiffness and deflection analysis of complex structure. Vol. 23: 805-823.

Wang T., Hsu T. C. (2001). Nonlinear finite element analysis of concrete structures using new constitutive models, Computers and Structures. 79(32): Page 2781–2791.

Wischers, G. (1978). Application of Effects of Compressive Loads on Concrete.Duesseldorf. Germany.

Zienkiewicz, (2005). The Finite Element Method: Its Basis and Fundamentals. 6^{the} Ed.

Zienkiewicz, O. C. (1977).The finite element method.3rd ed. McGraw-Hill.

Appendix A

Material properties

A. Concrete

Table A.1: Summary of concrete damage parameters

Concrete		Concrete Damage Parameter	
Grade	C25	Eccentricity (γ)	0.1
Density	2.40E-09	Dilation angle (β)	31
Modulus of elasticity	28960	K	0.667
Poisson's ratio	0.18	σ_{bo}/σ_{co}	1.16
		Viscosity parameter	0.0001

Table A.2: Compressive behaviour of concrete damage plasticity

Compressive behaviour		Compressive damage	
σ_c	e_{in}	d_c	e_{in}
10.20	0	0	0
13.44	8.6831E-05	0	8.6831E-05
18.46	0.0002244	0	0.0002244
22.90	0.0005023	0	0.0005023
24.83	0.00086645	0	0.00086645
25.00	0.00103674	0.00	0.00103674
24.66	0.00130338	0.0134837	0.00130338
22.70	0.00180231	0.09217729	0.00180231
19.19	0.00235449	0.23254493	0.00235449
14.34	0.00295272	0.42626595	0.00295272
13.67	0.00302771	0.45290305	0.00302771

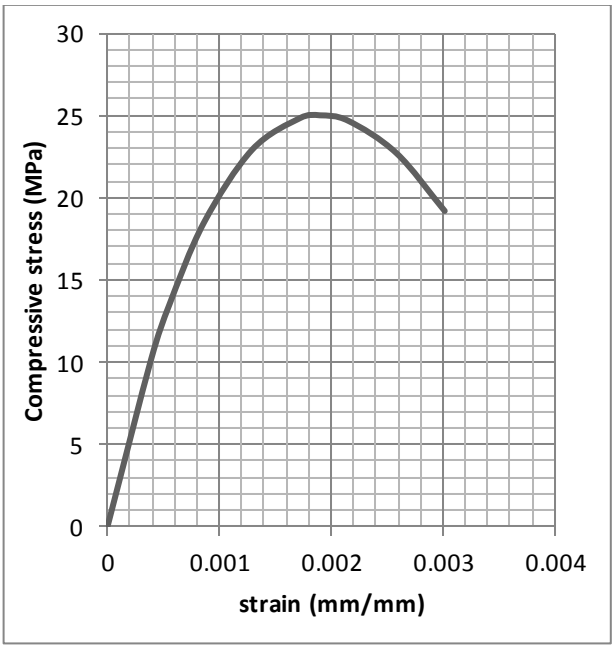

Figure A.1: Compressive stress versus inelastic strain

Table A.3: Tensile behaviour of concrete damage plasticity

Tensile stress		Tension damage	
f_t (Mpa)	c_r (mm/mm)	d_t	c_r
1.983	0.000000	0.00	0.000000
1.503	0.000085	0.24	0.000085
0.813	0.000609	0.59	0.000609
0.557	0.001618	0.72	0.001618
0.353	0.005125	0.82	0.005125
0.318	0.006626	0.84	0.006626
0.254	0.011628	0.87	0.011628
0.226	0.015629	0.89	0.015629

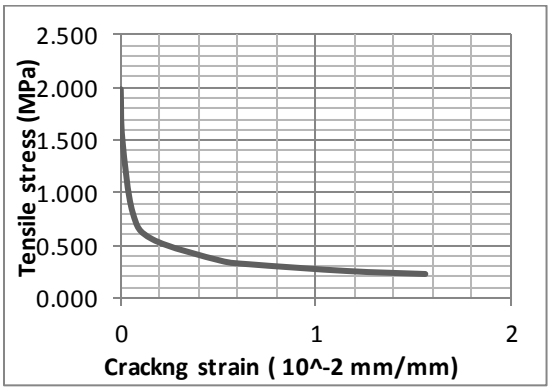

Figure A.2: Tensile versus cracking strain

B. Steel Reinforcement

Table A.4: Steel properties

Steel properties	Diameter of bar		
	ϕ4mm	ϕ10mm	ϕ12mm
Elastic Modulus	200000 MPa	200000 MPa	200000 MPa
Poisson's Ratio	0.3	0.3	0.3
Yield Strength	568	596	643

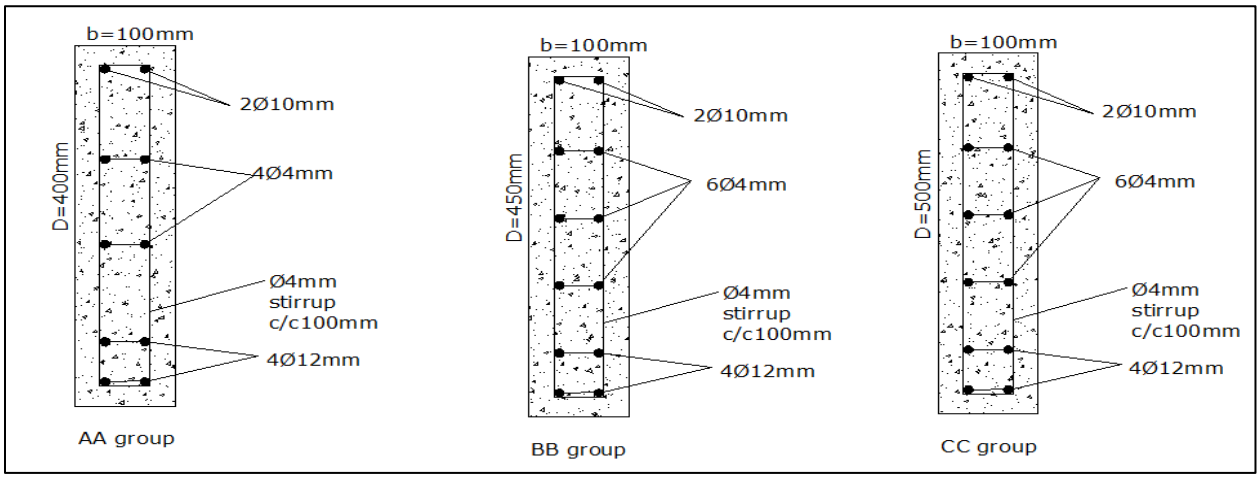

Figure A.3: Cross-sectional view of each group of deep beam

C. Detail reinforcement

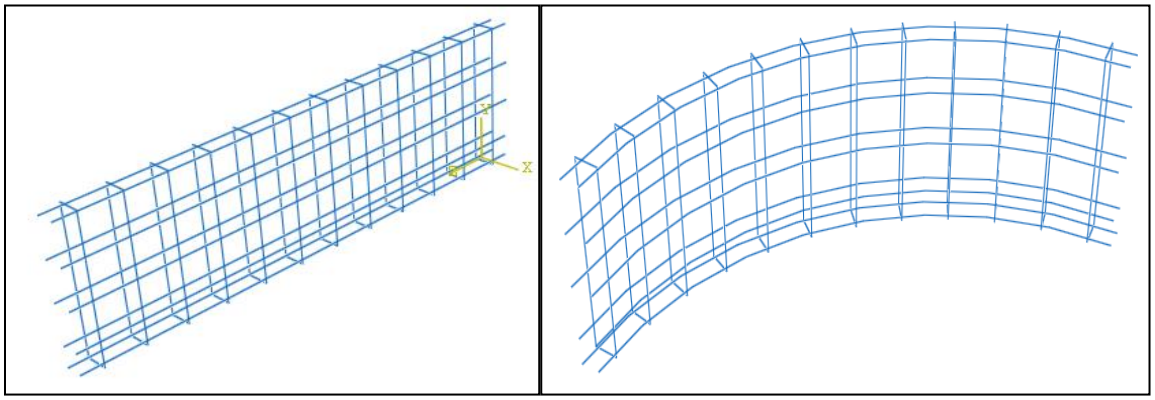

AA10 AA16

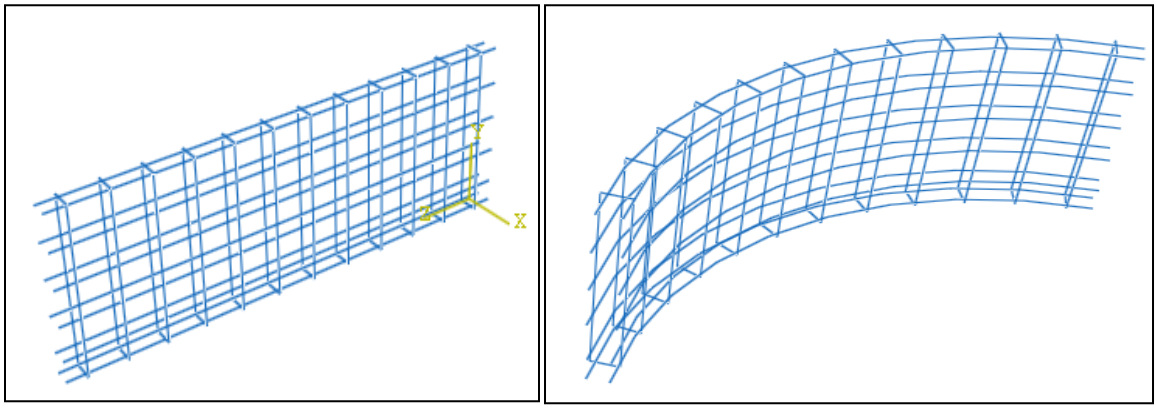

BB10 BB16

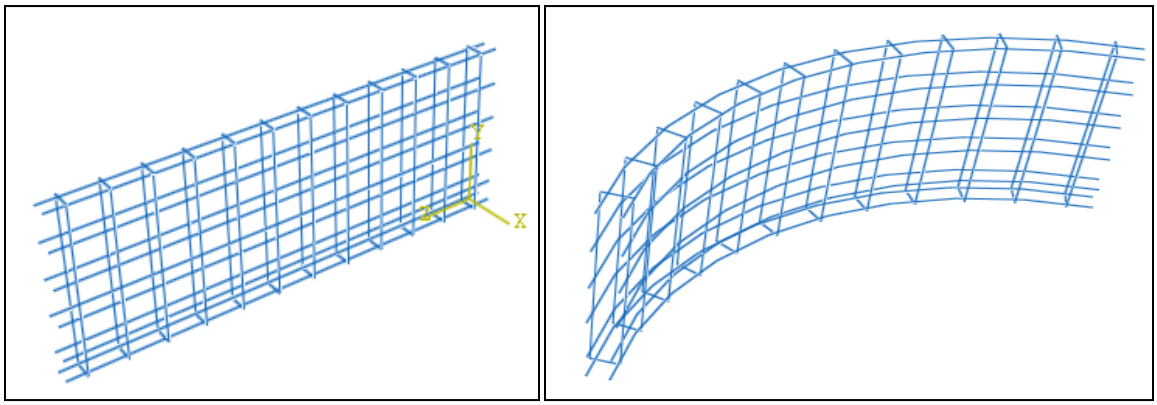

CC10 CC16

Figure A. 4: Sample detail reinforcement

Appendix B

Load versus deflection

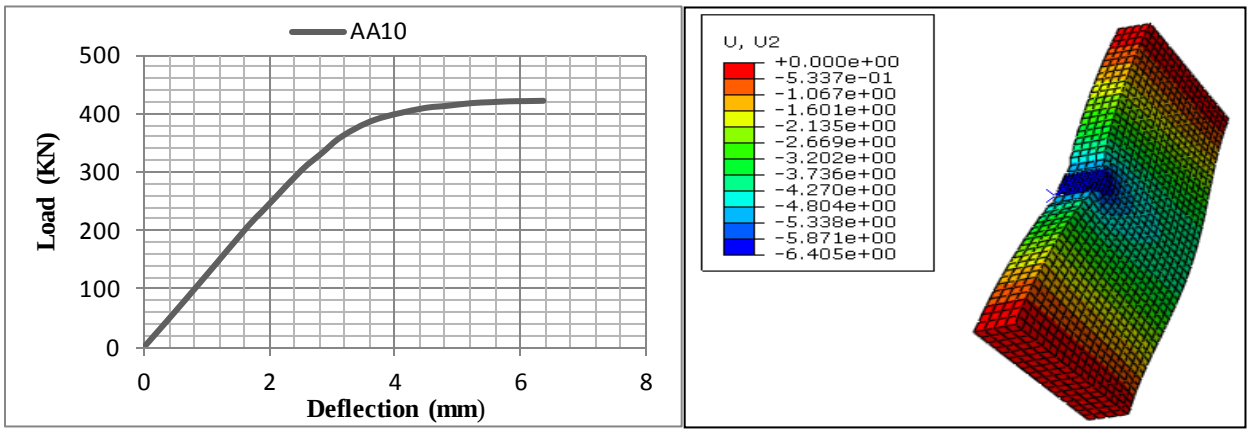

Figure B.1: load versus deflection of AA10

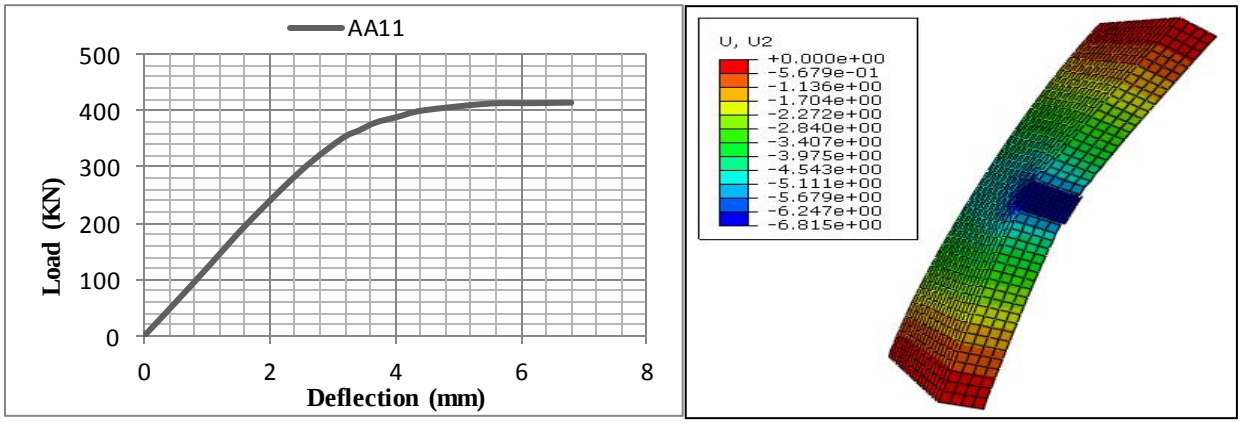

Figure B.2: load versus deflection of AA11

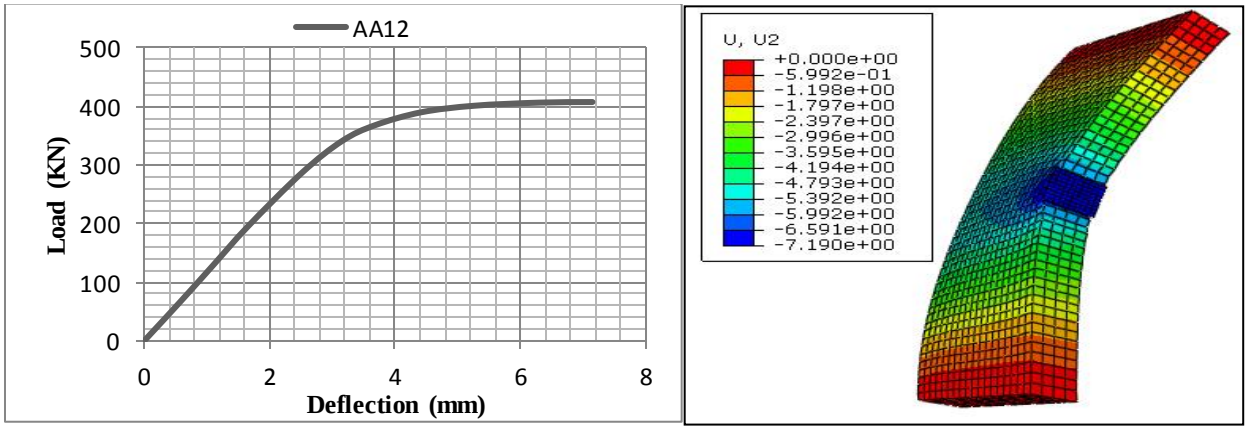

Figure B.3: load versus deflection of AA12

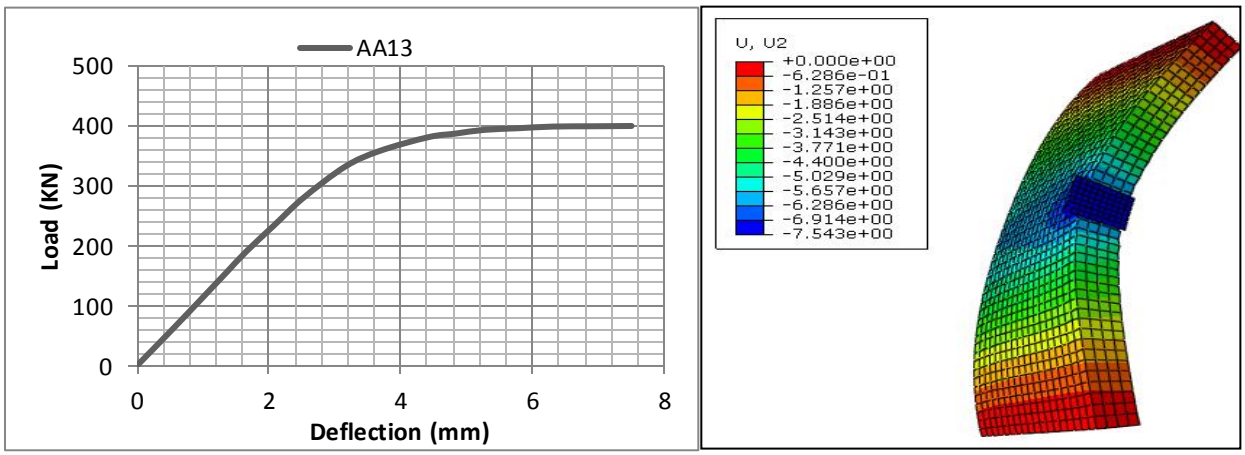

Figure B.4: load versus deflection of AA13

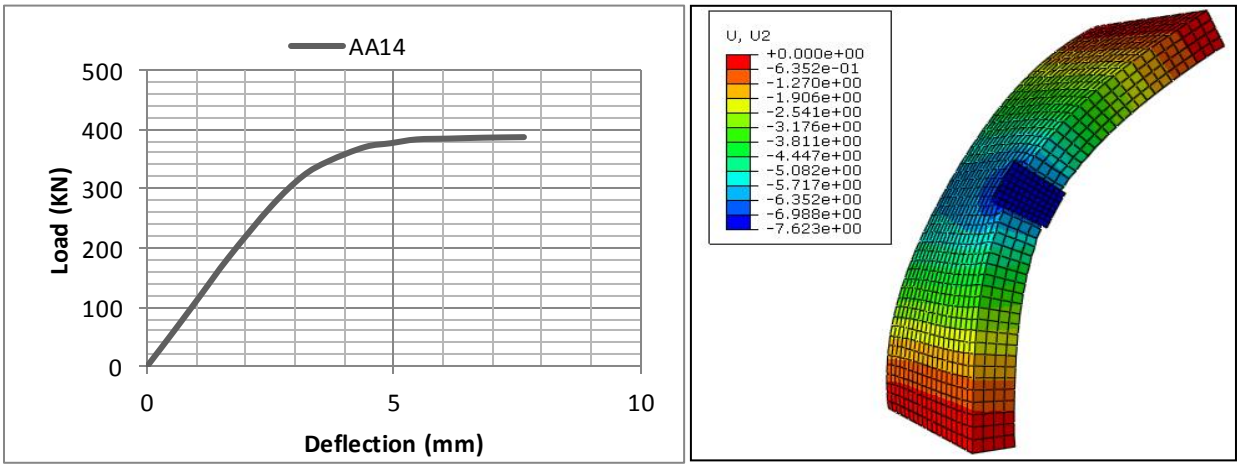

Figure B.5: load versus deflection of AA14

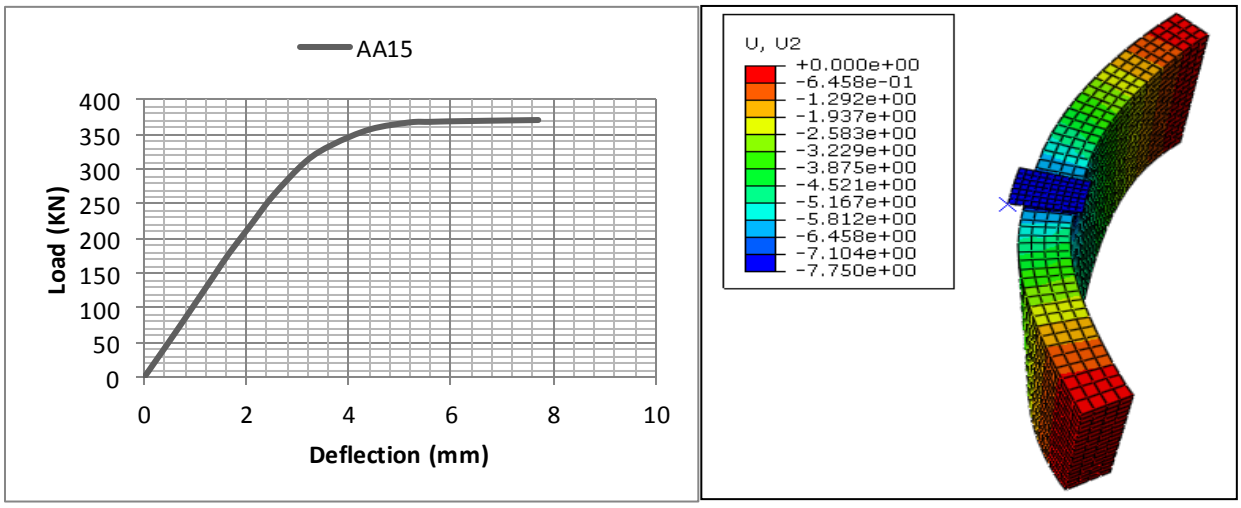

Figure B.6: load versus deflection of AA15

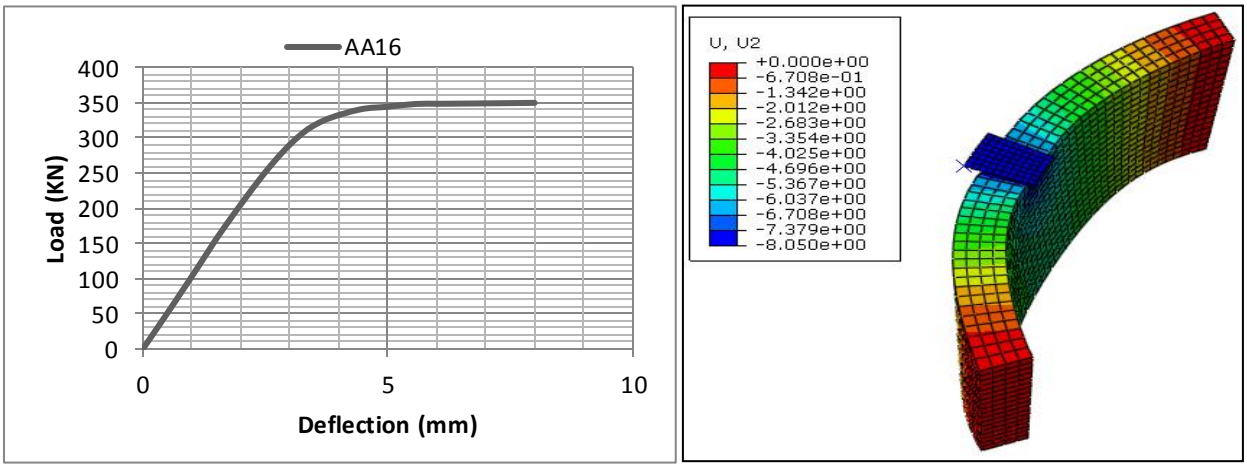

Figure B.7: load versus deflection of AA16

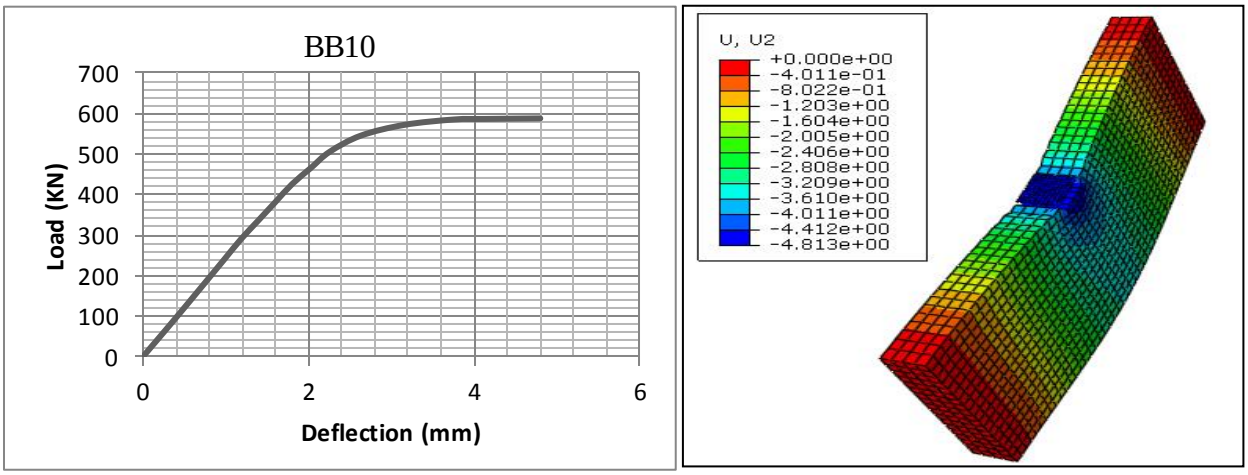

Figure B.8: load versus deflection of BB10

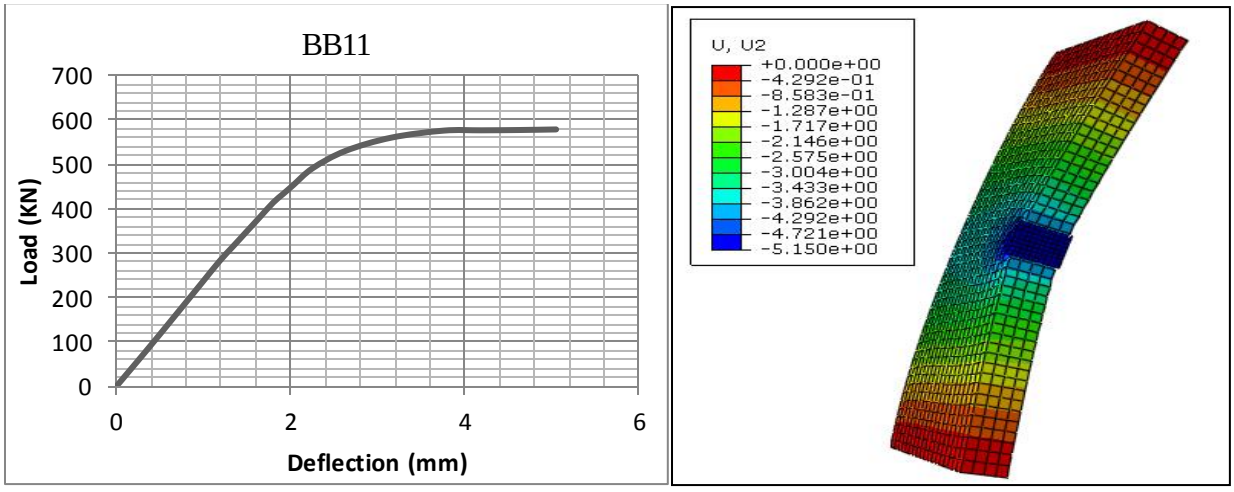

Figure B.9: load versus deflection of BB11

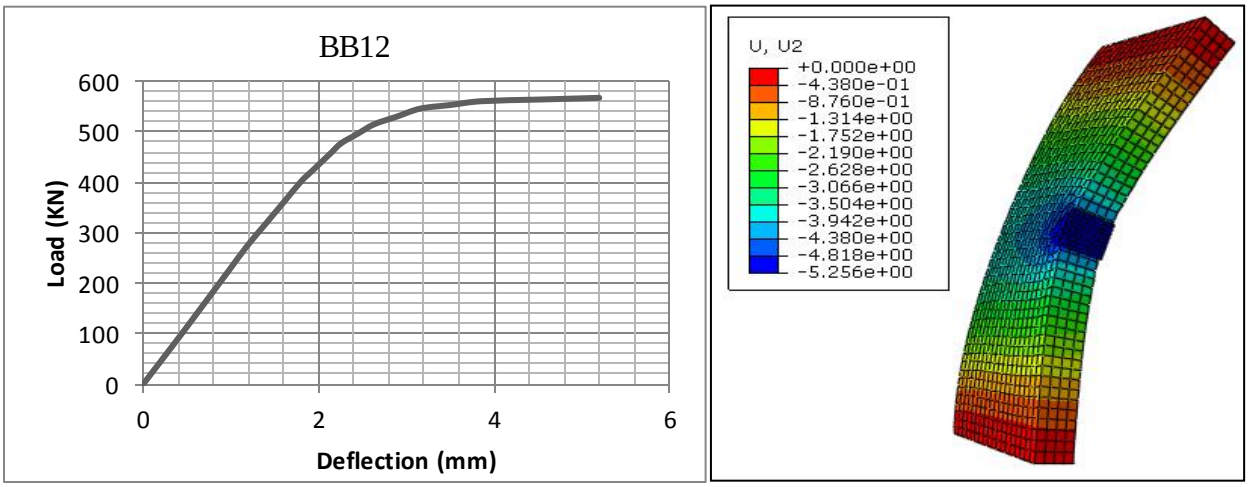

Figure B.10: load versus deflection of BB12

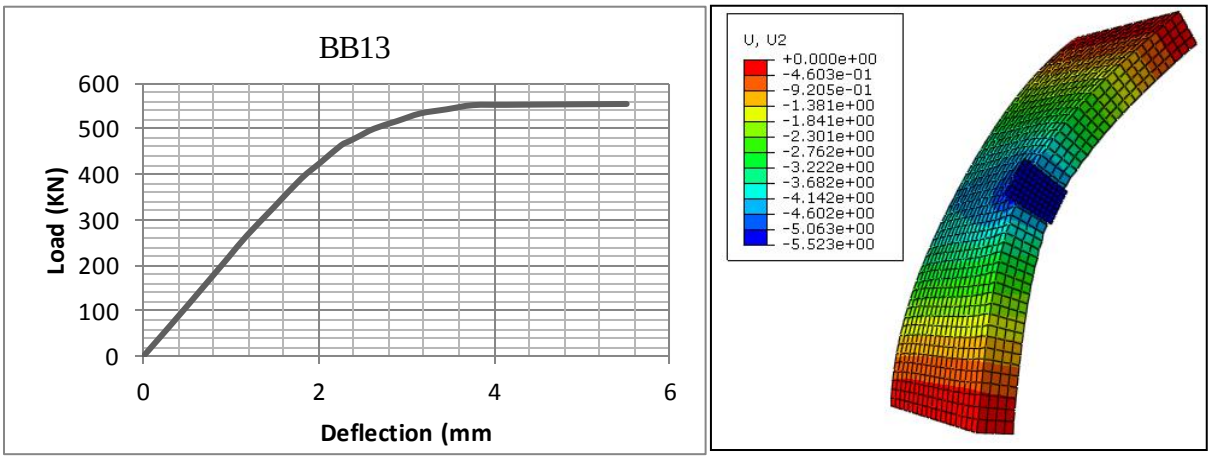

Figure B.11: load versus deflection of BB13

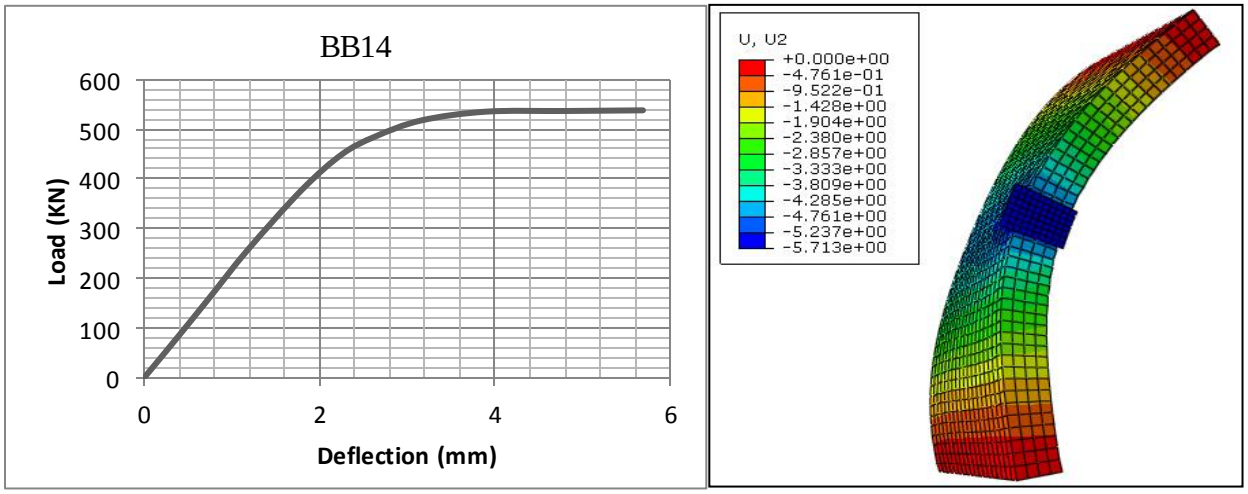

Figure B.12: load versus deflection of BB14

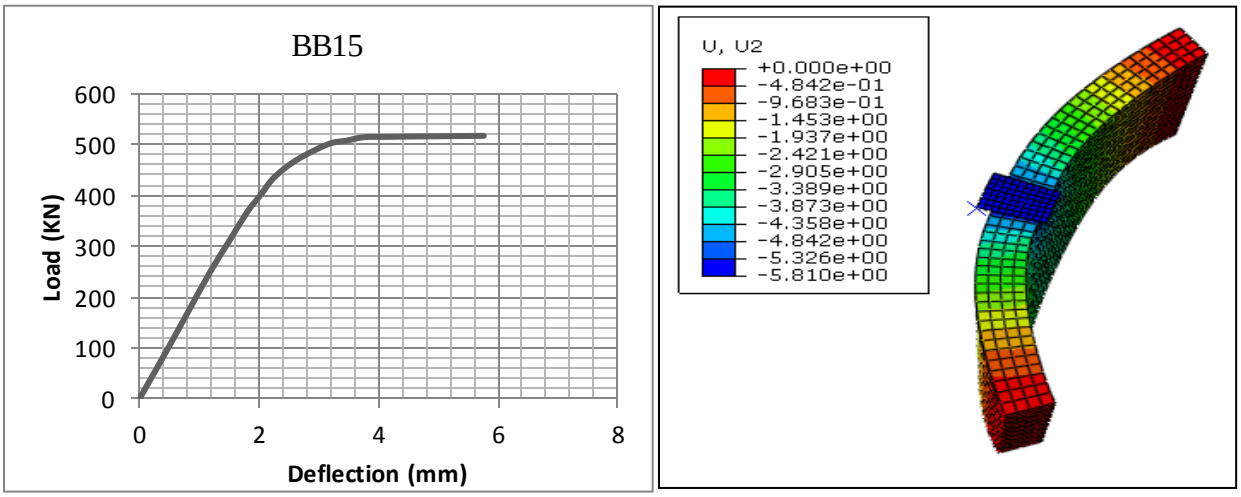

Figure B.13: load versus deflection of BB15

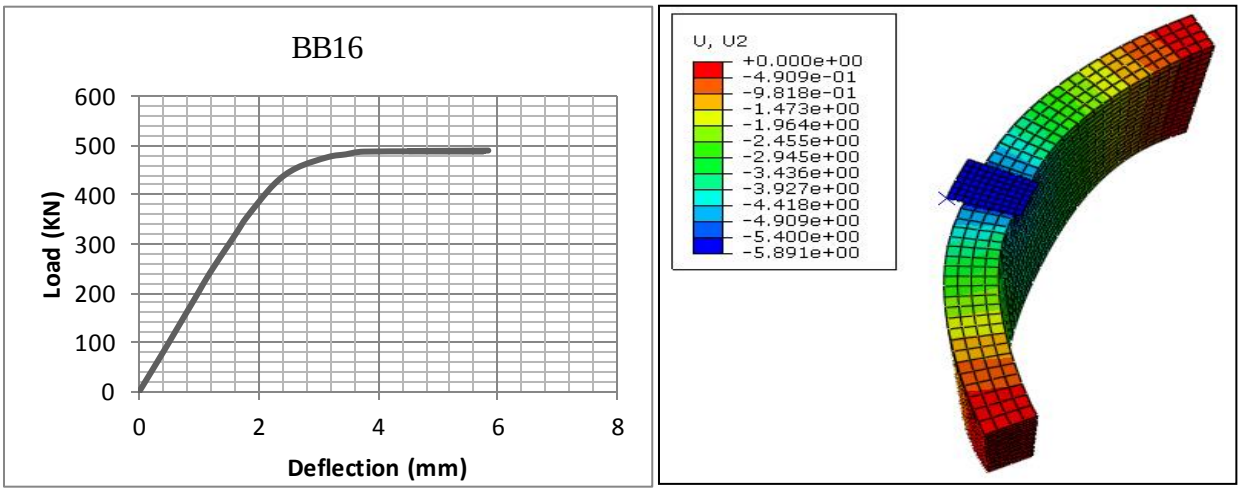

Figure B.14: load versus deflection of BB16

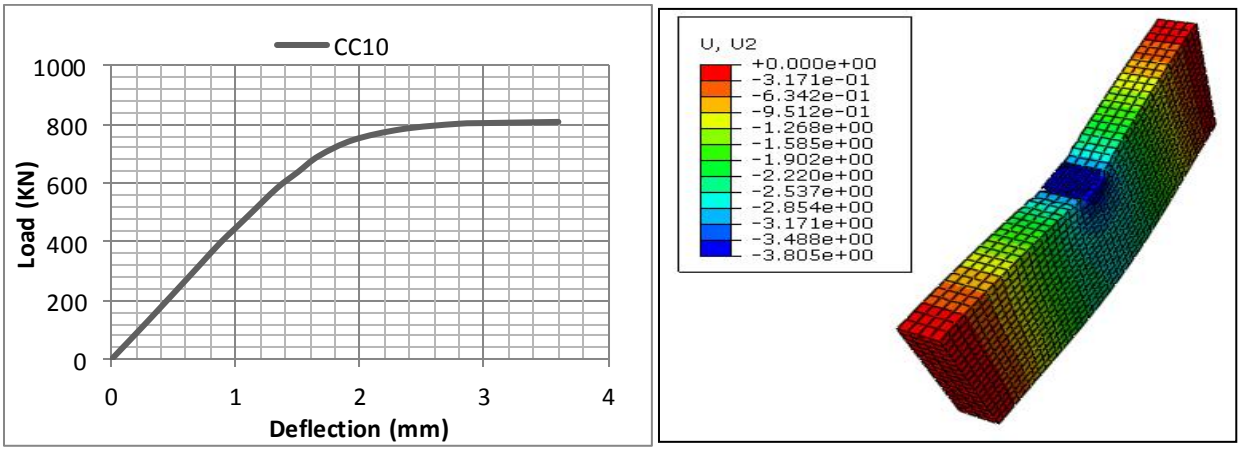

Figure B.15: load versus deflection of CC10

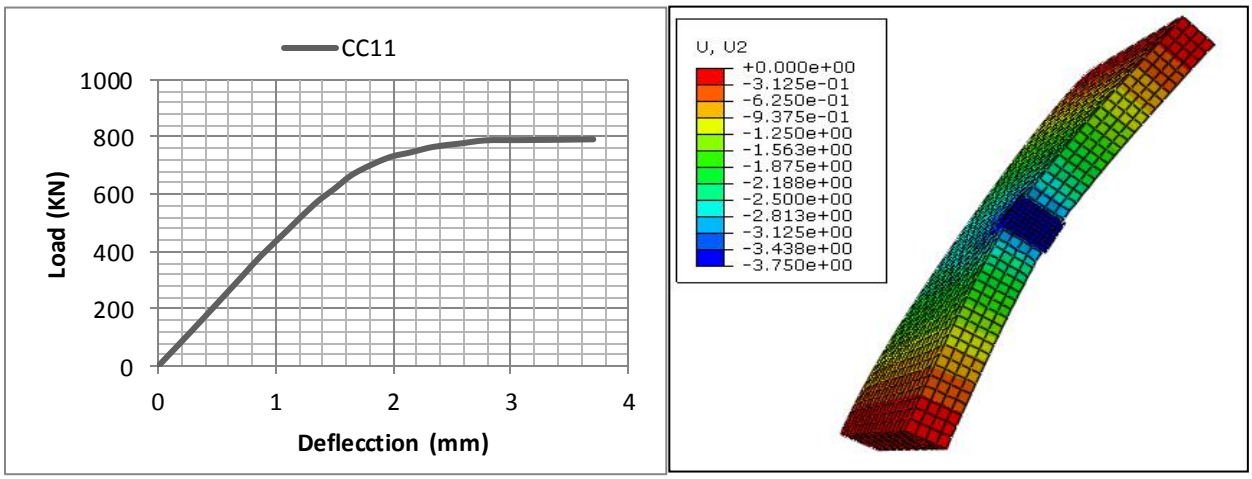

Figure B.16: load versus deflection of CC11

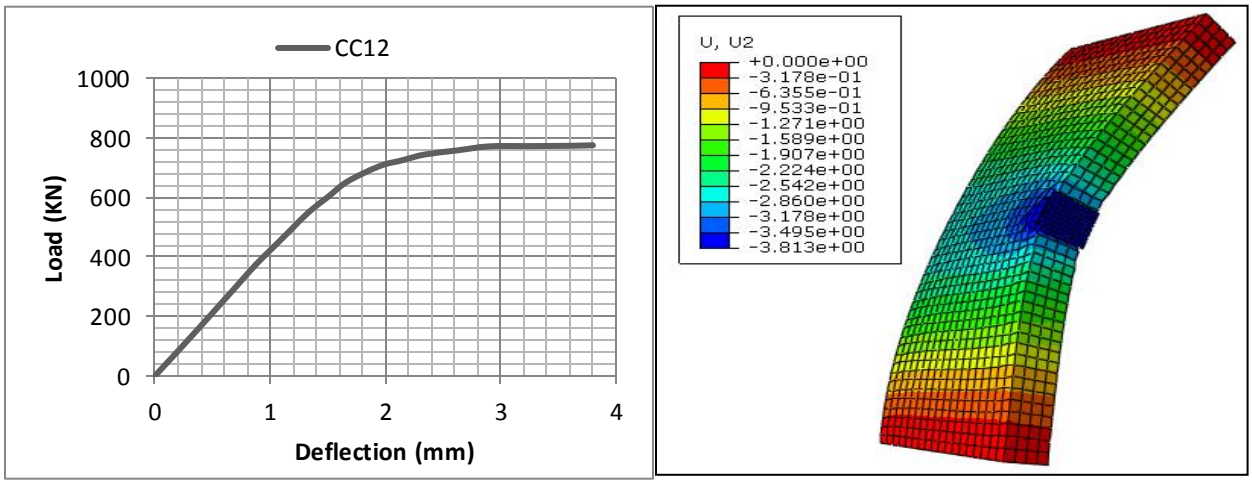

Figure B.17: load versus deflection of CC12

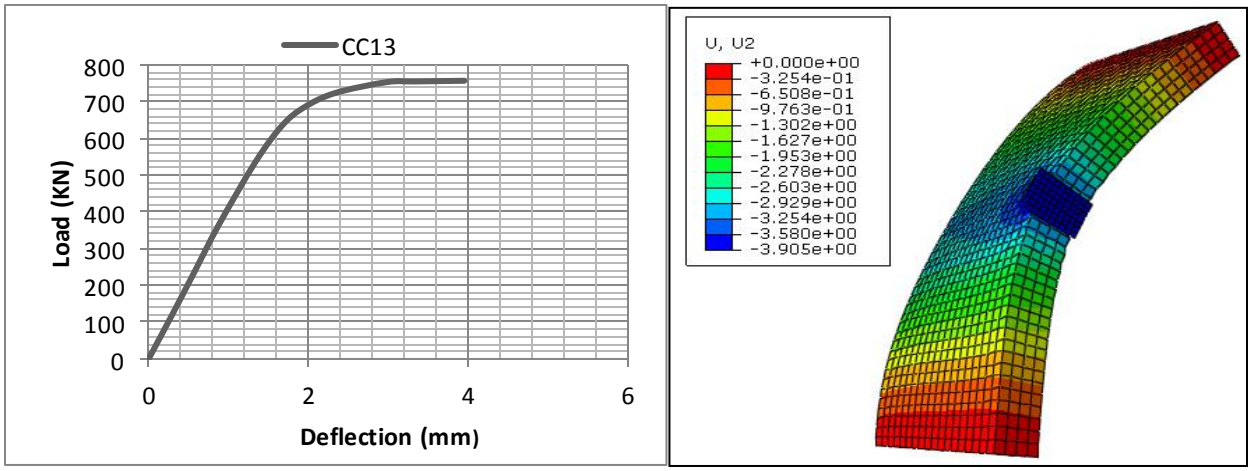

Figure B.18: load versus deflection of CC13

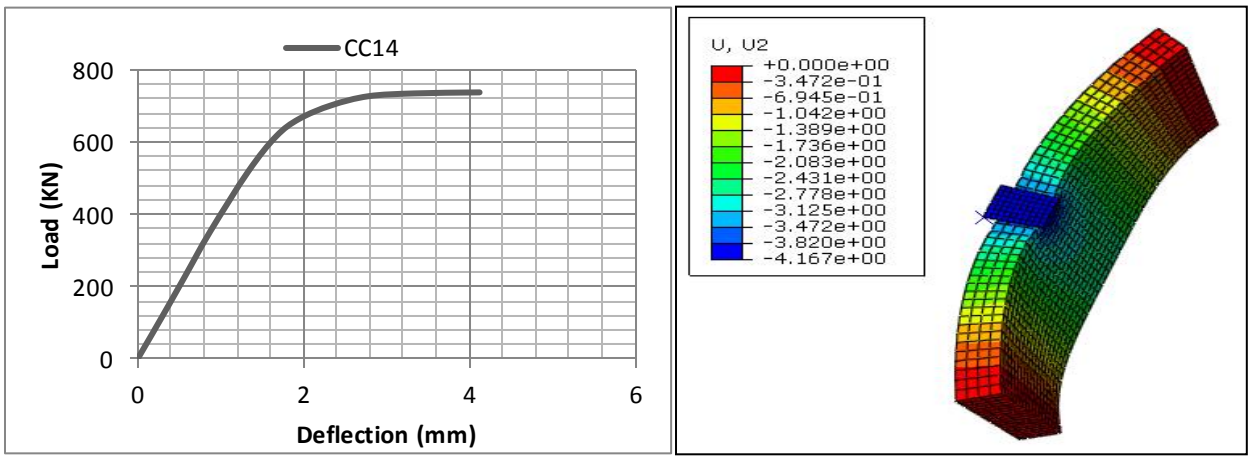

Figure B.19: load versus deflection of CC14

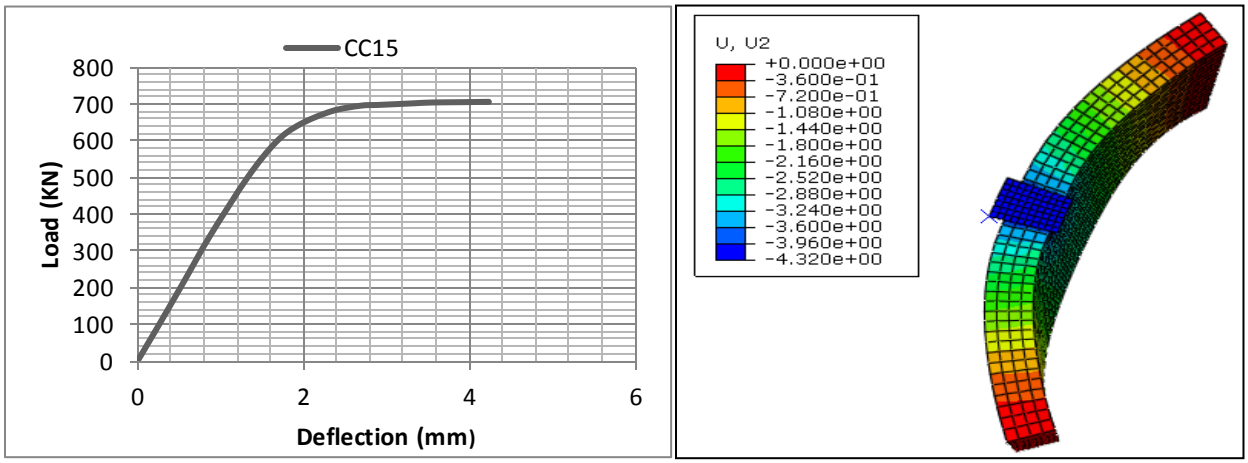

Figure B.20: load versus deflection of CC15

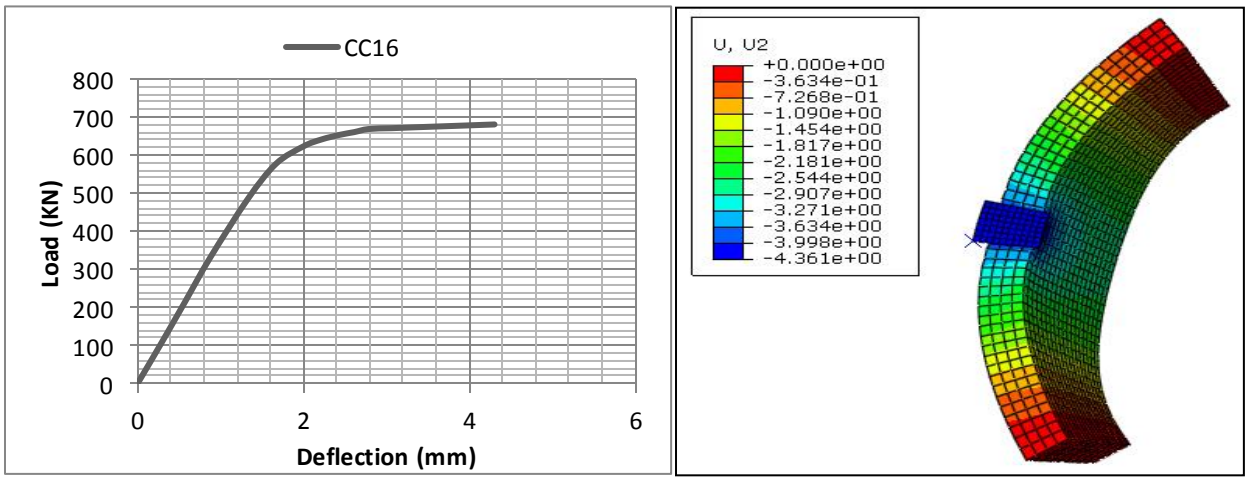

Figure B.21: load versus deflection of CC16

Appendix C

Load versus twisting angle

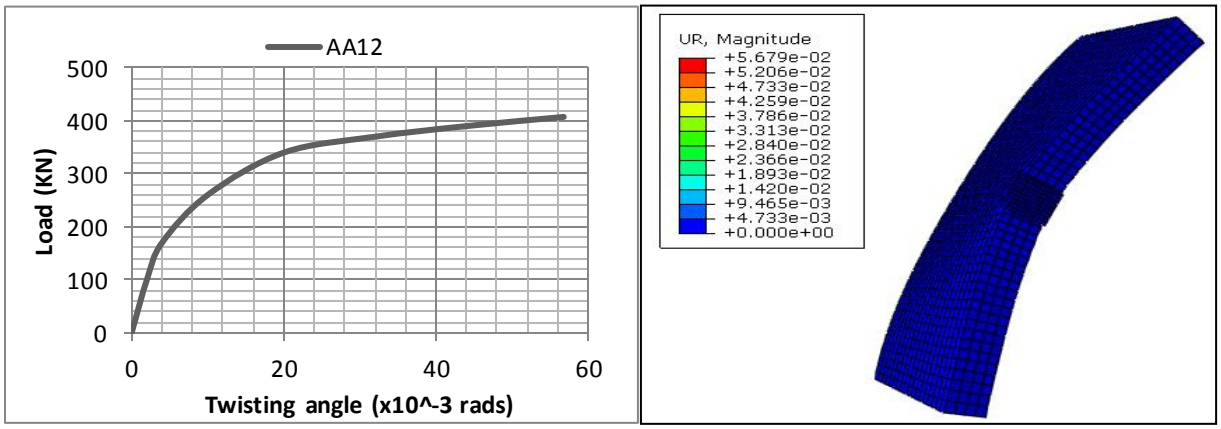

Figure C.22: load versus twisting angle of AA12

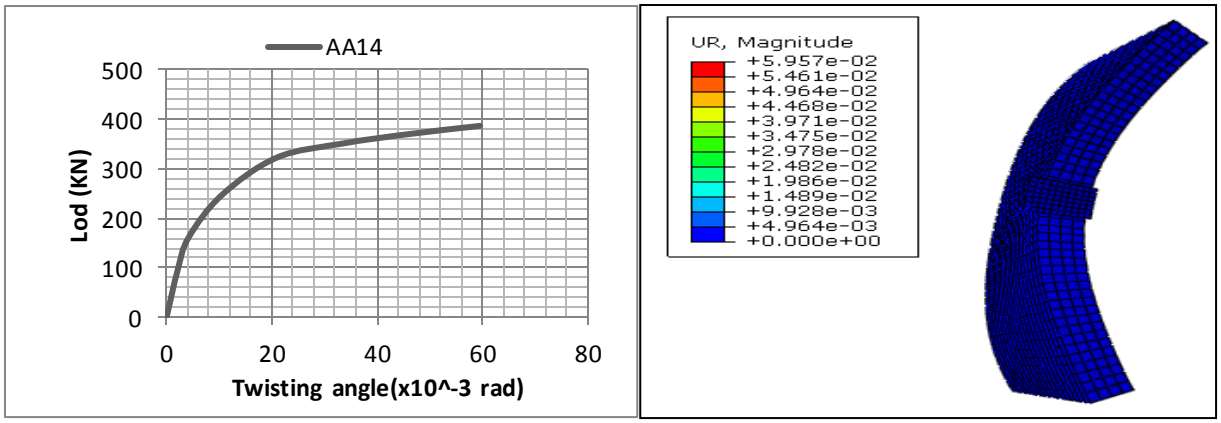

Figure C.23: load versus twisting angle of AA14

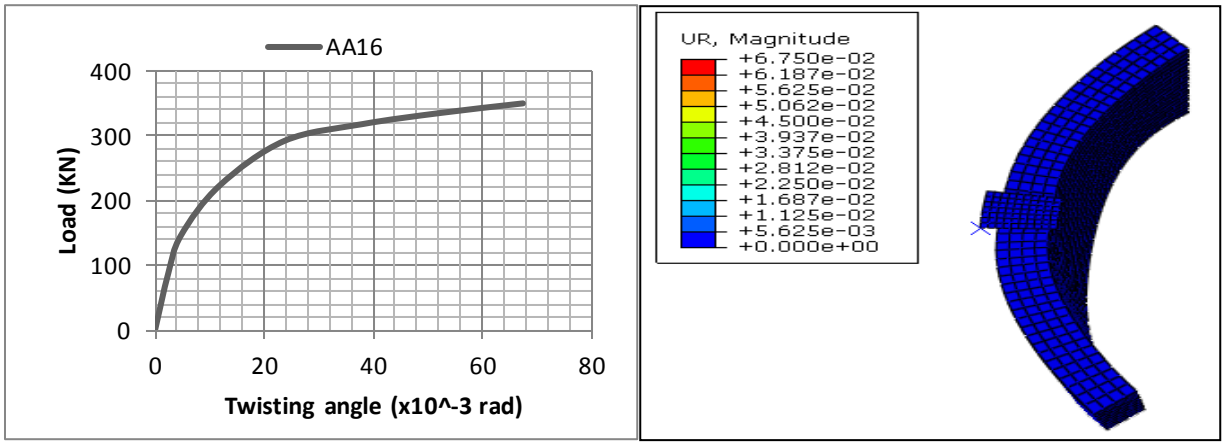

Figure C.24: load versus twisting angle of AA16

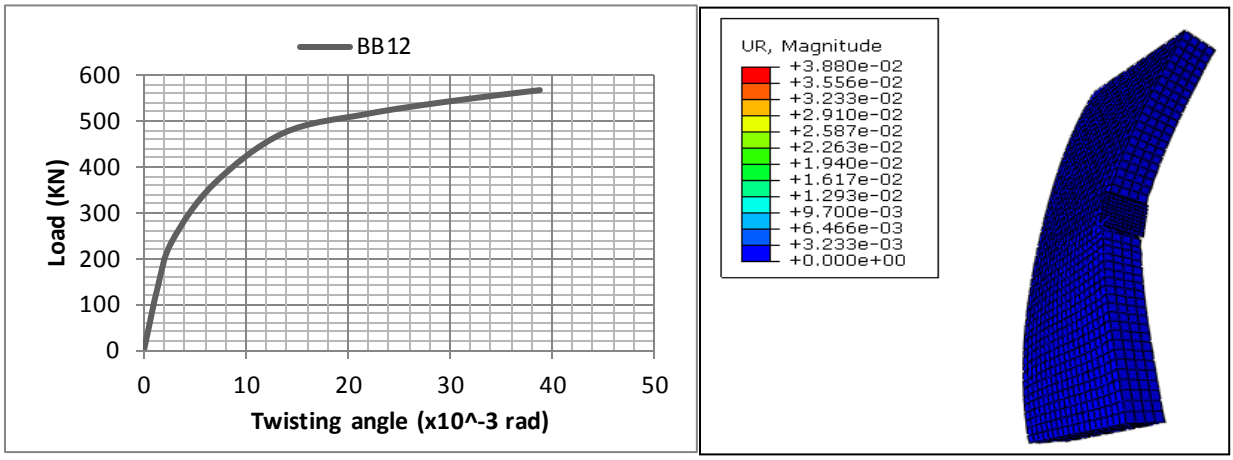

Figure C.25: load versus twisting angle of BB12

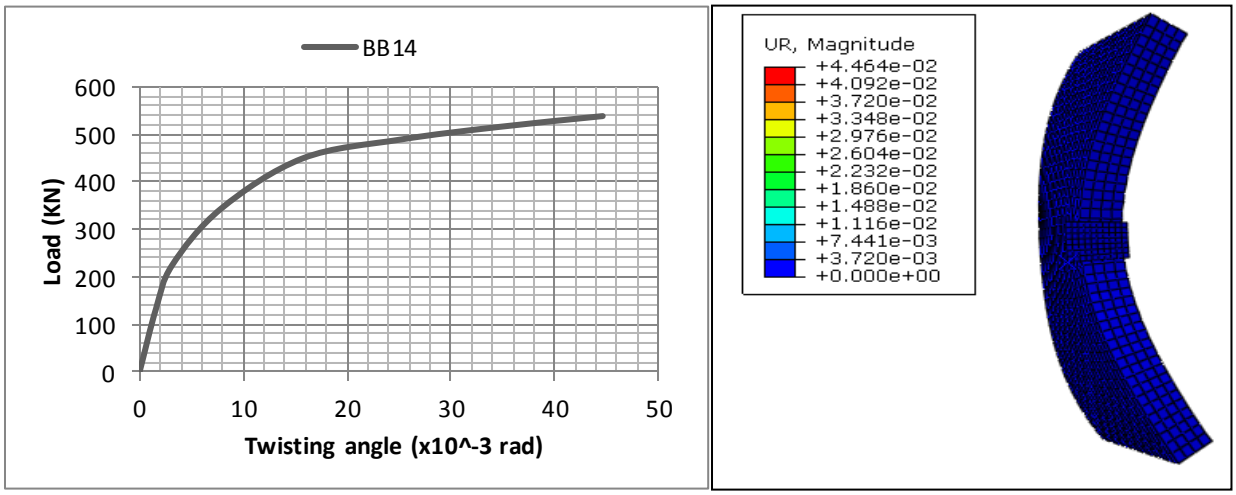

Figure C.26: load versus twisting angle of BB14

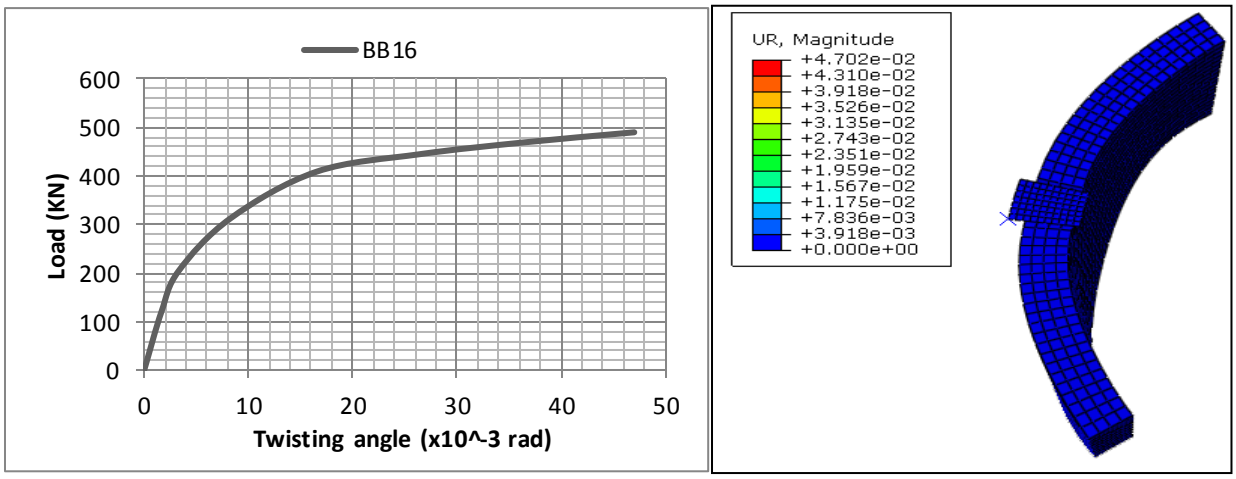

Figure C.27: load versus twisting angle of BB16

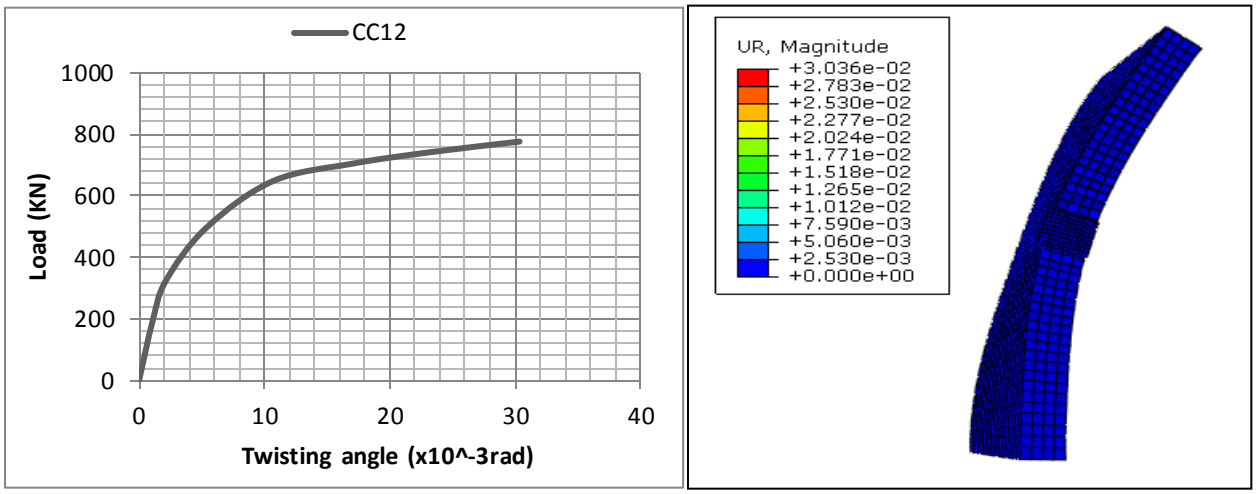

Figure C.28: load versus twisting angle of CC12

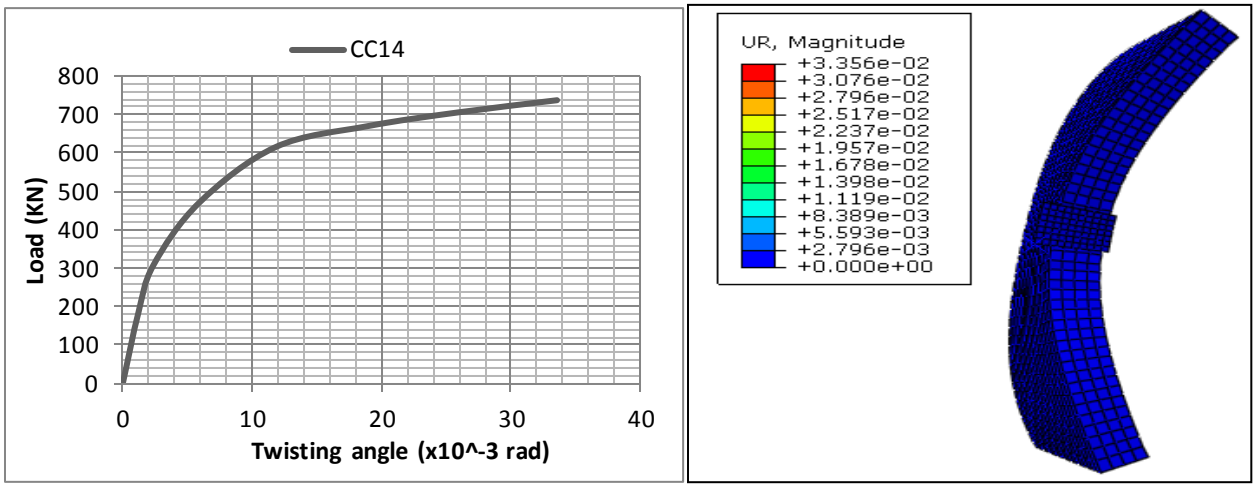

Figure C.29: load versus twisting angle of CC14

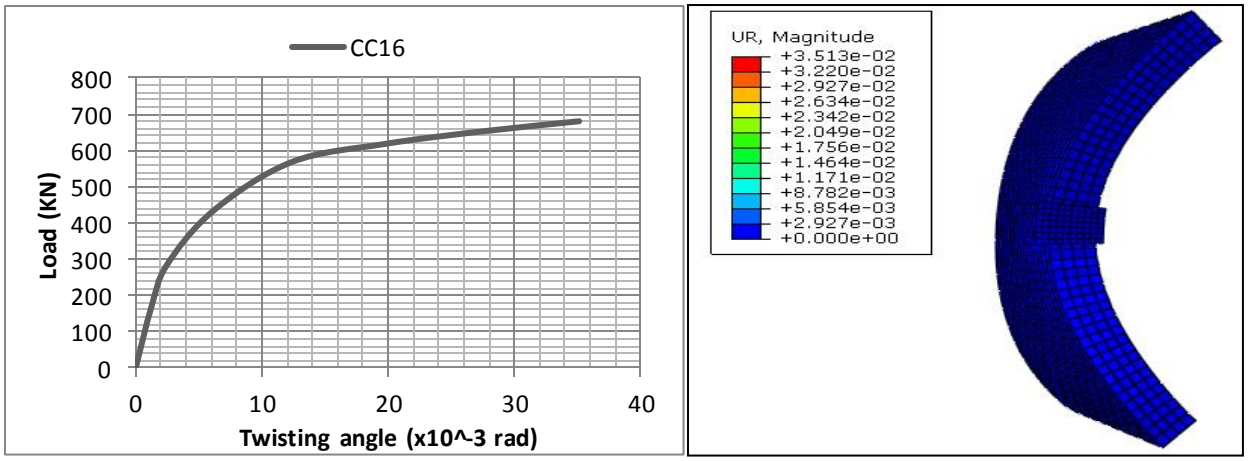

Figure C.30: load versus twisting angle of CC16